

國立交通大學

電信工程學系

博士論文



圓極化單極天線與小型化洩漏波天線

Circularly Polarized Monopole Antenna and
Compact Leaky-Wave Antenna

研究生：吳俊緯 (Jin-Wei Wu)

指導教授：周復芳 博士 (Dr. Christina F. Jou)

共同指導教授：王健仁 博士 (Dr. Chien-Jen Wang)

中華民國九十八年六月

圓極化單極天線與小型化洩漏波天線

Circularly Polarized Monopole Antenna and Compact Leaky-Wave Antenna

研究生：吳俊緯

Student: Jin-Wei Wu

指導教授：周復芳 博士

Advisor: Dr. Christina F. Jou

共同指導教授：王健仁 博士

Co-Advisor: Dr. Chien-Jen Wang



A Dissertation

Submitted to Department of Communication Engineering
College of Electrical and Computer Engineering
National Chiao Tung University
in Partial Fulfillment of the Requirements
for the Degree of Doctor of Philosophy
in
Communication Engineering
Hsinchu, Taiwan

2009 年 6 月

圓極化單極天線與小型化洩漏波天線

研究生：吳俊緯

指導教授：周復芳 博士

共同指導教授：王健仁 博士

國立交通大學 電信工程學系 博士班

摘 要

本論文主要包含三大部分：具圓極化輻射之單極天線、擁有抑制旁波功能之小型化洩漏波天線與漸進式洩漏波天線及利用共平面波導饋入之晶片型天線。第一部份提出兩種圓極化單極天線的設計與成果。第一支天線架構主要是在接地面上加入一倒 L 型的槽孔，使其能產生水平方向的電流分佈，進而與垂直分佈的單極天線激發出雙頻圓極化輻射波。第二支天線的設計目的是要提升第一支天線的阻抗頻寬與圓極化頻寬，設計方法是在接地面上加上一矩形金屬線與在天線主體嵌入一矩形槽孔，此方法不僅不會影響較低頻的圓極化波，同時能有效的增加阻抗頻寬與較高頻的圓極化頻寬。

第二部份描述可抑制旁波功能之小型化洩漏波天線與漸進式洩漏波天線。就抑制旁波功能之小型化洩漏波天線之設計而言，我們將洩漏波天線之接地面嵌入一些矩形槽孔，這些槽孔的大小會影響到洩漏波天線的相位係數與衰減係數，使洩漏波天線能達到小型化的設計。但是，由於此方法造成阻抗不匹配的情況，因此我們利用漸進式洩漏波天線架構之寬頻優點取代矩形的洩漏波天線。最後，我們嵌入兩個矩形槽孔來抑制洩漏波天線產生的旁波，使得這支天線不僅可以縮小洩漏波天線 20% 的寬度，也能有寬頻

的阻抗頻寬及有效抑制旁波。另外，就抑制旁波功能之漸進式洩漏波天線之設計而言，主要是由於漸進式洩漏波天線雖然可以激發出極寬頻的頻寬，但是卻會有非常嚴重的旁波的問題，故我們利用兩個槽孔與一接地針改善漸進式洩漏波天線的電流分佈進而解決此類問題。就量測結果，我們提出的方法雖然阻抗頻寬沒有傳統漸進式洩漏波天線那樣的寬頻，但是卻可以維持洩漏波天線有不錯的輻射特性。

第三部份在於研製適用於無線個人區域網路系統之晶片型天線。設計理念是將傳統往 Broadside 方向輻射的單極天線改變成往 End-Fire 方向輻射。由於在做整合時，天線與前端電路將會被設計在同一晶片上，因此傳統的單極天線所產生的輻射波容易干擾後方的電路，故此天線設計目的主要是為了減少天線與主動電路做整合時所產生的電磁干擾之問題。另外，就模擬的輻射場形結果，我們提出的天線不僅能有效的降低天線輻射對前端電路，而且可以多方向的接收或發射訊號。

Circularly Polarized Monopole Antenna and Compact Leaky-Wave Antenna

Student: Jin-Wei Wu

Advisor: Dr. Christina F. Jou

Co-Advisor: Dr. Chien-Jen Wang

Department of Communication Engineering

National Chiao Tung University

ABSTRACT

This thesis consists of three parts: Monopole antennas with dual-band circular polarization, study of compacting size of leaky-wave antenna and suppressing side lobe of tapered leaky-wave antenna, and on-chip antenna for wireless personal area network (WPAN) application. In the first part, novel designs of dual-band circular polarization (CP) monopole antenna are presented. The proposed antenna comprised of a ground plane embedded with an inverted-L slit, which is capable of generating a resonant mode for broadband impedance-bandwidth, and excites left-hand circular polarization (LHCP) at 2.5 GHz and right-hand circular polarization (RHCP) at 3.4 GHz. Furthermore, embedding an I-shaped slit in the rectangular radiator and adding an I-shaped stub in the ground plane, the impedance-bandwidth can be increased to 6.30 GHz, and the 3-dB AR-bandwidth at 3.4 GHz is greatly enhanced from 230 MHz to 900 MHz. In this design, we use a simple method to achieve the dual-band CP radiation and broad impedance bandwidth.

In the second part, a compact wideband leaky-wave antenna (LWA) with etched slot elements and suppressing side lobe of tapered leaky-wave antenna are studied. In compact wideband LWA case, by etching slot elements on the ground plane, the current distribution of LWA can be influenced to compact the width of conventional LWA. In order to achieve the impedance matching, this multi-section tapered short leaky-wave antenna is embedded with two rectangular slots. This technique not only improves the impedance matching but also suppresses the back lobe. In suppressing side lobe of tapered LWA case, the proposed LWA contains a tapered microstrip radiator with a shorting pin and two rectangular slots. This design of two slots and a shorting pin can interfere with the current distribution of tapered LWA to suppress the radiation of side lobe. In order to achieve the impedance matching, a matching stub is added along the feeding line. The propose LWAs not only successfully reduces the width of a conventional LWA by more than 20 %, but also suppresses the side lobe.

In the third part, an end-fired radiated on-chip monopole antenna for wireless personal area network (WPAN) application is designed. In general, if the on-chip antenna is integrated into RF front-end circuit, the effects electromagnetic interference (EMI) will be considered. Therefore, the proposed antenna can reduce the electromagnetic power to affect the circuit. The architecture of this antenna inherits rectangular monopole antenna except for its asymmetric-fed, slit, and shorting path approaches. The asymmetric-fed provides dual-band

around 60 GHz and end-fire radiation. Besides, by embedding a slit on the monopole antenna and shorting pin on the ground plane, this antenna can achieve wide impedance bandwidth. According the simulated results, the proposed antenna can reduce the radiated power at the feed line to affect the front-end circuit, and the impedance bandwidth can be achieved about 30% with respect to the center frequency at 5.38 GHz.



誌 謝

在這三年博士班的求學過程中，首先我要感謝指導教授周復芳博士給我的專業指導與鼓勵，也給我很大的研究空間，使我能順利完成博士學位。同時，我也要感謝共同指導教授王健仁博士從大學時期就開始栽培我，在我念博班時，提供我諸多的寶貴建議以及軟硬體上的協助。此外，也很感謝口試委員張道治院長、吳霖堃教授、鍾世忠教授、徐敬文教授、黃瑞彬教授、曾振東教授與陳一鋒教授的不吝指導，讓我知道有些問題是我沒考慮到，有些方法是我沒思考到，更讓我學習到不少專業知識。

在 919 實驗室的生活，要感謝全體的學長與學弟們，不論是已畢業的(如智元、班森(志豪)、沛遠、威廉、跳跳虎(昭竹)及昱舜)、剛畢業的(如奕霖、玠瑄、硬漢(昭維)、小老鼠(宗廷)及安東尼(子哲))、即將畢業的(匯儀)或是仍在努力中的(如智鵬、沈爽(宜星)、文斗、傑翔、文袖、冠儀及漢宗)，由於有你們存在，讓實驗室隨時隨地都充滿的歡樂的氣氛，也讓我過著充實又快樂的博士生活。另外，也很感謝碩班時的學長(德福、文才、佳宏及俊杰)、同學(志昌)及學弟們，因為有你們關心與支持，使得我博班這三年的光陰更加多采多姿。

在此，我要非常感謝我的家人，因為有你們的強力支持，雖然在求學過程中，有出現很多問題，也讓我一度有想放棄繼續攻讀博班的想法，但是一切都已過去了，不管醬來會是如何，我還是非常感激你們給我的鼓勵與包容，讓我無後顧之憂的完成學業。最後我要特別感謝我的女友宜君，這些年來對我無怨無悔的付出，陪我度過每個春夏秋冬，也伴我完成我的三個學位(大學、碩士及博士)，由於有妳的關係，我才能如此順順利利。或許還有許多我未感謝到的人，在下會抱著感恩的心來感謝你們的付出。

在此，謹將此論文及小小成果獻給我的父母、家人及我的女友宜君，並與你們分享我的喜悅，謝謝！

吳俊緯

於 風城交大

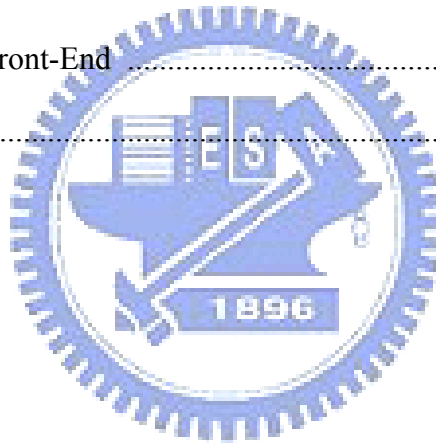
2009.06

Contents

Abstract (Chinese)	i
Abstract (English)	iii
Acknowledgments	vi
Contents	vii
List of Tables	x
List of Figures	xi
Chapter 1 Introduction	1
1.1 Objective of this Thesis	1
1.2 Motivation of Circularly Polarized Monopole Antenna	2
1.3 Motivation of Compact Wideband Leaky-Wave Antenna	7
1.4 Motivation of Suppressing Side Lobe of Tapered Short LWA	11
1.5 Motivation of End-Fire Radiated On-Chip Monopole Antenna for WPAN Application	14
1.6 Thesis Organization	18
1.7 References	20
Chapter 2 Dual-Band Circularly Polarized Monopole Antenna	24
2.1 Basic Monopole Antenna and Polarization Theory	25
2.1.1 Monopole Antenna Theory	25
2.1.2 Polarization Theory	27
2.2 Design of Dual-Band Circularly Polarized Monopole Antenna	30
2.2.1 Antenna 1 Design	31

2.2.2	Antenna 2 Design	33
2.3	Parametric Studies	37
2.3.1	Inverted-L Slit of Antenna 1	37
2.3.2	I-shaped Slit of Antenna 2	38
2.3.3	I-shaped Stub of Antenna 2	39
2.4	Simulation and Measurement Results	43
2.4.1	Impedance Bandwidth and Resonant Modes	43
2.4.2	Axial Ratios	51
2.4.3	Radiation Patterns and Gains	56
2.5	Summary	59
2.6	References	60
Chapter 3	Compact Wideband Leaky-Wave Antenna	61
3.1	Leaky-Wave Antenna Theory	62
3.2	Procedure of Leaky-Wave Antenna Design	67
3.2.1	Compact Leaky-Wave Antenna	68
3.2.2	Parameter Study of Etched Slot Elements	77
3.2.3	Increasing Bandwidth and Suppressing Back Lobe	81
3.3	Simulation and Measurement Results	85
3.4	Summary	89
3.5	References	90
Chapter 4	Suppressing Side Lobe of Tapered Short Leaky-Wave Antenna	92
4.1	Tapered Leaky-Wave Antenna Theory	93
4.2	Antenna Design	95
4.3	Simulation and Measurement Results	102
4.4	Summary	105

4.5	References	106
Chapter 5	End-Fire Radiated On-Chip Monopole Antenna for WPAN Application	107
5.1	Coplanar Waveguide (CPW) Theory	108
5.2	Antenna Design	111
5.3	Simulation Results	117
5.4	Summary	124
5.5	References	125
Chapter 6	Future Study	126
6.1	Radiation of Dual-Beam	126
6.2	Integration of Front-End	127
6.3	References	129



List of Tables

Table 2-1	Dimensions of the proposed printed Antenna 1 and 2	36
Table 2-2	Performance of Conventional and proposed antennas	55
Table 3-1	Dimensions of the proposed Leaky-Wave Antenna	73
Table 4-1	Dimensions of the proposed Tapered Short LWA	97
Table 5-1	Dimensions of the proposed Monopole Antenna	116



List of Figures

Figure 1-1	Microstrip-fed annular-ring patch for CP antenna [1-7]	5
Figure 1-2	Dual-band CP antenna [1-8]	5
Figure 1-3	Two prototypes of CP antenna: (a) annular-ring slot antenna [1-9], (b) microstrip- fed circularly polarized slot antenna [1-10]	6
Figure 1-4	Frequency-fixed beam-scanning microstrip leaky-wave antenna [1-17]	9
Figure 1-5	Microstrip leaky-wave antenna (MLWA) with parasitic elements [1-20]	9
Figure 1-6	Two prototypes of LWA: (a) EME microstrip leaky-mode antenna [1-21], (b) half-width antenna [1-22]	10
Figure 1-7	Active frequency-scanning leaky-mode antenna array [1-25]	12
Figure 1-8	Active feedback microstrip leaky wave antenna [1-26]	13
Figure 1-9	Aperture-fed patch antenna connected to the LWA [1-27]	13
Figure 1-10	On-chip antenna: (a) monopole antenna [1-28]; (b) PIFA [1-32]	15
Figure 1-11	On-chip dipole antenna: (a) dipole antenna with balun [1-33]; (b) dipole antenna with front-end circuit [1-34]	16
Figure 1-12	On-chip Yagi antenna: (a) Yagi antenna with director, driven, reflector element, and a ground plane [1-31]; (b) quasi-Yagi antenna [1-35]	17
Figure 2-1	Antenna 1, configurations of the proposed printed monopole antenna	

	with inverted-L slit	34
Figure 2-2	Antenna 2, configurations of the proposed printed monopole antenna with inverted-L slit, I-shaped slit, and I-shaped strip	34
Figure 2-3	Simulated surface current distribution of conventional monopole antenna at 3 GHz	35
Figure 2-4	Simulated AR of conventional monopole antenna	35
Figure 2-5	Simulated center frequency of axial ratio and 3-dB axial ratio bandwidth for the inverted-L length of Antenna 1: (a) lower band; (b) upper band	40
Figure 2-6	Simulated phase difference and axial ratio of the I-shape slit length of Antenna 2 at upper band: (a) axial ratio; (b) phase difference	41
Figure 2-7	Simulated phase difference and axial ratio of the I-shape stub length of Antenna 2 at upper band: (a) axial ratio; (b) phase difference	42
Figure 2-8	Simulated and measured return loss of the conventional antenna and Antenna 1	46
Figure 2-9	Simulated surface current distributions of Antenna 1: three resonant modes of monopole (a) 2.25 GHz; (b) 4.65 GHz; (c) 6.35 GHz; and one resonant mode of ground plane (d) 3.35 GHz	47
Figure 2-10	Comparison the measured return loss of Antenna 1 with and without the bevel	48
Figure 2-11	Simulated and measured return losses against frequency for the proposed Antenna 2	48

Figure 2-12	Simulated surface current distributions of Antenna 2: (a) 2.93 GHz; (b) 3.37 GHz; (c) 6.00 GHz; and (d) 8.00 GHz	49
Figure 2-13	Comparison the simulated return loss of Antenna 2	50
Figure 2-14	Simulated and measured axial ratio and phase difference of Antenna 1: (a) lower band; (b) upper band	53
Figure 2-15	Simulated and measured axial ratio and phase difference of Antenna 2: (a) lower band; (b) upper band	54
Figure 2-16	Measured radiation patterns of Antenna 1 in the XY- and XZ-plane: (a) 2.50 GHz; (b) 3.44 GHz	57
Figure 2-17	Measured radiation patterns of Antenna 2 in the XY- and XZ-plane: (a) 2.49 GHz; (b) 3.70 GHz; (c) 4.20 GHz	58
Figure 3-1	Field diagram for the (a) dominant mode and (b) first higher order mode (E field: solid line, H field: dashed line) [3-2]	65
Figure 3-2	Top view of the strip of microstrip line and dielectric region around it [3-6]	66
Figure 3-3	Normalized complex propagation constants of the conventional microstrip LWA. $H = 1.6$ mm, $W = 15$ mm, and $\epsilon_r = 4.4$. k_0 is the free space wave number	66
Figure 3-4	Configuration of the proposed leaky-wave antenna	72
Figure 3-5	Normalized complex propagation constants of the conventional microstrip LWA. $H = 1.6$ mm, $W = 15$ mm, and $\epsilon_r = 4.4$. k_0 is the free space wave number	73

Figure 3-6	Comparison of the theoretical, simulated, and measured θ_m and $\Delta\theta$ of a conventional LWA: (a) Radiation angle θ_m ; (b) Radiation beamwidth $\Delta\theta$	74
Figure 3-7	Simulated radiation angle and 3-dB radiation beamwidth of LWA with etched slot elements: (a) Radiation angle θ_m ; (b) Radiation beamwidth $\Delta\theta$	75
Figure 3-8	Simulated surface current distributions at 4.2 GHz: (a) conventional LWA; (b) LWA with 10 slot elements	76
Figure 3-9	Simulated radiation patterns of the slot widths, G_1 , in the YZ-plane at 3.70 GHz	79
Figure 3-10	Simulated radiation patterns of the slot lengths, G_2 , in the YZ-plane at 3.70 GHz	79
Figure 3-11	Comparison the simulated return losses of conventional LWA and LWA with 10 slot elements on the ground plane	80
Figure 3-12	Comparison the simulated impedance of the LWA of conventional, tapered, and tapered with Slot-A structure: (a) Real part; (b) Imaginary part	83
Figure 3-13	Comparison the simulated radiation patterns of the multi-section tapered short LWA without slot, that with Slot-A, and that with Slot-A and Slot-B at 4.3 GHz	84
Figure 3-14	Simulated and measured radiation patterns of the proposed LWA in the YZ-plane: (a) simulated patterns; (b) measured patterns	87
Figure 3-15	Maximum measured gains of the proposed LWA	88

Figure 3-16	Comparison the simulated and measured return losses of the conventional LWA and the proposed LWA	88
Figure 4-1	Three structure of tapered LWA: (a) Type I, (b) Type II, (c) Type III [4-1]	94
Figure 4-2	Structure of the proposed short length LWA	97
Figure 4-3	Measured normalized radiation patterns of the conventional tapered short LWA	98
Figure 4-4	Simulated return losses of the conventional tapered short LWA and the conventional tapered short LWA with Slot 1 structure	98
Figure 4-5	Structures of LWA and simulated radiation pattern in YZ-plane at 6.0 GHz: (a) conventional tapered short LWA; (b) LWA with Slot 1; (c) LWA with Slot 1 and 2; (d) proposed LWA; (e) Radiation pattern	99
Figure 4-6	Simulated surface current distributions at 6.0 GHz: (a) conventional tapered short LWA; (b) LWA with Slot 1; (c) LWA with Slot 1 and 2; (d) proposed LWA	100
Figure 4-7	Simulated radiation pattern in YZ-plane at 6.0 GHz	101
Figure 4-8	Simulated surface current distributions at 6.0 GHz: (a) $0.75 \lambda_0$ between Slot 1 and Slot 2; (b) $1.0 \lambda_0$ between Slot 1 and Slot 2	101
Figure 4-9	Measured normalized radiation patterns of the proposed LWA	103
Figure 4-10	Comparison of the measured main lobe to side lobe ratios (MSR) of tapered LWA and proposed LWA	103
Figure 4-11	Comparison of measured maximum gains of the tapered LWA and the	

	proposed LWA	104
Figure 4-12	Simulated and measured return losses of the proposed LWA	104
Figure 5-1	3D structure of conventional coplanar waveguide (CPW)	110
Figure 5-2	Structure of the proposed on-chip monopole antenna	113
Figure 5-3	Surface current distribution of the monopole antenna with central-fed and asymmetric-fed: (a) central-fed at 78.6 GHz; (b) asymmetric-fed at 60 GHz	114
Figure 5-4	Simulated normalized radiation patterns of the monopole antenna with asymmetric-fed at 60 GHz: (a) XY-Plane; (b) YZ-Plane	115
Figure 5-5	Simulated return losses of central-fed and asymmetric-fed	116
Figure 5-6	Proposed on-chip antenna: (a) layout photo; (b) micrographic	118
Figure 5-7	Simulated return loss of the proposed antenna	119
Figure 5-8	Current distribution of the on-chip antenna: (a) 58 GHz; (b) 63 GHz	120
Figure 5-9	Simulated normalized radiation patterns of on-chip antenna at 58 GHz: (a) XY-Plane; (b) YZ-Plane; (c) 3D	121
Figure 5-10	Simulated normalized radiation patterns of on-chip antenna at 63 GHz: (a) XY-Plane; (b) YZ-Plane; (c) 3D	122
Figure 5-11	Maximum simulated gain of the proposed LWA	123
Figure 5-12	Simulated gain of the proposed LWA at end-fire direction	123
Figure 6-1	Schematic configuration of the topology for dual-beam radiation	127

Figure 6-2 Configure of a beam-switchable scanning LWA [6-1] 128

Figure 6-3 Configure of frond-end: (a) transmitter [6-2], (b) receiver [6-3] 128



CHAPTER 1

INTRODUCTION

1.1 Objective of this Thesis

In this thesis, three topics are proposed. The first topic is the monopole antennas with dual-band circular polarization. The research includes how to transform the polarization from the linearly polarized monopole antenna to circularly polarized antenna, and how to increase the axial ratio bandwidth. The second topic includes two types: compacting size of leaky-wave antenna and suppressing side lobe of tapered leaky-wave antenna. These researches include the studies of reducing width of leaky-wave antenna, increasing impedance bandwidth, and suppressing side lobe. These properties provide a lot of advantages for the scanning systems, traffic control, and collision avoidance system such as compact size, low cost, wideband, and easy fabrication. The third topic is the study of on-chip antenna for wireless personal area network (WPAN) application. The on-chip antenna is fabricated by using TSMC 0.18- μm CMOS process. The above antenna not only provides 7.7 GHz bandwidth for WPAN band, but also excites end-fire radiation.

1.2 Motivation of Circularly Polarized Monopole Antenna

In recent years, printed monopole antennas have been developed since they have many attractive features such as simple structure, low profile, light weight, wide impedance-bandwidth, and omni-directional radiation patterns [1-1] ~ [1-3]. The antennas are widely used for the wireless communication systems such as GSM, DCS, PCS, IMT-2000, WLAN, and UWB. However, these printed antennas are both tall and wide; they are few applications in handheld devices.

In general, the radiation patterns of printed monopole antennas are linearly polarized (LP); they are difficult to radiate circularly polarized (CP) radiation wave which was generated by two near-degenerated orthogonal resonant modes of equal amplitude and 90° phase difference (PD). Recent the applications of circularly polarized (CP) wave have attracted much attention due to their significant superiority on resisting of inclement weather over linearly polarized (LP) wave. They have been especially employed in modern communication systems sensitive to atmospheric variation, such as radar tracking, navigation, satellite systems, radio frequency identification (RFID), sensor systems, and mobile communication systems [1-4]. The hazard caused by misalignment could be neglected to simplify antenna mounting as well as to benefit receiving efficiency, and the essential feature of polarization diversity is that the signal reception performance can be improved in the multi-path fading environment. If the monopole antenna can generate the LP and CP radiation

waves, the applications of the monopole antenna will be greatly enhanced.

Typically, the planar CP antenna is achieved through using patch antenna [1-5] ~ [1-8] and slot antenna [1-9] ~ [1-12]. Previous reports in [1-5] and [1-6] show that a CP patch antenna is introduced by cutting slot. A coupling method of a fan-shaped patch for CP antenna has been proposed in Fig. 1-01 [1-7]. To reduce the size of CP antenna, see Fig. 1-02, a cross-patch with a dual-band hybrid is proposed [1-8]. These antennas can excite a pure CP radiation wave, but the impedance- and AR-bandwidth are narrower than 10%. To generate wider AR-bandwidth, many printed slot antennas are designed [1-9] ~ [1-12]. In [1-9] and [1-10], the antenna structures contain a ring slot which produces CP radiation waves by embedding a slot or adding a shorted strip (see Fig. 1-03). In addition to ring slot, a crosspatch-loaded is added in the centre of the square slot [1-11] and a mono-strip is added in the circular slot [1-12] to excite two near-degenerate orthogonal resonant modes of equal amplitude and 90° phase difference for CP. In fact, the 3-dB AR-bandwidth of slot antennas can be larger than 10%. However, the 10-dB impedance-bandwidth is less than 50%.

In chapter 2, novel broadband monopole antennas with dual-band CP are proposed. A microstrip-fed monopole antenna with an inverted-L slit in the ground plane, called Antenna 1. It gives a broadband impedance-bandwidth of 102.5% at the center frequency of 4.35 GHz and the dual-band CP radiation waves of 6.0% LHCP at the center frequency of 2.485 GHz (lower band) and 6.7% RHCP at the center frequency of 3.425 GHz (upper band). In addition,

Antenna 2 is designed by embedding an I-shaped slit in monopole radiator and adding an I-shaped stub in ground plane. It can further increase the impedance-bandwidth to 118.4% and enhance the 3-dB AR-bandwidth at the upper band to 23.1%. The results show that the two novel antennas can achieve broadband impedance-bandwidth and dual-band CP. The impedance- and AR-bandwidth are better than patch and slot antenna.



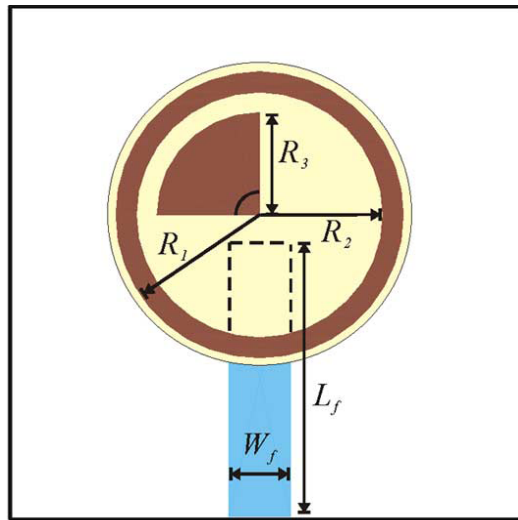


Fig. 1-1. Microstrip-fed annular-ring patch for CP antenna [1-7].

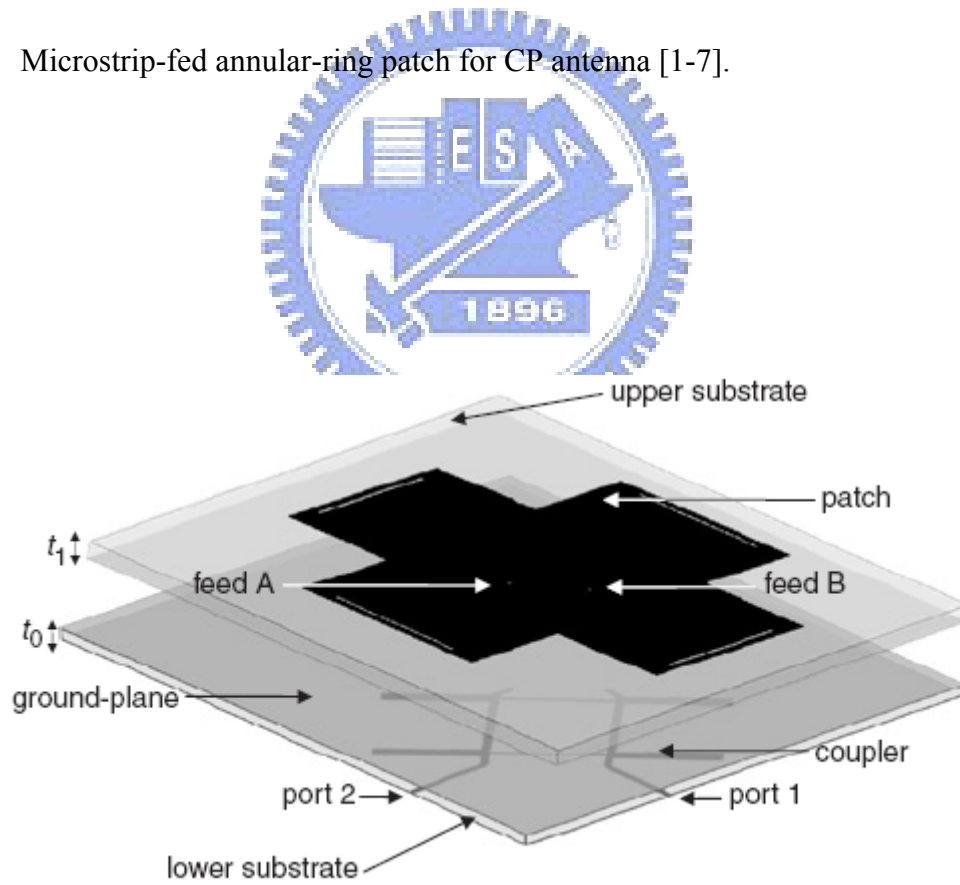
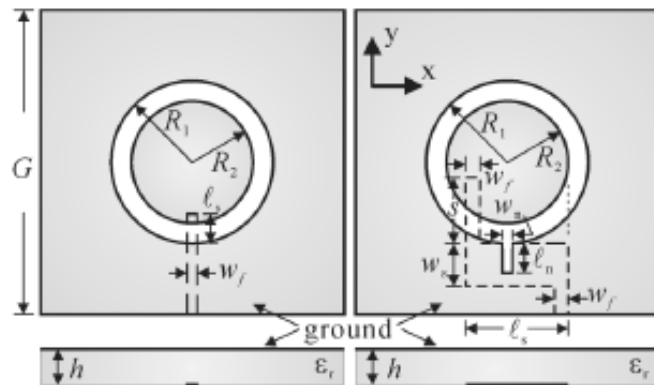
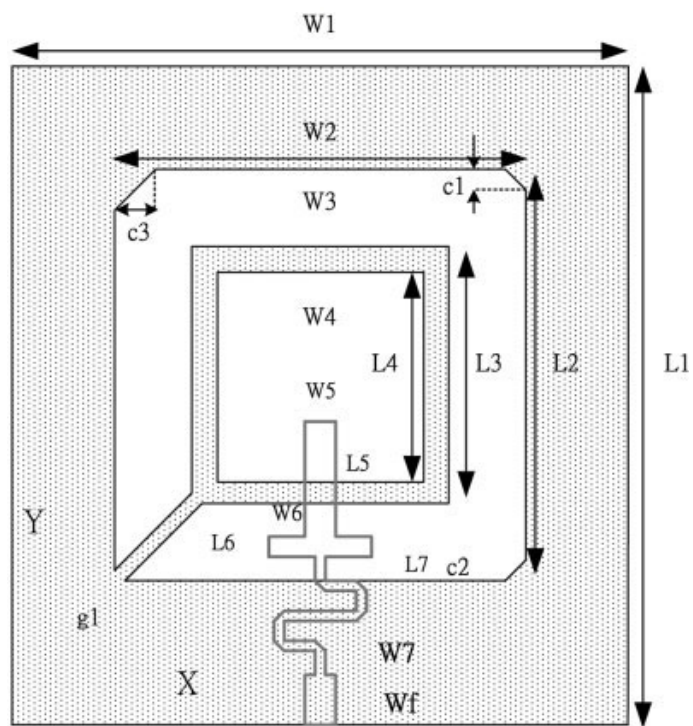


Fig. 1-2. Dual-band CP antenna [1-8].



(a)



(b)

Fig. 1-3. Two prototypes of CP antenna: (a) annular-ring slot antenna [1-9], (b) microstrip-fed circularly polarized slot antenna [1-10].

1.3 Motivation of Compact Wideband Leaky-Wave Antenna

Leaky wave antennas (LWAs) have been presented nearly thirty years, the structure of which was proposed in 1979 by Menzel [1-13] and the theory of which was derived in 1986 by Oliner and Lee [1-14]. LWAs are usually used in the radar system and the satellite communication because they possess the advantages of narrow beam, frequency-scanning capability, wideband bandwidth, and fabrication simplicity [1-15] and [1-16]. For enhancing the applications of LWA, the frequency-fixed beam-scanning LWAs are proposed [1-17] and [1-18]. In [1-17], the structure of microstrip leaky-wave antenna, which is plotted in Fig. 1-04, contained many feeding terminals and control switches which achieved the ability of frequency fixed beam-scanning by switching different feeding terminal. In addition to use of the switch, an active microstrip leaky wave antenna which derived the dual-beam asymmetrically scanning pattern by the active circuit was designed [1-18].

Although owning many advantages, LWA is faced with a major problem of large size. As well known, the length and the width of LWA are respectively required about four and half wavelengths to radiate effectively. There are two ways to reduce the antenna size: shortening the length and reducing the width. In general, if the length is shortened, the induced back lobes, which are caused by the reflected power, will be increased. For suppressing the back lobes of short LWA, a radiating element was added at the end of short LWA to radiate the remaining power in [1-19]. Recently, a method of utilizing two patches with short-circuit

edges, see Fig. 1-05, was designed to couple the radiation power, and then suppressed the back lobe [1-20]. Excluding short LWA, the techniques of compressing the width have been presented in [1-21] and [1-22]. The structures of the LWA are shown in Fig. 1-06. The electric-magnetic-electric (EME) microstrip was added in the LWA to affect the first higher order mode, and a half width LWA was designed to compact the width of conventional LWA by the image theory.

In chapter 3, we propose a novel method to achieve compact size, wide bandwidth, and low back lobes. This antenna is composed of etched slot elements on the ground plane. Although this method can shift the cutoff frequency to lower frequency in order to reduce the width of conventional LWA, these etched slot elements on the ground plane causes the impedance mismatching. Therefore, we embedded two rectangular slots, Slot-A and Slot-B, on the multi-section tapered short LWA. These two slots can achieve the impedance matching and suppress the back lobe. Detail design rules and results of the short LWA antenna (only about $1.14 \lambda_0$ at 3.4 GHz) demonstrate that the impedance bandwidth can be achieved about 33 % at the center frequency of 3.95 GHz for 7-dB return loss. The cutoff frequency of this antenna can be shifted about 750 MHz from 4.15 GHz to 3.40 GHz in order to reduce the width of the LWA by more than 20 %. The back lobe can be suppressed by 7.5 dB at 4.3 GHz.

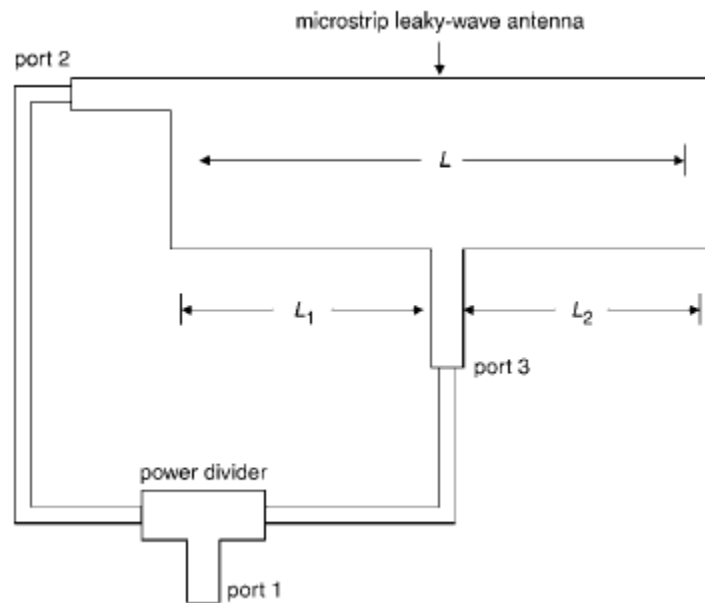


Fig. 1-4. Frequency-fixed beam-scanning microstrip leaky-wave antenna [1-17].

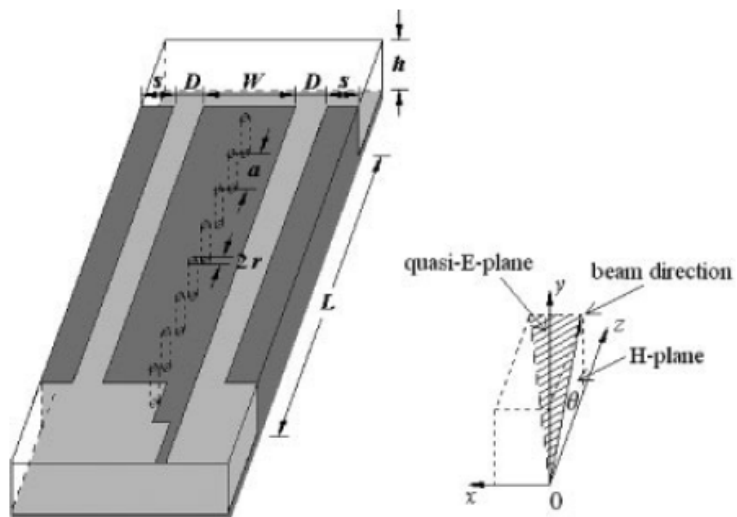
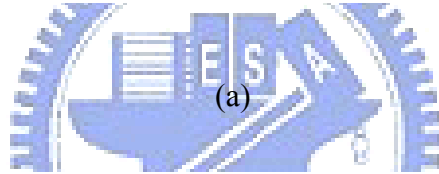
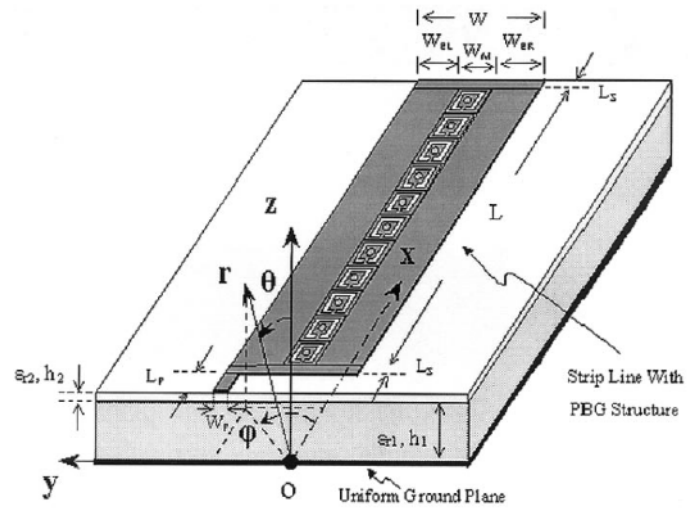
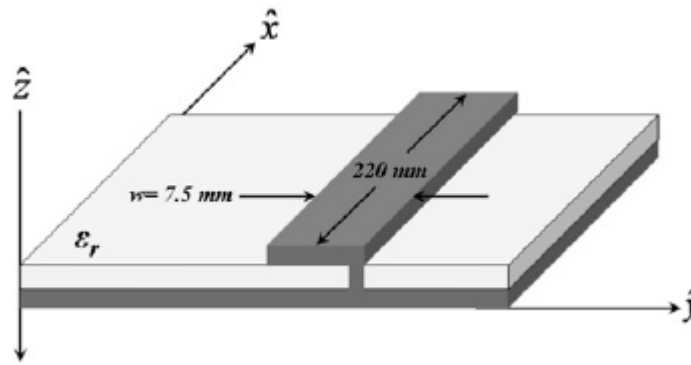


Fig. 1-5. Microstrip leaky-wave antenna (MLWA) with parasitic elements [1-20].



(a)

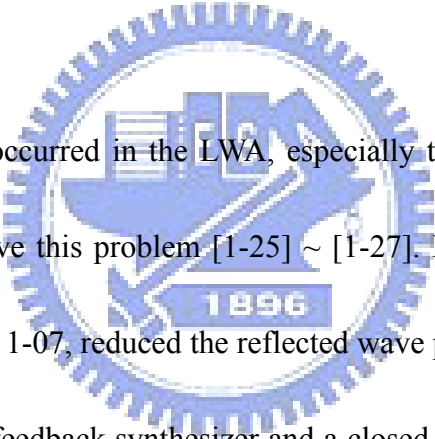


(b)

Fig. 1-6. Two prototypes of LWA: (a) EME microstrip leaky-mode antenna [1-21], (b) half-width antenna [1-22].

1.4 Motivation of Suppressing Side Lobe of Tapered Short LWA

LWA is mainly operated in the first higher order mode, so it possesses the advantages of frequency scanning capability, narrow beamwidth, and high gain. However, the radiation bandwidth is controlled by the width of LWA, the thickness of the substrate, and the dielectric constant. To improve the radiation bandwidth, the tapered structure leaky wave antenna was proposed [1-23] and [1-24]. Although realizing broad impedance bandwidth, the tapered LWA results in a serious problem of spurious side lobe which is generated by the backward radiation.



The side lobe is often occurred in the LWA, especially the short LWA, so that several researches are studied to solve this problem [1-25] ~ [1-27]. In [1-25], the method of LWA array, which is plotted in Fig. 1-07, reduced the reflected wave power and increased the power gain. In Fig. 1-08, an active feedback synthesizer and a closed loop were designed; therefore, the side lobe level was greatly decreased [1-26]. The design of the LWA with aperture-fed antenna (see Fig. 1-09) offered another radiated path of the reflected wave from the open end of LWA to suppress the side lobe [1-27]. These topologies achieved good result of suppressing side lobe.

In chapter 4, we present a novel method to solve the problem of spurious side lobe of tapered short LWA (about only $1.5\lambda_0$ at 4.5 GHz). The proposed LWA is composed of two rectangular slots and a shorting pin on the tapered short LWA. From the measured results, the

side lobe is suppressed over 5 dB at higher frequency band (6.0~6.4 GHz), the main lobe scanning angle is achieved about 43° from 14° to 57° between 4.6 to 6.4 GHz, and the 7-dB impedance bandwidth is about 1.6 GHz from 4.58 to 6.18 GHz.

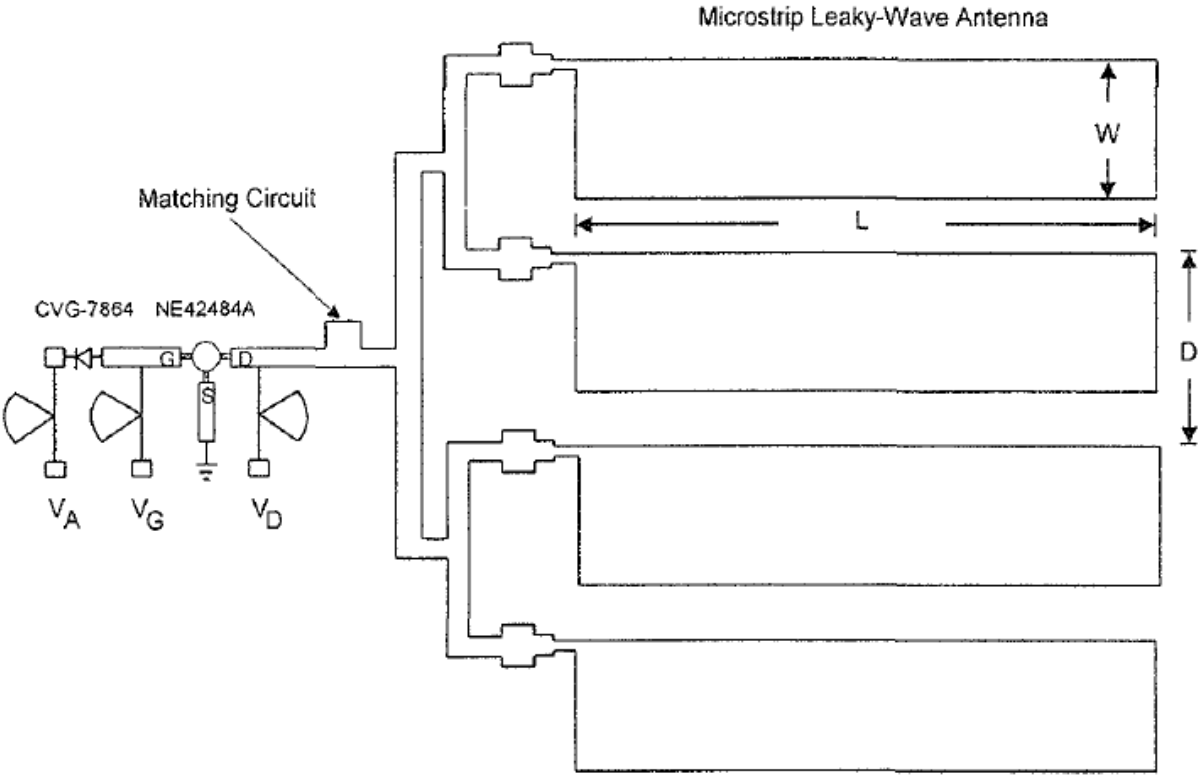


Fig. 1-7. Active frequency-scanning leaky-mode antenna array [1-25].

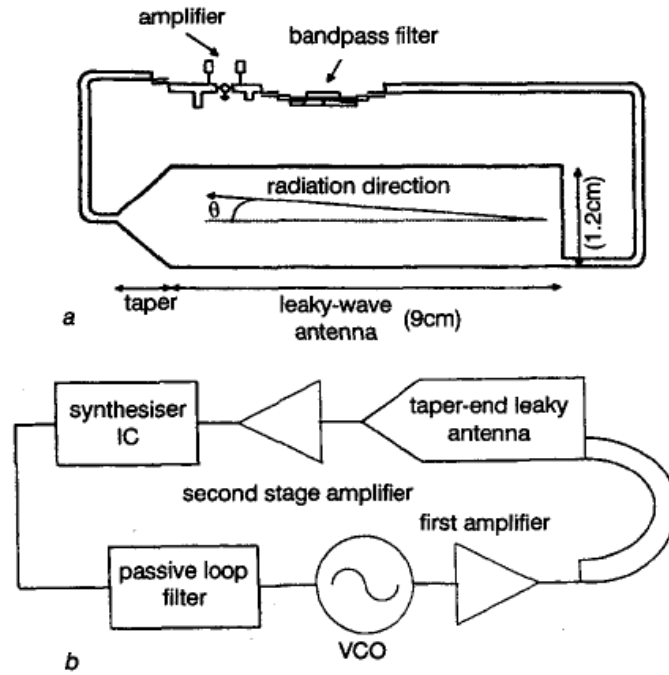


Fig. 1-8. Active feedback microstrip leaky wave antenna [1-26].

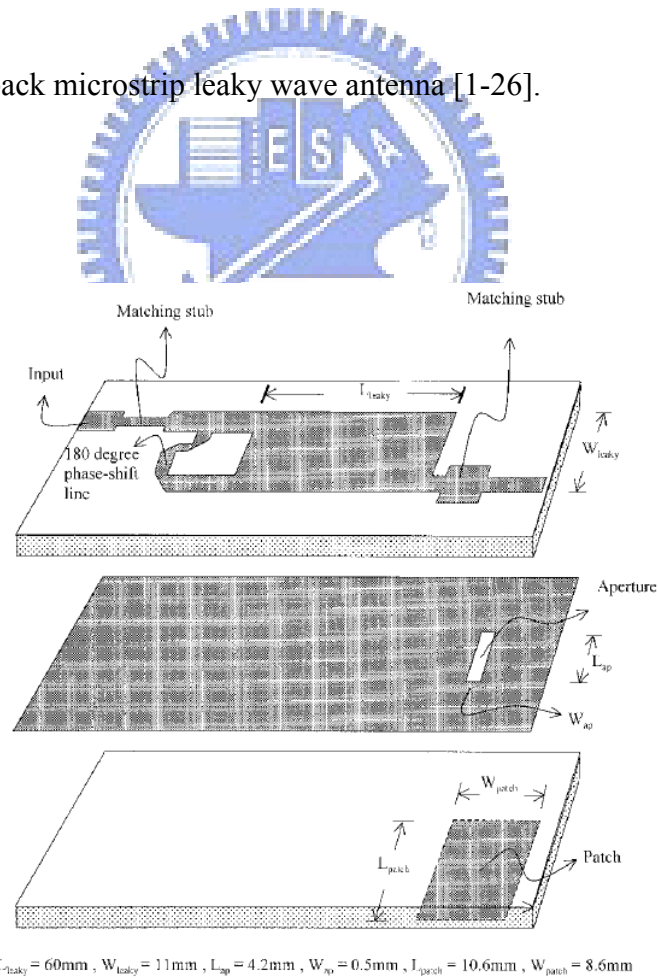


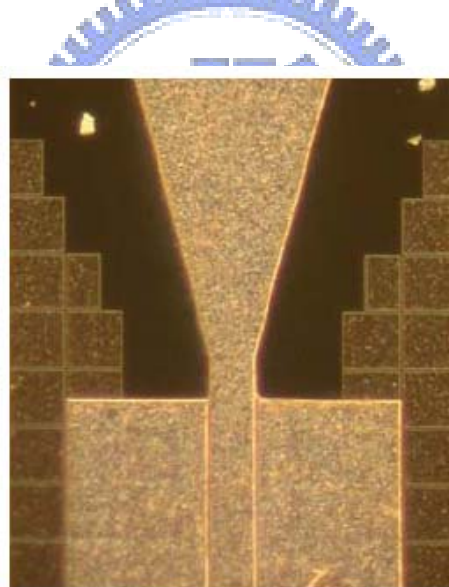
Fig. 1-9. Aperture-fed patch antenna connected to the LWA [1-27].

1.5 Motivation of End-Fire Radiated On-Chip Monopole Antenna for WPAN Application

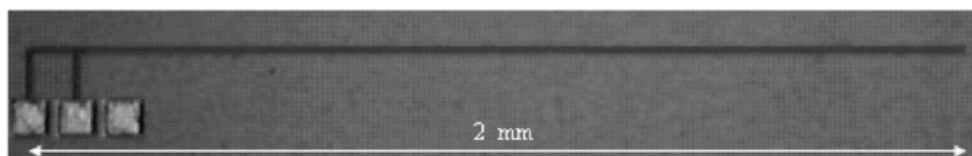
Recently, 7GHz of unlicensed bandwidth around 60-GHz band for wireless personal area network (WPAN) is interested in the short-range communications and high data rate wireless consumer applications [1-28] ~ [1-31]. The attenuation characteristics of 60 GHz nowadays contain atmospheric oxygen of 10–15 dB/km in wide bandwidth, high-speed wireless LAN, Gb/s point-to-point links, vehicular radar at nearby frequencies, and wireless home video and data link that need lots of bandwidth. Due to these reasons, it is very attractive to the WPAN design today.

Millimeter-wave CMOS RFICs and on-chip antenna have been attempted to develop [1-30] ~ [1-35]. Monopole antenna [1-28], PIFA [1-32], dipole antennas [1-33] and [1-34], and Yagi antennas [1-31] and [1-35] are commonly used to design the CMOS on-chip antennas. These antennas, shown in Fig. 1-10 to Fig. 1-12, are utilized the traditional structures to design. However, the on-chip antenna will be integrated into RF front-end circuit, so the effects of electromagnetic compatibility (EMC) and electromagnetic interference (EMI) are considered. Because the radiation pattern of dipole antenna, monopole antenna, and PIFA is omni-direction, the electromagnetic wave will interfere with the frond-end circuit. Yagi antennas is the end-fired radiated, so the electromagnetic power of back side is lower, and effects of EMC and EMI can be reduced to influence the front-end circuit.

In chapter 5, in order to reduce the radiated wave of antenna to interfere with the front-end circuit, an end-fired radiated on-chip monopole antenna for wireless personal area network (WPAN) application is proposed. This antenna is composed of a coplanar waveguide (CPW) asymmetric-fed, a rectangular monopole antenna with a slit, and a shorting path which connects the monopole antenna and the ground plane. The on-chip antenna is fabricated in TSMC 0.18- μm CMOS process, and the antenna size is only about $0.62 \times 1.00 \text{ mm}^2$. It gives a wide impedance bandwidth of 7.7 GHz at the center frequency of 60.25 GHz, the radiation patterns of end-fire direction, and the higher gain in the WPAN band.

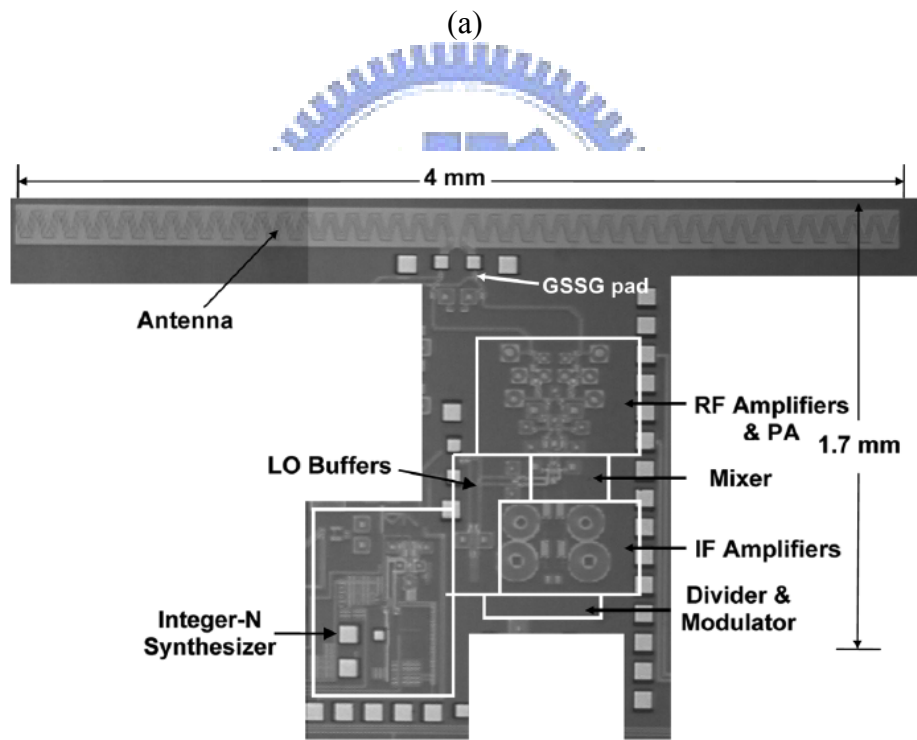
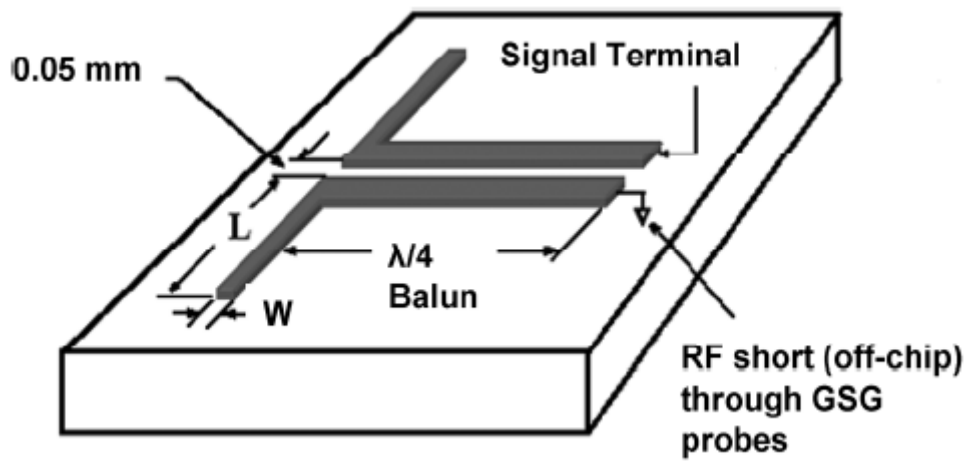


(a)



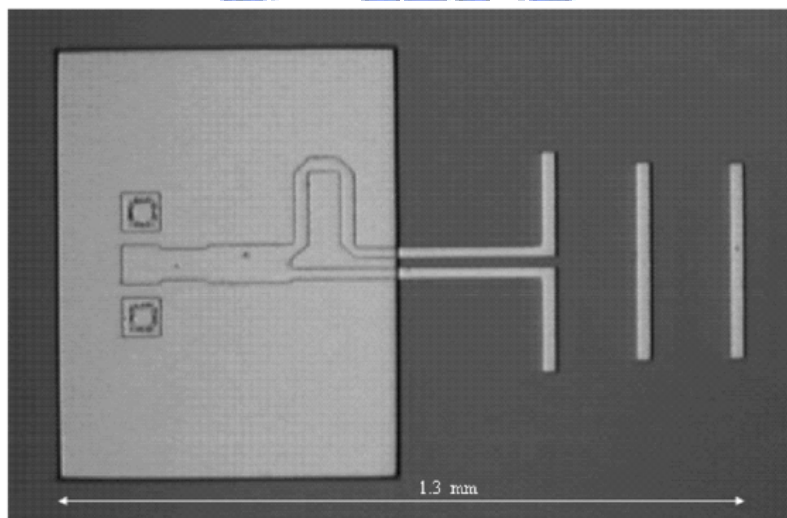
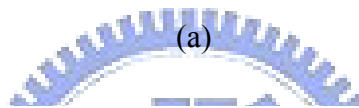
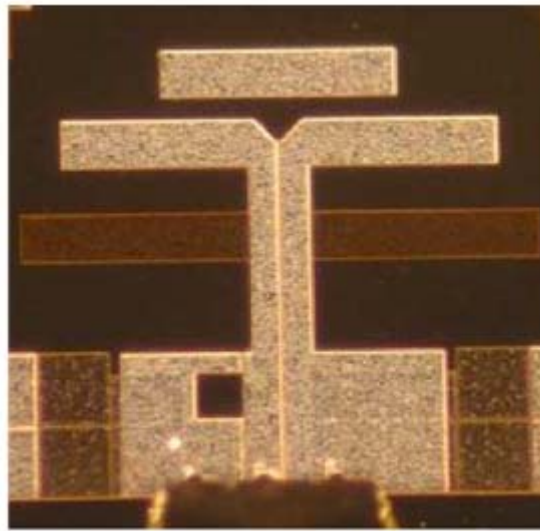
(b)

Fig. 1-10. On-chip antenna: (a) monopole antenna [1-28]; (b) PIFA [1-32].



(b)

Fig. 1-11. On-chip dipole antenna: (a) dipole antenna with balun [1-33]; (b) dipole antenna with front-end circuit [1-34].



(b)

Fig. 1-12. On-chip Yagi antenna: (a) Yagi antenna with director, driven, reflector element, and a ground plane [1-31]; (b) quasi-Yagi antenna [1-35].

1.6 Thesis Organization

This dissertation is divided to six chapters and is organized as follows:

In chapter 1, the outline and the motivations of four researches are introduced.

Chapter 2 documents the design of dual-band circular polarization (CP) monopole antenna.

And before that, the basic theories of monopole antenna and polarization will be reviewed.

Then we will begin to propose our first research which includes two antennas. The current distribution of these antennas is change to achieve broad impedance bandwidth and dual-band axial ratio bandwidth (AR-BW) simultaneously.

Chapter 3 describes a compact wideband leaky-wave antenna (LWA) with etched slot elements and tapered structure. Here, we will review the basic theory of leaky-wave antenna first. After that, we will demonstrate that our study not only reduces the antenna size but also suppresses the back lobe.

In chapter 4, a method for suppressing side lobe of tapered short leaky-wave antenna is demonstrated. The basic theory of tapered leaky-wave antenna will be introduced in the first section. After that, the proposed LWA, which contains a tapered microstrip radiator with a shorting pin and two rectangular slots, will be shown that the radiation of side lobe can be successfully suppressed.

In chapter 5, an end-fired radiated on-chip monopole antenna for wireless personal area

network (WPAN) application is designed. In first section, we will introduce the basic theory of coplanar waveguide. Then the on-chip antenna will be analyzed to demonstrate that this proposed antenna can reach wide bandwidth and excite end-fire direction pattern.

Finally, future studies will be made in chapter 6.



1.7 References

- [1-1] J. Liang, C. C. Chiau, X. Chen, and C. G. Parini, "Printed circular disc monopole antenna for ultra-wideband applications," *Electron. Lett.*, vol. 40, no. 20, pp. 1246-1247, Sep. 2004.
- [1-2] Z. N. Chen, M. J. Ammann, M. Y. W. Chia, and T. S. P. See, "Annular planar monopole antennas," *IEE Proc.-Microw. Antennas Propag.*, vol. 149, no. 4, pp. 200-203, Aug. 2002.
- [1-3] C. C. Lin, Y. C. Kan, L. C. Kuo, and H. R. Chuang, "A planar Triangular monopole antenna for UWB communication," *IEEE Microw. Wireless Compon. Lett.*, vol. 15, no. 10, pp. 624-626, Oct. 2005.
- [1-4] S. H. Hsu and K. Chang, "A novel reconfigurable microstrip antenna with switchable circular polarization," *IEEE Antennas Wireless Propag. Lett.*, vol. 6, pp. 160-162, 2007.
- [1-5] S. M. Kim, K. S. Yoon, and W. G. Yang, "Dual-band circular polarization square patch antenna for GPS and DMB," *Microw. Opt. Technol. Lett.*, vol. 49, no. 12, pp. 2925-2926, Dec. 2007.
- [1-6] K. F. Tong and T. P. Wong, "Circularly polarized U-slot antenna," *IEEE Trans. Antennas Propag.*, vol. 55, no. 8, pp. 2382-2385, Aug. 2007.
- [1-7] Y. F. Lin, H. M. Chen, and S. C. Li, "A new coupling mechanism for circularly polarized annular-ring patch antenna," *IEEE Trans. Antennas Propag.*, vol. 56, no. 1, pp. 11-16, Jan. 2008.
- [1-8] H. Y. A. Yim, C. P. Kong, and K. K. M. Cheng, "Compact circularly polarised microstrip antenna design for dual-band applications," *Electron. Lett.*, vol. 42, no.7, pp. 380-381, Mar. 2006.

- [1-9] J. Y. Sze, C. I. G. Hsu, M. H. Ho, Y. H. Ou, and M. T. Wu, "Design of circularly polarized annular-ring slot antennas fed by a double-bent microstripline," *IEEE Trans. Antennas Propag.*, vol. 55, no. 11, pp. 3134-3139, Nov. 2007.
- [1-10] K. M. Chang, R. J. Lin, I. C. Deng, and Q. X. Ke, "A novel design of a microstrip-fed shorted square-ring slot antenna for circular polarization," *Microw. Opt. Technol. Lett.*, vol. 49, no. 7, pp. 1684-1687, Jul. 2007.
- [1-11] C. C. Chou, K. H. Lin, and H. L. Su, "Broadband circularly polarised crosspatch-loaded square slot antenna," *Electron. Lett.*, vol. 43, no. 9, pp. 485-486, Apr. 2007.
- [1-12] I. C. Deng, J. B. Chen, Q. X. Ke, J. R. Chang, W. F. Chang, and Y. T. King, "A circular CPW-fed slot antenna for broadband circularly polarized radiation," *Microw. Opt. Technol. Lett.*, vol. 49, no. 11, pp. 2728-2733, Nov. 2007.
- [1-13] W. Menzel, "A new travelling-wave antenna in microstrip," *Archiv. Elektrik, Ubertrag Tech.*, pp. 137-140, Apr. 1979. Band 33.
- [1-14] A. A. Oliner and K. S. Lee, "The nature of the leakage from higher modes on microstrip line," in *Int. Microw. Symp. Digest, MTT-S*, Jun. 1986, vol.86, no. 1, pp. 57-60.
- [1-15] C. Luxey and J. M. Laheurte, "Simple design of dual-beam leaky-wave antennas in microstrips," *IEE Proc. Microw. Antennas Propag.*, vol. 144, no. 6, pp. 397-402, Dec. 1997.
- [1-16] J. L. Gómez-Tornero, A. d. I. T. Martínez, D. C. Rebenaque, M. Gugliemi, and A. Álvarez-Melcón, "Design of tapered leaky-wave antennas in hybrid waveguide-planar technology for millimetre waveband applications," *IEEE Trans. Antennas Propag.*, vol. 53, no. 8, pp. 2563-2577, Aug. 2005.
- [1-17] Y. Li and Y. Long, "Frequency-fixed beam-scanning microstrip leaky-wave antenna with multi-terminals," *Electron. Lett.*, vol. 42, no.1, pp. 7-8, Jan. 2006.

- [1-18] C. J. Wang, Y. H. Sheu, and C. F. Jou, "A dual-beam asymmetrically scanning leaky-wave antenna by utilizing a HEMT resistive upconverter," *IEEE Microw. Wireless Compon. Lett.*, vol. 11, no.12, pp. 492-494, Dec. 2001.
- [1-19] I. Y. Chen, C. J. Wang, H. L. Guan, and C. F. Jou, "Studies of suppression of the reflected wave and beam-scanning features of the antenna arrays," *IEEE Trans. Antennas Propag.*, vol. 53, no. 7, pp. 2220-2225, Jul. 2005.
- [1-20] Y. X. Li, Q. Xue, E. K. N. Yung, and Y. L. Long, "TRadiation patterns of microstrip leaky-wave antenna with parasitic elements," *Microw. Opt. Technol. Lett.*, vol. 50, no. 6, pp. 1565-1567, Jun. 2008.
- [1-21] C. K. Wu, Y. C. Chen, and C. K. C. Tzuang, "Compressed-width leaky EH₁ mode PBG antenna," *IEEE Microw. Wireless Compon. Lett.*, vol. 13, no. 8, pp. 343-344, Aug. 2003.
- [1-22] G. M. Zelinski, G. A. Thiele, M. L. Hastriter, M. J. Havrilla and A. J. Terzuoli, "Half width leaky wave antennas," *IET Microw. Antennas Propag.*, vol. 1, no. 2, pp. 341-348, Apr. 2007.
- [1-23] V. Nalbandian and C. S. Lee, "Tapered leaky-wave ultra wide-band microstrip antenna," in *Proc. IEEE AP-S Int. Symp.*, 1999, pp. 1236-1239.
- [1-24] W. Hong, T. L. Chen, C. Y. Chang, J. W. Sheen, and Y. D. Lin, "Broadband tapered microstrip leaky-wave antenna," *IEEE Trans. Antennas Propag.*, vol. 51, no. 8, pp. 1922-1928, Aug. 2003.
- [1-25] C. J. Wang, C. F. Jou, J. J. Wu, and S. T. Peng, "Radiation characteristic of active frequency-scanning leaky-mode antenna arrays," *IEIEC Trans. Electron.*, vol. E82-C, no. 7, pp. 1223-1228, Jul. 1999.
- [1-26] Y. C. Shih, S. K. Chen, C. C. Hu, and C. F. Jou, "Active feedback microstrip leaky wave antenna-synthesizer design with suppressed back lobe radiation," *Electron. Lett.*, vol. 35 no. 7, pp. 513-514, Apr. 1999.

- [1-27] C. J. Wang, H. L. Guan, and C. F. Jou, "A novel method for short leaky-wave antennas to suppress the reflected wave," *Microw. Opt. Technol. Lett.*, vol. 36, no. 2, pp. 129-131, Jan. 2003.
- [1-28] C. C. Lin, S.-S. Hsu, C. Y. Hsu, and H. R. Chuang, "A 60-GHz millimeter-wave CMOS RFIC-on-chip triangular monopole antenna for WPAN applications," in *Proc. IEEE AP-S Int. Symp.*, Jun. 2007, pp. 2522-2525.
- [1-29] Federal Communications Commission, "Amendment of parts 2, 15 and 97 of the commission's rules to permit use of radio frequencies above 40 GHz for new radio applications", *FCC 95-499*, ET Docket No. 94-124, RM-8308, 15 Dec., 1995.
- [1-30] C. H. Doan, S. Emami, A. M. Niknejad, and R. W. Brodersen, "Design of CMOS for 60 GHz applications," in *Proc. IEEE Solid-State Circuits Conf.*, 2004, pp. 440-449.
- [1-31] Y. P. Zhang, M. Sun, and L. H. Guo, "On-chip antennas for 60-GHz radios in silicon technology," *IEEE Trans. Electron Devices*, vol. 52, no. 7, pp. 1664-1668, Jul. 2005.
- [1-32] Y. P. Zhang, L. H. Guo, and M. Sun, "High transmission gain inverted-F antenna on low-resistivity Si for wireless interconnect," *IEEE Electron Device Lett.*, vol. 27, no. 5, pp. 374-376, May 2006.
- [1-33] A. Shamim, L. Roy, N. Fong, and N. G. Tarr, "24 GHz on-chip antennas and Balun on bulk Si for air transmission," *IEEE Trans. Antennas Propag.*, vol. 56, no. 2, Feb. 2008.
- [1-34] C. Cao, Y. Ding, X. Yang, J. J. Lin, H. T. Wu, A. K. Verma, J. Lin, F. Martin, K. O. Kenneth, "A 24-GHz transmitter with on-chip dipole antenna in 0.13- μm CMOS," *IEEE J. Solid-State Circuits*, vol. 43, no. 6, pp.1394-1402, Jun. 2008.
- [1-35] S. S. Hsu, K. C. Wei, C. Y. Hsu, and H. R. Chuang, "A 60-GHz millimeter-wave CPW-fed Yagi antenna fabricated by using 0.18- μm CMOS technology," *IEEE Electron Device Lett.*, vol. 29, no. 6, pp. 625-627, Jun. 2008.

CHAPTER 2

DUAL-BAND CIRCULARLY POLARIZED MONOPOLE ANTENNA

Novel designs of dual-band circular polarization (CP) monopole antenna are presented. Broad impedance bandwidth and dual-band axial ratio bandwidth (AR-BW) can be simultaneously achieved. The proposed antenna comprised of a ground plane embedded with an inverted-L slit, which is capable of generating a resonant mode for broadband impedance-bandwidth, and excites two orthogonal E vectors with equal amplitude and 90° phase difference (PD) for radiating left-hand circular polarization (LHCP) at 2.5 GHz and right-hand circular polarization (RHCP) at 3.4 GHz. A bevel is cut in the rectangular radiator to increase the impedance-bandwidth. According to the measurement results, the measured result of the impedance-bandwidth is about 4.46 GHz for 10-dB return loss from 2.12 to 6.58 GHz; the 3-dB axial ratio (AR) bandwidths are about 150 MHz at the lower band (2.5 GHz) and 230 MHz at the upper band (3.4 GHz). Furthermore, embedding an I-shaped slit in the rectangular radiator and adding an I-shaped stub in the ground plane, the impedance-bandwidth can be further increased to 6.30 GHz (2.17 ~ 8.47 GHz), and the 3-dB AR-bandwidth at the upper band is greatly enhanced from 230 MHz to 900 MHz.

2.1 Basic Monopole Antenna and Polarization Theory

2.1.1 Monopole Antenna Theory

Monopole antenna is formed from dipole antenna by the principles of image theory. Firstly, dipole antenna is introduced in this section. Two metal elements, the total length of which is a half wavelength, are symmetrically fed by a balanced two-wire transmission line to construct a half-wave dipole antenna. The current distribution of the dipole antenna is nearly one-half of a sine wave, and the maximum amplitude is at the center of the dipole [2-1]. The current distribution is defined as

$$I(z) = I_m \sin \left[\frac{2\pi}{\lambda} \left(\frac{\lambda}{4} - |z| \right) \right] \quad (2-01)$$

where I_m is the maximum current magnitude, z is the current from the maximum at the center of the dipole to zero at the ends, $z = \pm\lambda/4$. From this current equation, the radiation pattern can be calculated. The electric field is found as

$$E_\theta = j\omega\mu \frac{I_m}{\pi} \frac{e^{-jk_0 r}}{4\pi r} \frac{\cos[(\pi/2)\cos\theta]}{\sin\theta} \quad (2-02)$$

The normalized far field pattern is derived as

$$F(\theta) = \frac{\cos[(\pi/2)\cos\theta]}{\sin\theta} \quad (2-03)$$

The total radiated power is

$$P_{rad} = \int_0^\pi \int_0^{2\pi} U(r, \theta) r^2 \sin\theta d\phi d\theta, \quad U(r, \theta) = \frac{1}{2\eta_0} |E_\theta|^2 \quad (2-04)$$

So,

$$P_{rad} = \frac{1.22\eta_0}{4\pi} I_m^2 \quad (2-05)$$

The radiation resistance and the complete impedance of the dipole are written as

$$R_r = \frac{2P_{rad}}{I_m^2} = \frac{1.22\eta_0 I_m^2}{2\pi I_m^2} = 73(\Omega) \quad (2-06)$$

and

$$Z_D = 73 + j42.5\Omega \quad (2-07)$$

The directivity of the dipole antenna is defined as

$$D = \frac{4\pi U_m}{P_{rad}} = 1.64 = 2.15dB \quad (2-08)$$

where

$$U_m = \frac{r^2}{2\eta_0} |E_\theta|_{\max}^2 = \frac{\eta_0 I_m^2}{8\pi^2} \quad (2-09)$$

The performances of monopole antenna are similar to dipole antenna except the impedance and directivity. Because the length and the voltage of monopole antenna is a half of dipole antenna, the impedance of monopole is only half of dipole. It is derived as

$$Z_M = \frac{V_{in,M}}{I_{in,M}} = \frac{1}{2} \frac{V_{in,D}}{I_{in,D}} = \frac{1}{2} Z_D \quad (2-10)$$

Directivity of monopole is twice as large as the dipole in free space. The equation is shown as

$$D_M = \frac{4\pi}{\Omega_M} = \frac{4\pi}{1/2\Omega_M} = 2D_D \quad (2-11)$$

2.1.2 Polarization Theory

According to the concept of polarization, the polarization of antennas is related to the polarization of the wave radiated in a given direction [2-1] and [2-2]. The polarization of a plane wave describes the time-varying behavior of the instantaneous electric field at a fixed observation point. Generally, the polarized wave includes three important types: linearly polarized (LP), elliptically polarized (EP), and circularly polarized (CP).

Linear Polarization: LP is excited when the electric field vector moves positive or negative along a line. The situation can be written as

$$\vec{E} = \hat{n}E_n \quad (2-12)$$

where \vec{E} is the instantaneous electric field vector. There are two cases of linear polarization: vertical and horizontal linear polarization. The radiation of commercial antennas is linear polarization such as dipole, monopole, horn, and Yagi-Uda antenna.

Circular Polarization: CP is generated by two orthogonal E vectors with equal amplitude and 90° phase difference. It is defined as

$$\vec{E} = \vec{E}_{Hor} + e^{j\delta} \vec{E}_{Ver} \quad (2-13)$$

$$\vec{E}_{RHCP} = \frac{1}{\sqrt{2}}(\vec{E}_{Hor} + j\vec{E}_{Ver}) \quad (2-14)$$

and

$$\bar{E}_{LHCP} = \frac{1}{\sqrt{2}}(\bar{E}_{Hor} - j\bar{E}_{Ver}) \quad (2-15)$$

where \bar{E} is the instantaneous electric field vector, \bar{E}_{Hor} and \bar{E}_{Ver} respectively denote the electric field vector in the horizontal and vertical plane, and δ is the phase difference. If the amplitudes of \bar{E}_{Hor} and \bar{E}_{Ver} can be equal and $\delta = \pm 90^\circ$, the polarized wave is right-hand circularly polarized (RHCP) or left-hand circularly polarized (LHCP) [2-1]. Patch, helical, and spiral antenna are usually designed to radiate CP radiation wave.

Elliptical Polarization: EP is produced by two E vectors. In general, these two E vectors are considered that the phase difference between two E vectors is 90° , and the amplitude of two E vectors is not equal. It is expressed as

$$\bar{E} = \bar{E}_{Hor} + e^{j90} \bar{E}_{Ver} \quad (2-16)$$

and

$$E_{Hor} \neq E_{Ver} \quad (2-17)$$

The phenomenon of EP which can excite right-hand elliptically polarized (RHEP) or left-hand elliptically polarized (LHEP) is similar to CP. In physical sense, when the structure of conventional linearly polarized antenna is varied for reducing size, the antenna will produce two electric field vectors to form EP.

Axial Ratio: The value of axial ratio (AR) can represent the characteristic of polarization. AR is defined by the ratio of the major to the minor axis electric field [2-1], [2-3], and [2-4]

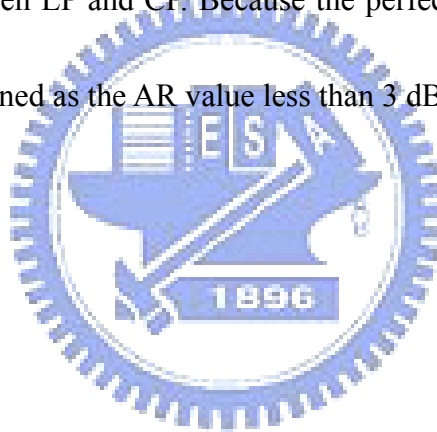
or by RHCP and LHCP, and it is written as

$$1 \leq AR = \frac{|E_{Major}|}{|E_{Minor}|} = \frac{|E_{RHCP} + E_{LHCP}|}{|E_{RHCP} - E_{LHCP}|} \leq \infty \quad (2-18)$$

or

$$0dB \leq AR = 20 \log \frac{|E_{RHCP} + E_{LHCP}|}{|E_{RHCP} - E_{LHCP}|} \leq \infty dB \quad (2-19)$$

For a perfect CP wave, the AR value is 0 dB or 1, and for a LP wave, the AR value is infinite. EP is defined between LP and CP. Because the perfect CP wave with AR = 0 dB is ideal, the CP is typically defined as the AR value less than 3 dB.



2.2 Design of Dual-Band Circularly Polarized Monopole Antenna

The schematic diagrams of the proposed monopole antennas are illustrated in Fig. 2-1 and Fig. 2-2, respectively. These proposed antennas are etched on a FR4 substrate with relative permittivity $\epsilon_r = 4.4$, loss tangent $\tan \delta = 0.024$, and thickness $H = 1.6$ mm. The overall dimensions of the antennas are about $40 \times 39 \times 1.6$ mm³. In general, the length of monopole antenna is usually about a quarter-wavelength. The approximate value for the length L_0 of monopole radiating strip is given by

$$L_0 \approx \frac{\lambda_g}{4} = \frac{\lambda_r}{4\sqrt{\epsilon_{eff}}} = \frac{c}{4\sqrt{\epsilon_{eff}} f_r} \quad (1)$$

with

$$\epsilon_{eff} = \frac{\epsilon_r + 1}{2} \quad (2)$$

where c is the speed of light, λ_r is the free-space wavelength of the monopole resonant frequency f_r , and ϵ_{eff} is the approximated effective dielectric constant [2-5]. The dimensions of the rectangular radiator of the antennas ($L_0 \times W_0$) are 23.5×12 mm².

2.2.1 Antenna 1 Design

The general behavior of a monopole antenna is either vertical or horizontal linearly polarized. If the conventional monopole antenna is vertically linearly polarized, the radiation in the horizontal direction is very weak. For example, Fig. 2-3 presents the simulated surface current distribution of the conventional monopole antenna, which can be divided into vertical and horizontal current. The distribution of horizontal current excites two components with 180° out of phase. Therefore, radiation at the horizontal direction in the far field is very weak. Thus the monopole antenna excites LP. The simulated AR results of the conventional monopole antenna at the broadside direction are shown in Fig. 2-4. The antenna radiates an LP radiation wave with an AR value greater than 40 dB. For this reason, the conventional monopole antenna is very difficult to excite CP. CP is generated by two orthogonal E vectors (E_{Hor} , E_{Ver}) with equal amplitude and 90° phase difference (PD), where E_{Hor} and E_{Ver} denote the complex voltage in the horizontal and vertical plane, respectively.

To achieve the CP radiation wave, see Fig. 2-1, an inverted-L slit is embedded in the ground plane at the left side of the feed line. The E_{Hor} of the inverted-L slit and E_{Ver} of the rectangular radiator have a phase difference of 90° which can excite CP. The phase of the E_{Hor} leads E_{Ver} about 90° and the LHCP wave at the lower frequency (2.5 GHz) can be generated. At the upper frequency (3.4 GHz), a RHCP wave is also excited, because there is a 90° phase lag instead of 90° phase lead as in the lower band. The effect of the length of inverted-L slit

(S_2+S_3) on the AR will be discussed in section 2.3.

The impedance-bandwidth can also be increased by this technique. In the operating frequency range, three resonant modes are excited by the rectangular radiator and one resonant mode is excited by the ground plane with the inverted-L slit.

Furthermore, a bevel is cut to adjust the impedance matching [2-6]. Also, a 50 Ohm microstrip feed line of width W_1 and length L_1 is terminated with the standard SMA connector and connected to an impedance transformer of width W_2 and length L_2 .



2.2.2 Antenna 2 Design

To further enhance the impedance- and AR-bandwidth, the I-shaped slit and stub are added in the rectangular radiator and ground plane, respectively. The geometry of this Antenna 2 is shown in Fig. 2-2. The I-shaped slit of length L_4 in the rectangular radiator can excite a RHCP wave at the upper frequency band. The I-shaped stub of length L_3 in the ground plane can affect the phase difference. The AR-bandwidth of the upper band can be increased by adjusting the sizes of L_3 and L_4 . The detail effects about the length (L_3, L_4) will be studied in section 2.3. Furthermore, the I-shaped slit and stub can excite a mode at 8.0 GHz, so that the impedance-bandwidth is further extended to 6.30 GHz.

The positions of the I-shaped slit and stub can interfere with the antenna performance resulting from tuning the inverted-L slit. If the positions of the I-shaped slit and stub are designed at the left side of the feed line, the characteristics of the extremely wide impedance-bandwidth and dual-band CP will be destroyed. Therefore, they are embedded at the right side of the feed line. Detailed dimensions are listed in Table 2-1.

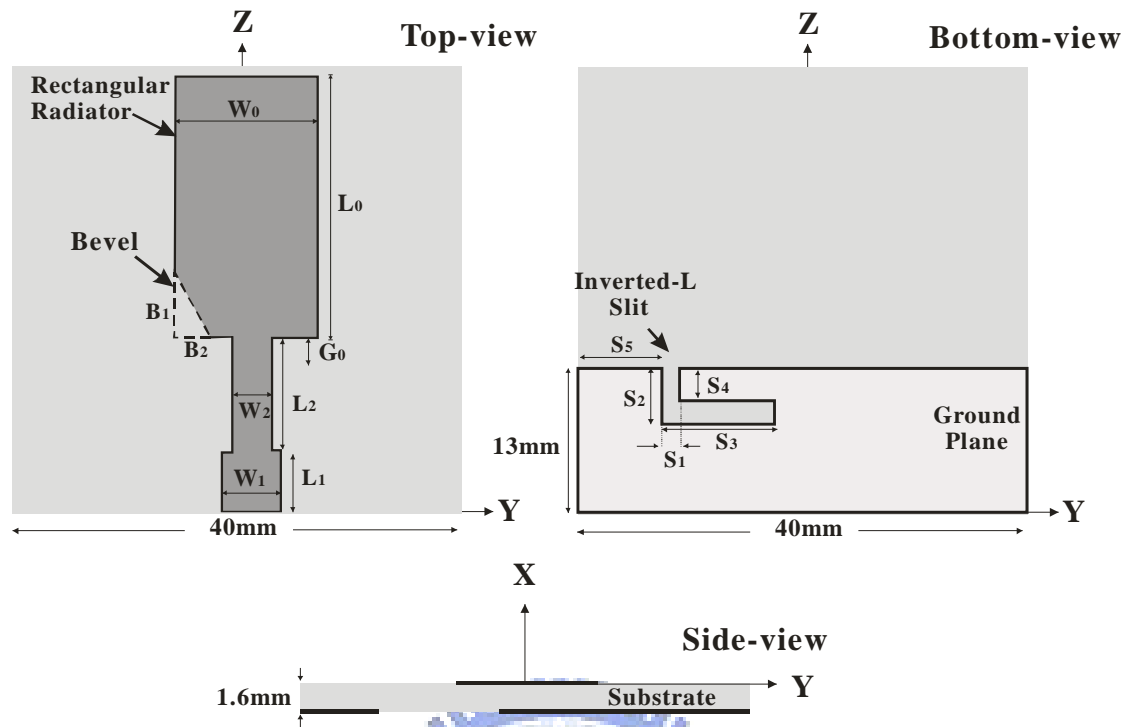


Fig. 2-1. Antenna 1, configurations of the proposed printed monopole antenna with inverted-L slit.

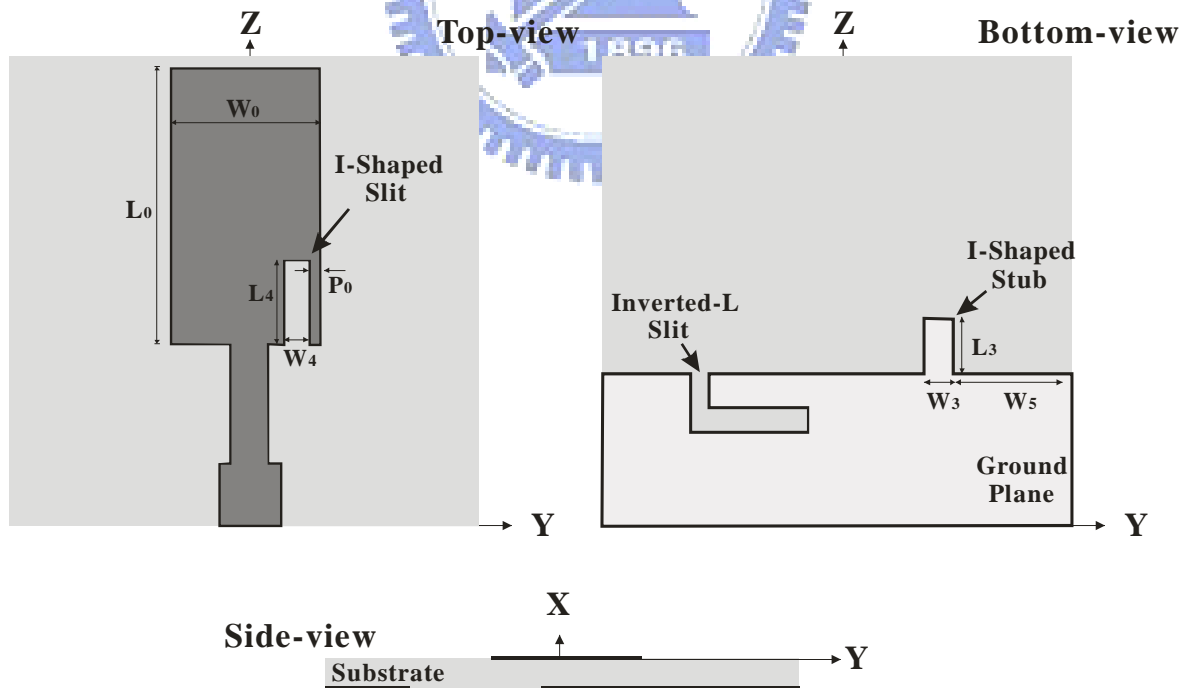


Fig. 2-2. Antenna 2, configurations of the proposed printed monopole antenna with inverted-L slit, I-shaped slit, and I-shaped strip.

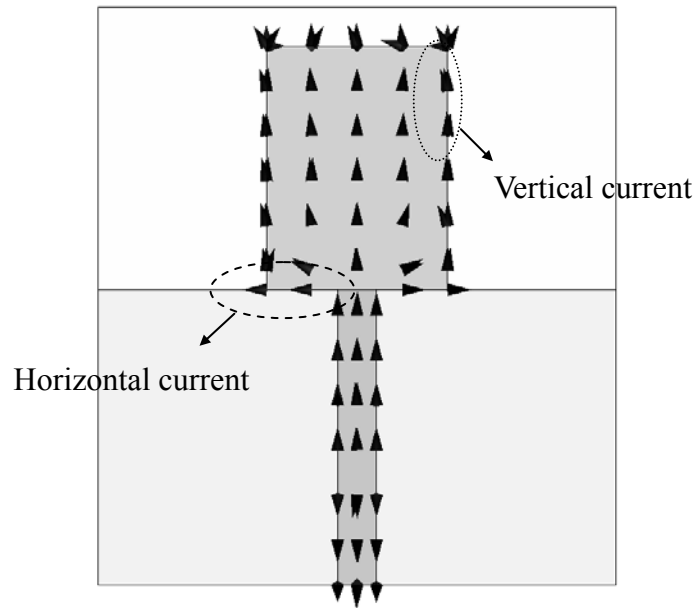


Fig. 2-3. Simulated surface current distribution of conventional monopole antenna at 3 GHz.

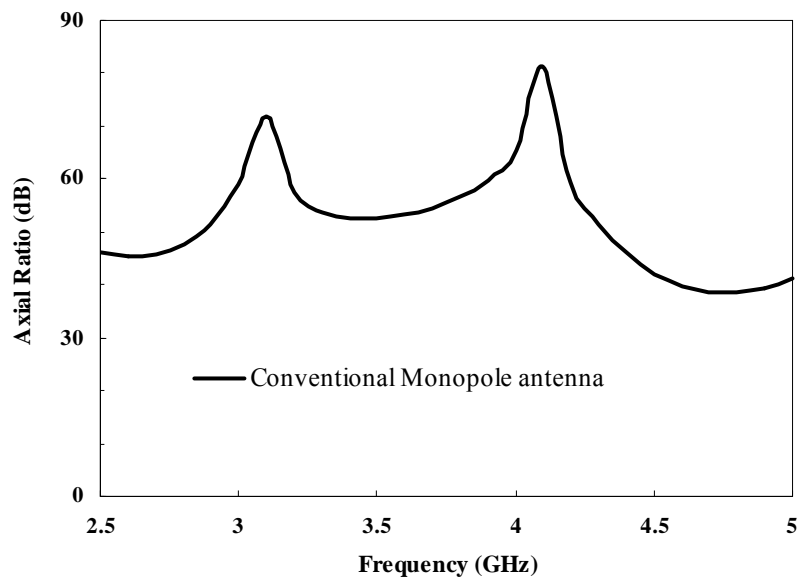


Fig. 2-4. Simulated AR of conventional monopole antenna

TABLE 2-1
DIMENSIONS OF THE PROPOSED PRINTED ANTENNA 1 AND 2

	Antenna 1	Antenna 2		Antenna 1	Antenna 2
L ₀	23.5 mm	23.5 mm	W ₀	12 mm	12 mm
L ₁	6.0 mm	6.0 mm	W ₁	3.0 mm	3.0 mm
L ₂	9.5 mm	9.1 mm	W ₂	2.4 mm	2.4 mm
L ₃	-	3.5 mm	W ₃	-	0.5 mm
L ₄	-	8.2 mm	W ₄	-	1.2 mm
S ₁	1.0 mm	1.0 mm	W ₅	-	13 mm
S ₂	6.0 mm	6.0 mm	P ₀	-	1.0 mm
S ₃	11.0 mm	11.0 mm	B ₁	5.0 mm	-
S ₄	4.7 mm	4.0 mm	B ₂	2.5 mm	-
S ₅	7.0 mm	7.0 mm	G ₀	2.5 mm	2.1 mm

2.3 Parametric Studies

This section focuses on the effects of various parameters on the AR. The performance of AR at the broadside direction is mainly affected by the inverted-L slit (S_2+S_3) of Antenna 1, and the I-shaped slit (L_4) and the I-shaped stub (L_3) of Antenna 2.

2.3.1 Inverted-L Slit of Antenna 1

Fig. 2-5 exhibits the effects of adjusting the total length of inverted-L slit (S_2+S_3) of Antenna 1 on the center frequency of AR and 3-dB AR-bandwidth at the lower band frequency. The lower and upper bands are affected by the total length of inverted-L slit. It is clearly seen that the center frequency of AR decreased as the length of the inverted-L slit increased. Therefore, the center frequency of CP is mainly controlled by the inverted-L slit. In addition, the 3-dB AR-bandwidth is affected by the total length of inverted-L slit, which can be optimized by tuning the parameters (S_2+S_3).

From the simulated results, the characteristic of CP is determined by the length of inverted-L slit (S_2+S_3).

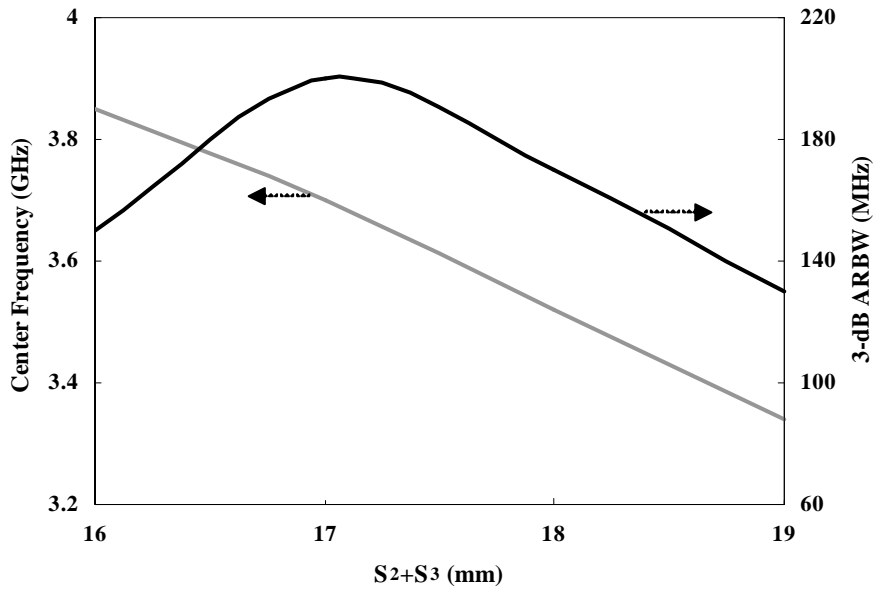
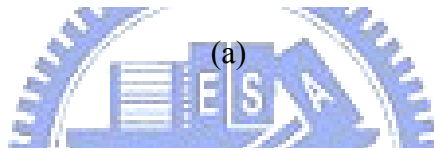
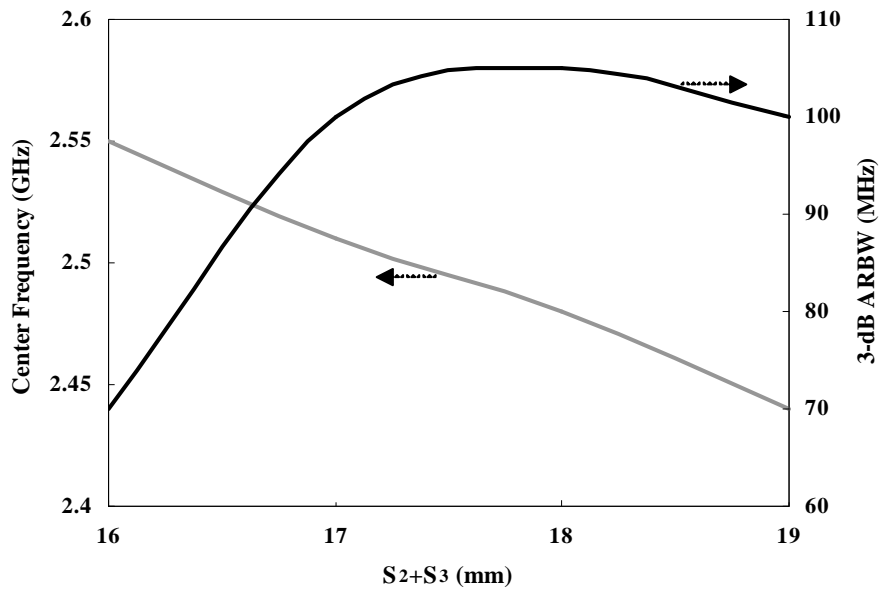
2.3.2 I-shaped Slit of Antenna 2

The simulated upper band AR and PD results of Antenna 2 at the different length of I-shaped slit (L_4) are plotted in Fig. 2-6. The I-shaped slit with three different lengths, 7.2, 8.2, and 9.2 mm, are analyzed as other parameters are fixed. From Fig. 2-6(a), the first CP mode is about 3.5 GHz, which is excited by inverted-L slit, and it is affected slightly when varying the length L_4 . However, the second CP mode is strongly dependent on L_4 . When $L_4 = 9.2$ mm, there is only one CP mode. Thus, the 3-dB AR-bandwidth is quite narrow. From the case of $L_4 = 8.2$ mm, two CP modes are shown and the two bands resulting from the two CP modes are merged into one broad CP band. As L_4 is decreased to 7.2 mm, the frequency of the second CP mode is increased to 4.36 GHz, so that the upper band is turned into two bands. Therefore, by properly tuning L_4 , the two CP modes can be combined to form a wider AR-bandwidth. However, from Fig. 2-6(b), it can clearly be found that although for $L_4 = 7.2$ mm, the PD is kept roughly -90° at 3.8 GHz, but the AR (see Fig. 2-6(a)) is not less than 3-dB at 3.8 GHz. Therefore, because the magnitudes of two orthogonal E vectors are not equal, this radiation wave becomes elliptic polarization instead of circular polarization at 3.8 GHz. Based on this study, we choose $L_4 = 8.2$ mm.

2.3.3 I-shaped Stub of Antenna 2

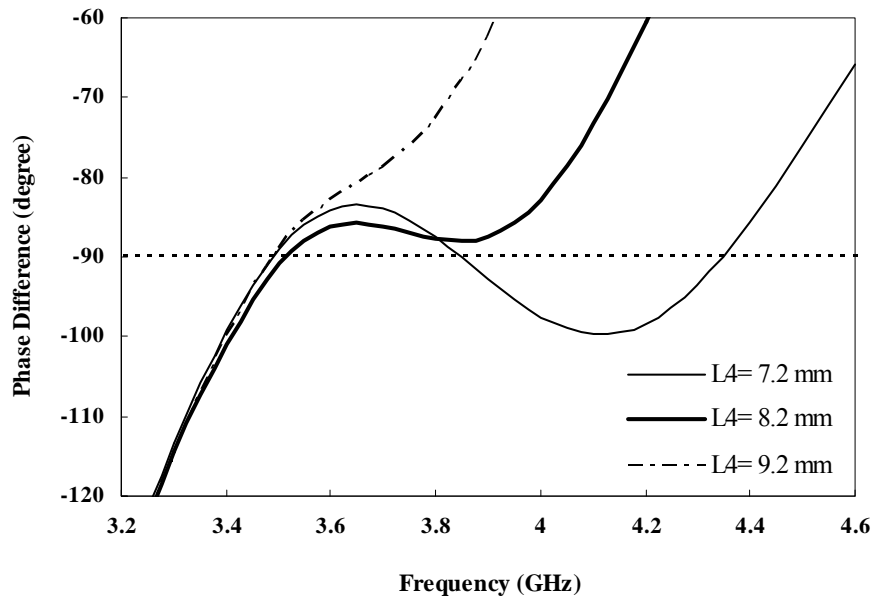
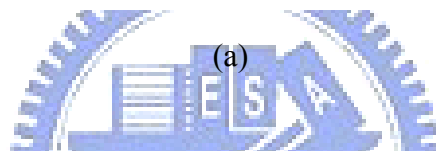
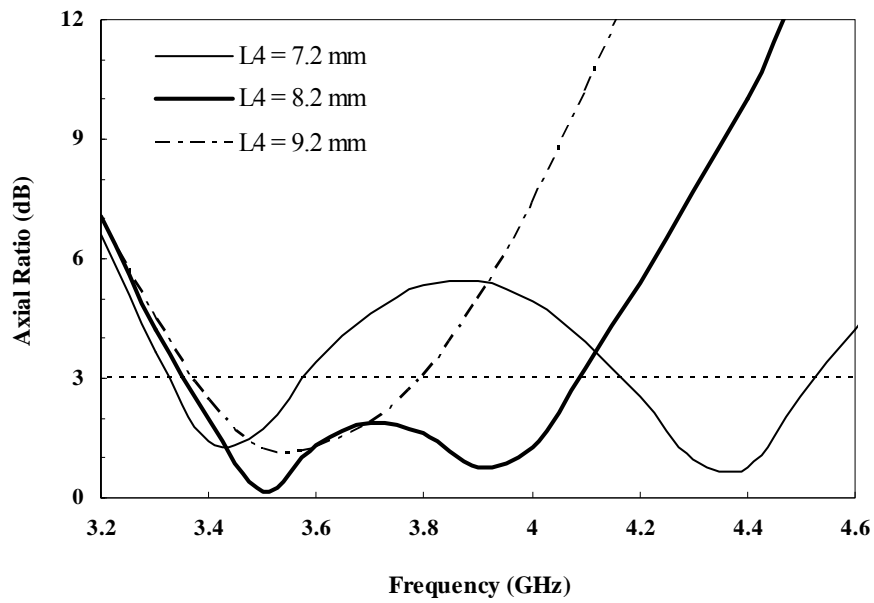
The effects of the length of I-shaped stub L_3 on AR and PD at the upper band are depicted in Fig. 2-7. From studying these data, there are two important points to be found. First, in Fig. 2-7(a), the length of I-shaped stub can affect the second CP mode of the upper band. However, compared with Fig. 2-6(a), L_4 is more affective than L_3 for tuning the second CP mode. Second, from Fig. 2-7(b), it is observed that the variation of PD can be tuned by different L_3 . Note that the variation of PD is important for CP. When $L_3 = 4.0$ mm, the variation of PD from 3.5 to 3.9 GHz is kept roughly -90° in Fig. 2-7(b), and the AR is also less than 1.5 dB to activate a good CP in Fig. 2-7(a).

According to these study results of L_4 and L_3 , the frequency of the second CP mode is mainly controlled by L_4 , and the PD of the second CP mode is mainly controlled by L_3 . Therefore, the widest 3-dB AR-bandwidth can be reached at the upper band by properly adjusting L_4 and L_3 .



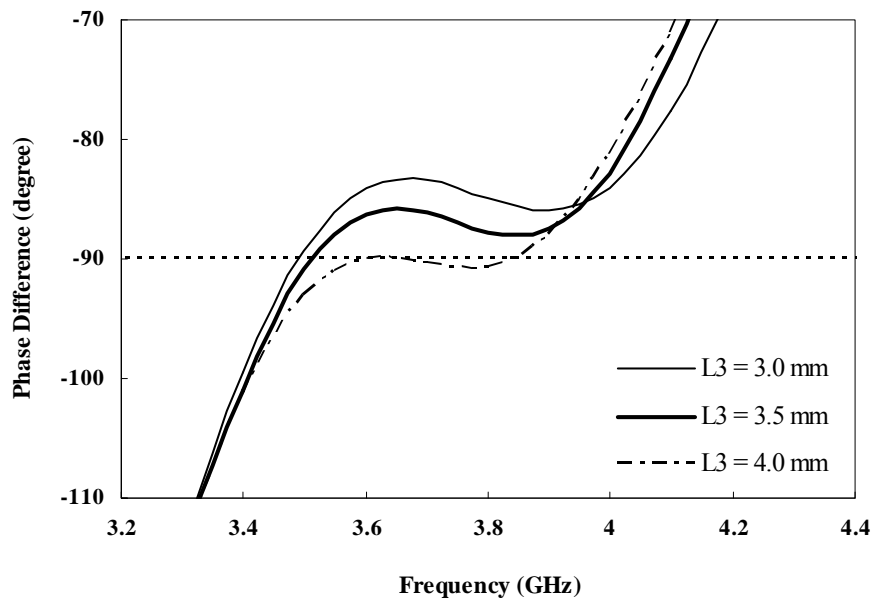
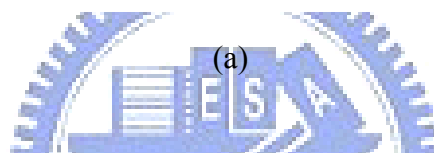
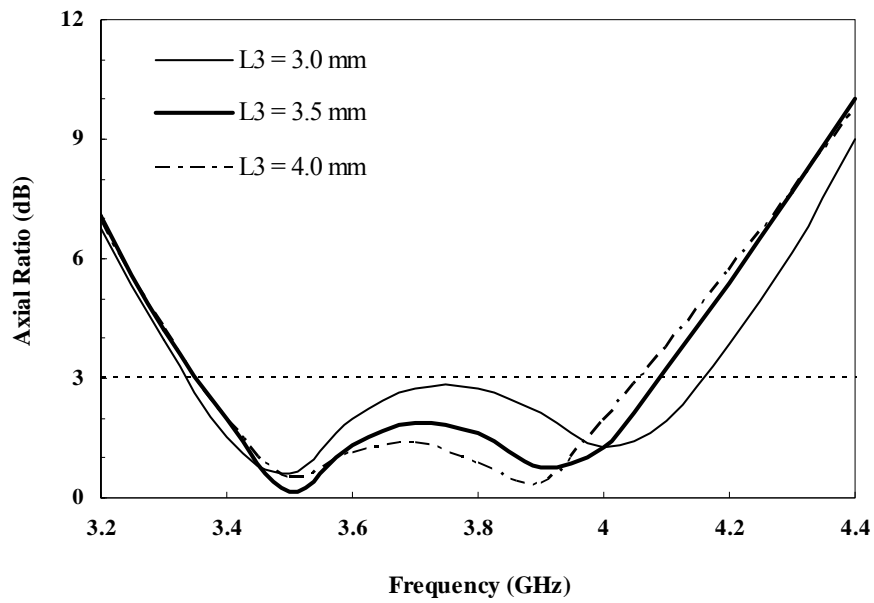
(b)

Fig. 2-5. Simulated center frequency of axial ratio and 3-dB axial ratio bandwidth for the inverted-L length of Antenna 1: (a) lower band; (b) upper band.



(b)

Fig. 2-6. Simulated phase difference and axial ratio of the I-shape slit length of Antenna 2 at upper band: (a) axial ratio; (b) phase difference.



(b)

Fig. 2-7. Simulated phase difference and axial ratio of the I-shape stub length of Antenna 2 at upper band: (a) axial ratio; (b) phase difference.

2.4 Simulation and Measurement Results

There are three subsections: 2.4.1) Studying the impedance-bandwidth and resonant modes. The simulated and measured return loss of Antenna 1 and 2 are discussed. The resonant modes are explained by the simulated surface current distributions for Antenna 1 and 2. 2.4.2) Analyzing axial ratios. The simulated and measured results of AR will show that Antenna 1 has dual-band CP and Antenna 2 enhances the AR-bandwidth at the upper band. The many methods can be used to measure the AR such as using the 3D chamber and utilizing the polarizer in the 2D chamber. 2.4.3) Illustrating the measured radiation patterns and gains.

2.4.1 Impedance Bandwidth and Resonant Modes

The characteristics of the two monopole antennas were calculated by Ansoft High Frequency Structure Simulator (HFSS) software [2-7] and measured by HP 8722C network analyzer.

Antenna 1: Fig. 2-8 compares the simulated and measured return loss for a conventional monopole antenna and Antenna 1. In our experiments, the conventional monopole antenna consists of a feed line, a rectangular radiator without the slit and bevel, and a ground plane without the slit and stub. The measured impedance-bandwidth of Antenna 1 for 10-dB return loss is from 2.12 to 6.58 GHz, which has about 4.46 GHz bandwidth (102.5 %), comparing to the conventional antenna only has 0.73 GHz bandwidth (27 %) from 2.34 to 3.07 GHz.

According to the result of measured return loss, Antenna 1 performs a wide bandwidth due to the four resonant modes which are influenced and excited by the inverted-L slit. From the simulated result, these four resonant modes are: the three resonant modes of monopole antenna at the center frequencies of 2.25, 4.65, and 6.35 GHz, and one resonant mode of the ground plane at the center frequency of 3.35 GHz. In Fig. 2-9, the simulated surface current distributions are presented for these four resonant modes. In Fig. 2-9(a), (b), and (c), the simulation results show that the three resonant modes of monopole antenna are influenced by the inverted-L slit. Fig. 2-9(d) shows the most surface current distributions are formed along the inverted-L slit to excite the resonant mode of the ground plane. Therefore, the ground embedded inverted-L slit can be used to excite extra resonant mode, which provides extended bandwidth.

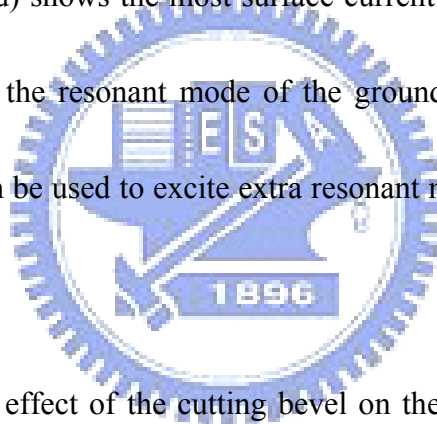


Fig. 2-10 describes the effect of the cutting bevel on the measured return loss. For the rectangular radiator without the bevel, the third and fourth resonant modes of the Antenna 1 are excited at 4.40 and 6.40 GHz, respectively. With the presence of the cutting bevel, the third mode is shifted to higher frequency and the fourth mode is shifted to the lower frequency. Thus, the impedance-bandwidth can be increased.

Based on the discussion above, we can realize that due to the combination of the four resonant modes, the impedance-bandwidth can be increased from 27 % of conventional monopole antenna to 102.5 % of Antenna 1. The experimental results verify that the method

of embedding inverted-L slit in ground plane and cutting the bevel in the rectangular radiator can increase impedance-bandwidth.

Antenna 2: Fig. 2-11 illustrates the simulated and measured return loss of Antenna 2. The 10-dB bandwidth of measured return loss is extended to 6.30 GHz or about 118.4%, covering the range from 2.17 to 8.47 GHz. The resonant modes of Antenna 2 are at: 2.93, 3.37, 6.0, and 8.0 GHz which are affected by embedding the I-shaped slit and adding I-shaped stub. Therefore, these resonant modes are differed from Antenna 1. From Fig. 2-12(a), (b), and (c), it can be clearly seen that the resonances at 2.93, 3.37, and 6.0 GHz are interfered with the I-shaped slit in the rectangular radiator and the I-shaped stub in the ground plane. In addition, this method excites one resonant mode at 8.0 GHz. In Fig. 2-12(d), the maximum surface current is localized in the I-shaped stub and slit to yield a resonant mode at 8.0 GHz. Due to the four resonant modes affected by the I-shaped stub and slit, they combined to form a broadband impedance-bandwidth.

The simulated return loss of the Antenna 2 with and without I-shaped stub is compared in Fig. 2-13. A resonant mode at the center frequencies of 9.0 GHz can be shifted to 8.0 GHz by using I-shaped stub to increase the impedance-bandwidth. Furthermore, this technique of embedding the I-shaped slit and stub can also improve the AR-bandwidth at the upper band (3.4 GHz band). Details of the results of AR will be described in next subsection.

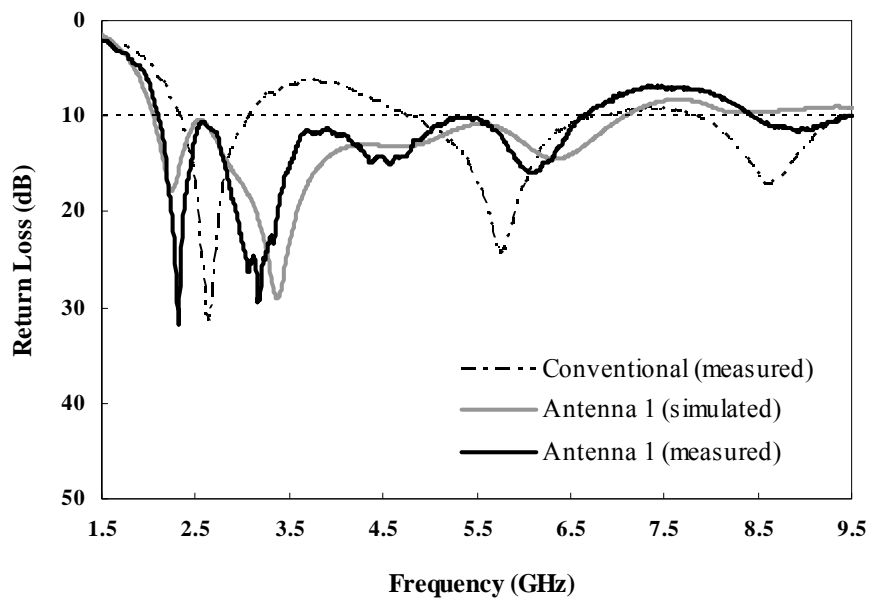


Fig. 2-8. Simulated and measured return loss of the conventional antenna and Antenna 1.

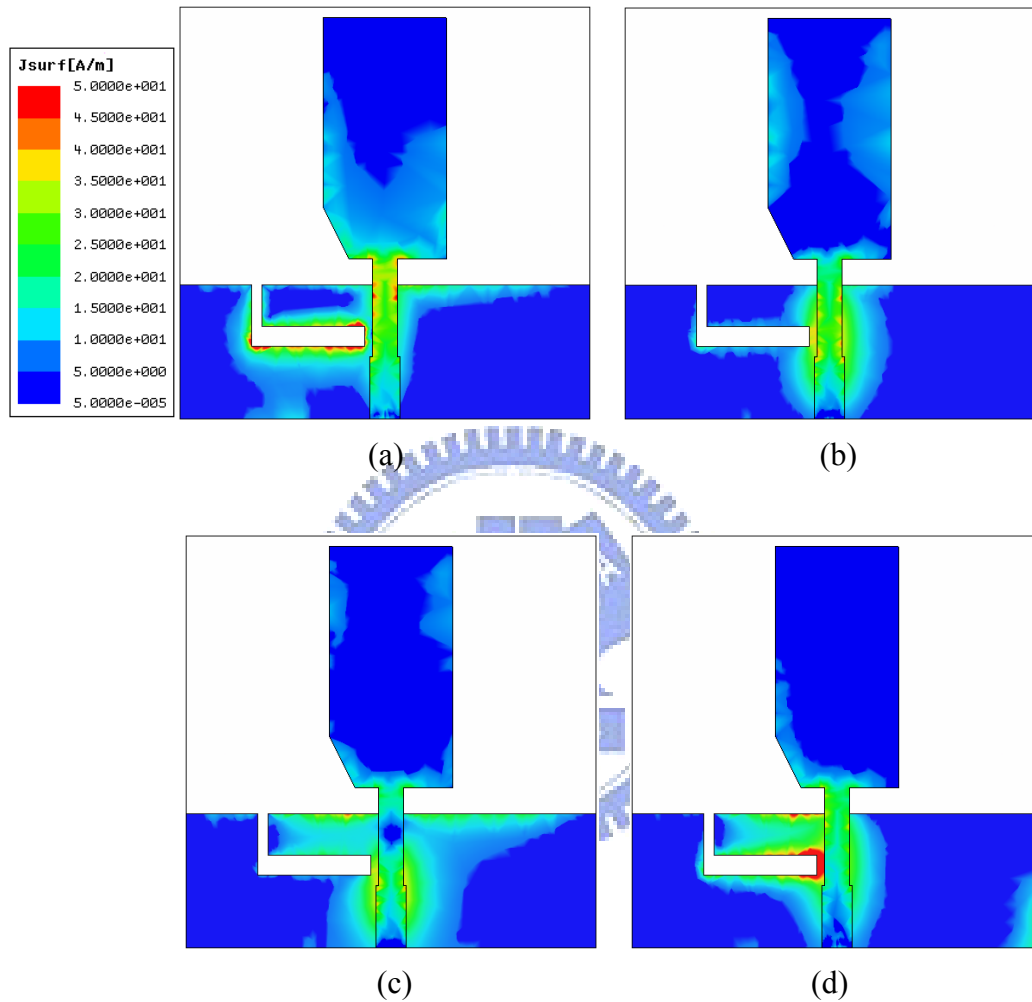


Fig. 2-9. Simulated surface current distributions of Antenna 1: three resonant modes of monopole (a) 2.25 GHz; (b) 4.65 GHz; (c) 6.35 GHz; and one resonant mode of ground plane (d) 3.35 GHz.

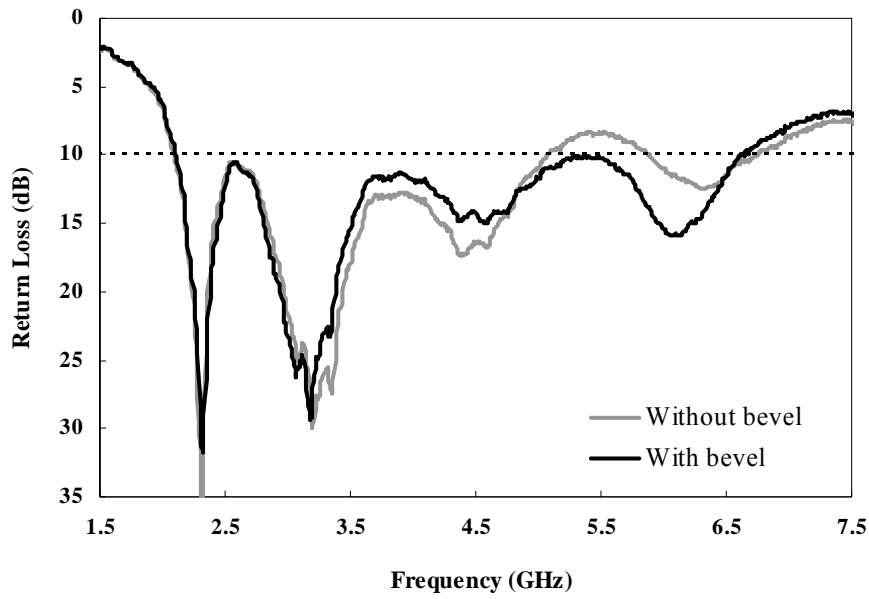


Fig. 2-10. Comparison the measured return loss of Antenna 1 with and without the bevel.

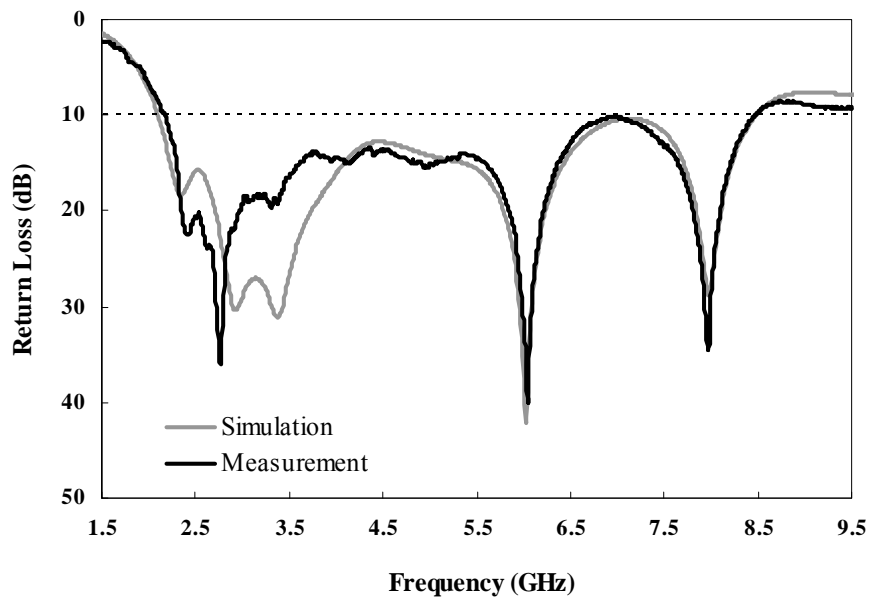


Fig. 2-11. Simulated and measured return losses against frequency for the proposed Antenna 2.

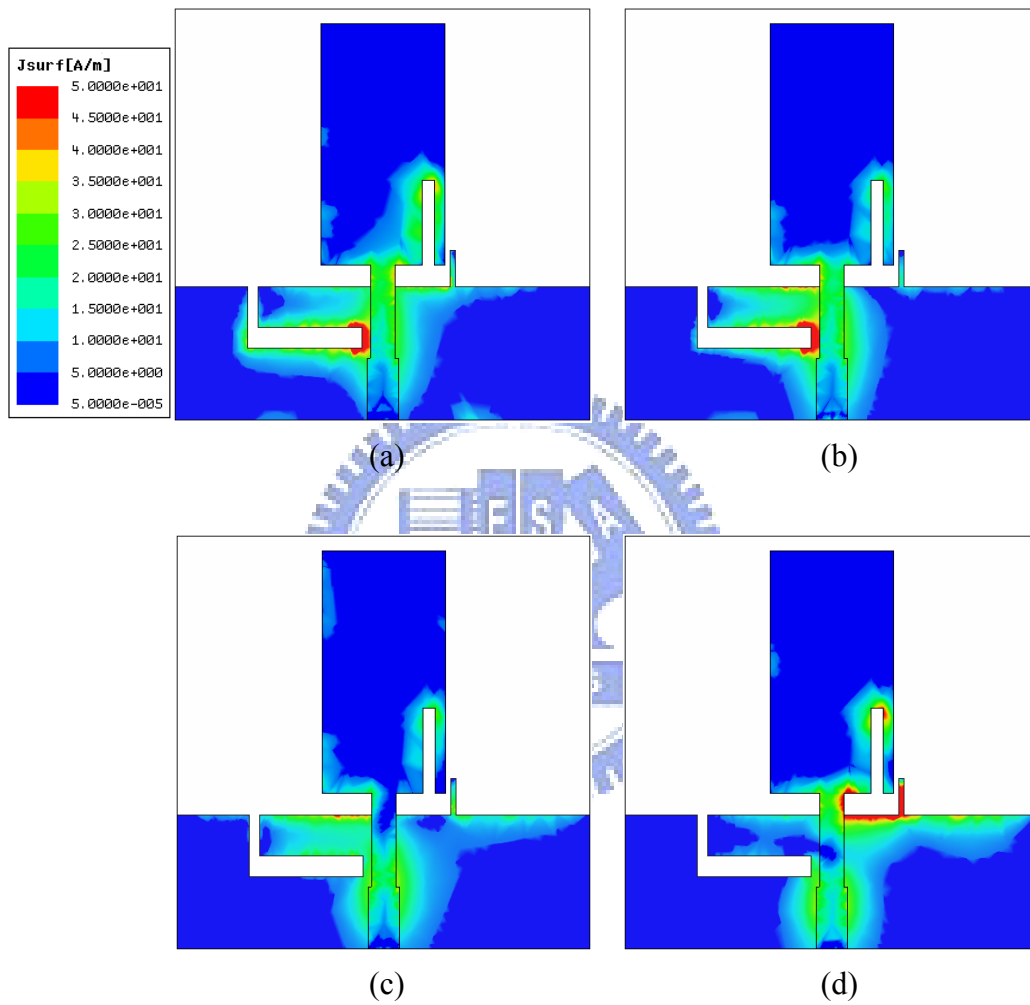


Fig. 2-12. Simulated surface current distributions of Antenna 2: (a) 2.93 GHz; (b) 3.37 GHz; (c) 6.00 GHz; and (d) 8.00 GHz.

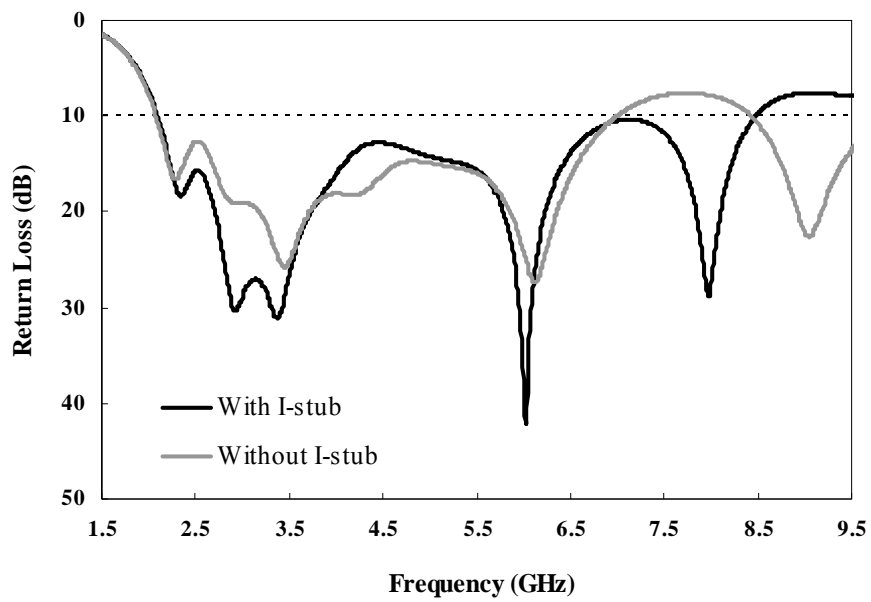


Fig. 2-13. Comparison the simulated return loss of Antenna 2.

2.4.2 Axial Ratios

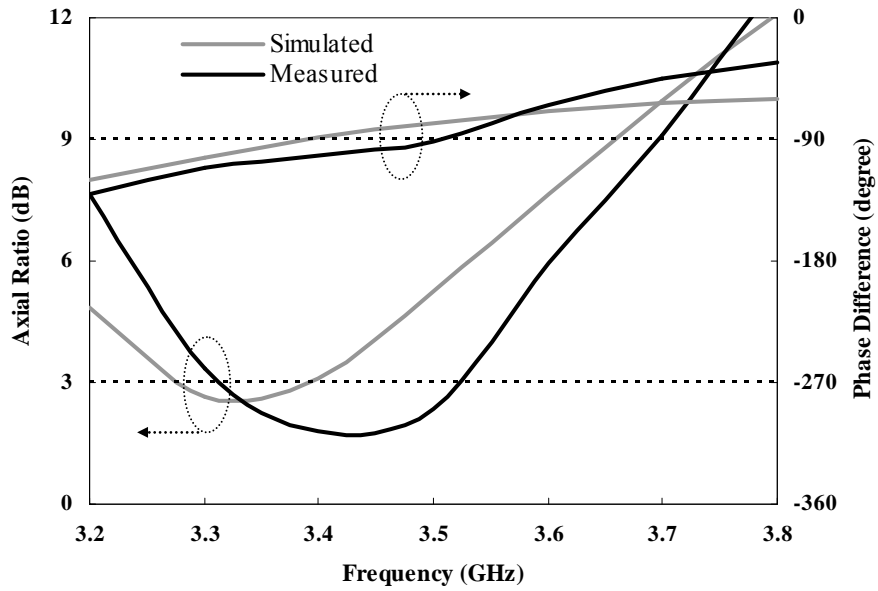
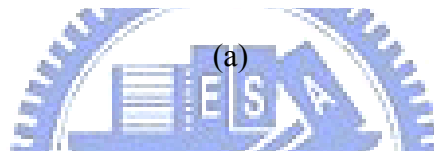
Antenna 1: The simulated and measured AR and PD results of the lower and upper bands at the broadside direction are plotted in Fig. 2-14(a) and (b). The measured 3-dB AR-bandwidths reach 150 MHz from 2.41 to 2.56 GHz (lower band) or about 6.0% with respect to the center frequency at 2.485 GHz, and 230 MHz from 3.31 to 3.54 GHz (upper band) or about 6.7% with respect to the center frequency at 3.425 GHz. From the measured PD results, the PD of the lower band is close to 90° to generate a LHCP wave, and a RHCP wave is achieved at the upper band by the PD of -90° . In addition, the measured PD as function of frequency varies less than the simulation result; therefore the measured 3-dB AR-bandwidth is wider than the simulation. From the results, we can see that the AR-bandwidth could be greatly increased, if the variation of the PD can be kept about 90° or -90° as function of frequency.

Antenna 2: Fig. 2-15(a) and (b) show the simulated and measured AR and PD results of the lower and upper bands at the broadside direction. From Fig. 2-15(a), it appears that the 3-dB AR-bandwidth is from 2.41 to 2.55 GHz approximately 5.6% with respect to the center frequency at 2.48 GHz. Compare Fig. 2-14(a) with Fig. 2-15(a), it can be found that the characteristic of AR at the lower band is slightly affected by the I-shaped slit and stub.

From the measured results of upper band which compare Fig. 2-15(b) with Fig. 2-14(b), we can see the first CP mode (3.6 GHz) excited by inverted-L slit and the second CP mode

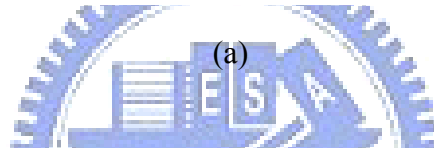
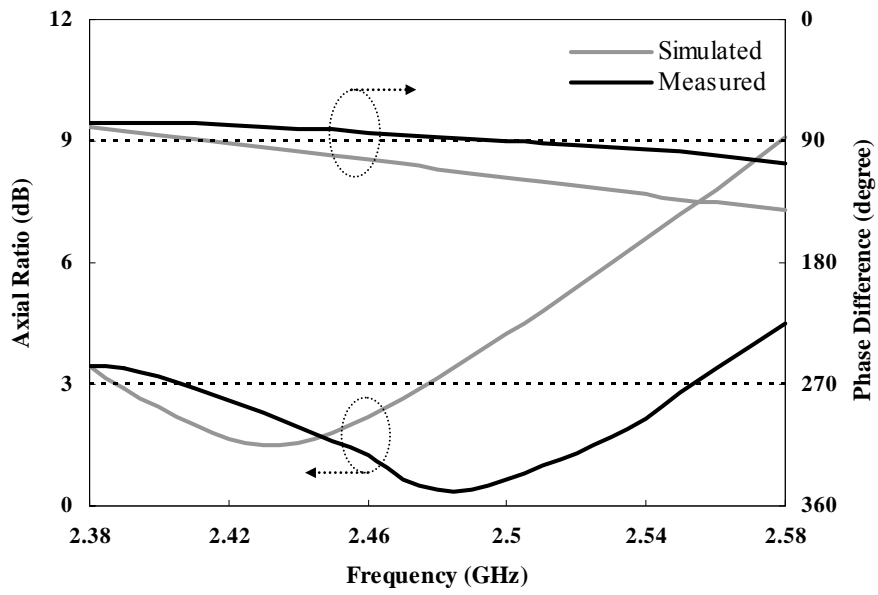
(4.2 GHz) generated by the I-shaped slit and stub are combined to form a wider AR-bandwidth at the upper band than Antenna 1. In addition, the variation of the PD at the upper band can be kept about -90° from 3.5 to 4.2 GHz by the I-shaped slit and stub. The measured 3-dB AR-bandwidth can greatly extend to about 900 MHz from 3.45 to 4.35 GHz or about 23.1% with respect to the center frequency at 3.90 GHz. Thus, the AR-bandwidth of Antenna 2 at the upper band has been improved from 6.7% of Antenna 1 to 23.1% of Antenna 2. The measured minimum AR of LHCP is 0.41dB at 2.49 GHz and RHCP is 0.71 dB at 4.2 GHz.

The performances of the conventional and two proposed Antennas are summarized in Table 2-2. In Antenna 1, inverted-L slit can greatly increase impedance-bandwidth and excite dual-band CP. In Antenna 2, the impedance- and AR-bandwidth at the upper band can be further improved by embedding an I-shaped slit and adding an I-shaped stub.

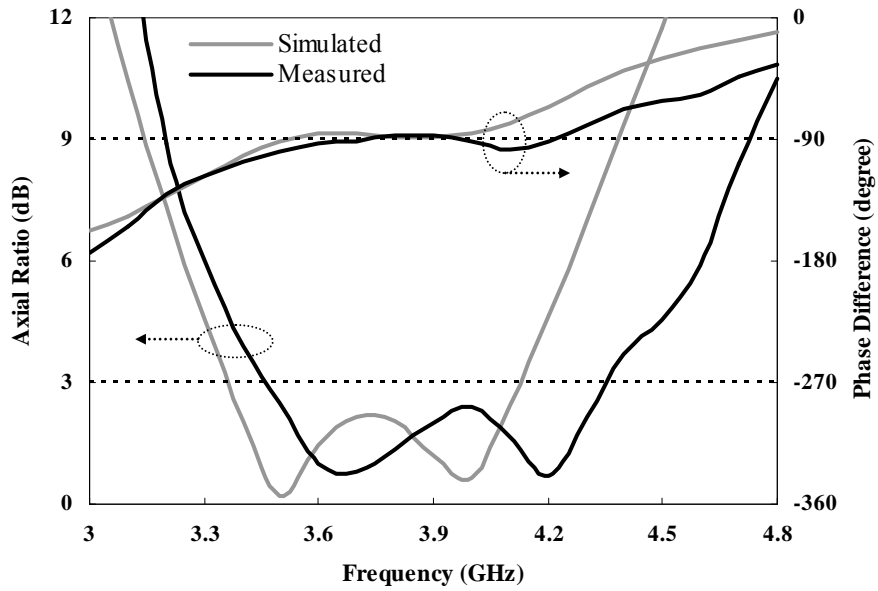


(b)

Fig. 2-14. Simulated and measured axial ratio and phase difference of Antenna 1: (a) lower band; (b) upper band.



(a)



(b)

Fig. 2-15. Simulated and measured axial ratio and phase difference of Antenna 2: (a) lower band; (b) upper band.

TABLE 2-2
PERFORMANCE OF CONVENTIONAL AND PROPOSED ANTENNAS

	Conventional	Antenna 1	Antenna 2
f_{lowest} (GHz)	2.34	2.12	2.17
Imp. BW (GHz, %)	0.73, 27 %	4.46, 102.5 %	6.30, 118.4 %
Lower-band AR-BW (MHz, %)	none	150, 6.0 %	140, 5.6 %
Upper-band AR-BW (MHz, %)	none	230, 6.7 %	900, 23.1 %
Polarization	LP	CP : 2.41 ~ 2.56 GHz 3.31 ~ 3.54 GHz LP : others	CP : 2.41 ~ 2.55 GHz 3.45 ~ 4.35 GHz LP : others

2.4.3 Radiation Patterns and Gains

The measured normalized radiation patterns at XY -plane and XZ -plane of Antenna 1 are displayed in Fig. 2-16. It is noted that the radiation patterns are not omnidirectional because the structure of the proposed antennas is not symmetrical and the radiation patterns are influenced by slit and stub. Therefore, it can not achieve the requirement for handheld devices. We observe that good LHCP and RHCP radiation patterns are excited in the lower and upper band, respectively. The measured 3-dB AR beam widths in the XY - and XZ -plane are 101° and 34° , respectively, at 2.50 GHz in Fig. 2-16(a). In Fig. 2-16(b), the 3-dB AR beam widths are 49° and 24° at 3.44 GHz. The measured normalized radiation patterns of Antenna 2 at three different frequencies of 2.49, 3.70, and 4.20 GHz are showed in Fig. 2-17. The measured 3-dB AR beamwidths of Antenna 2 at 2.49, 3.70, and 4.20 GHz are 88° , 76° , and 66° , respectively, in the XY -plane. In the XZ -plane are 27° , 31° , and 27° . In addition, the maximum measured gains of Antenna 2 at 2.40, 3.70, and 4.20 GHz are about 0.77, 0.97, and 1.92 dBi, respectively. From Fig. 2-16 and 2-17, the CP of the antenna at +X and -X direction is the opposite polarization, the reason is because the E_{Ver} on the top and bottom surface of the substrate remains the same phase; however, the E_{Hor} on the top and bottom surface of the substrate is 180° out of phase.

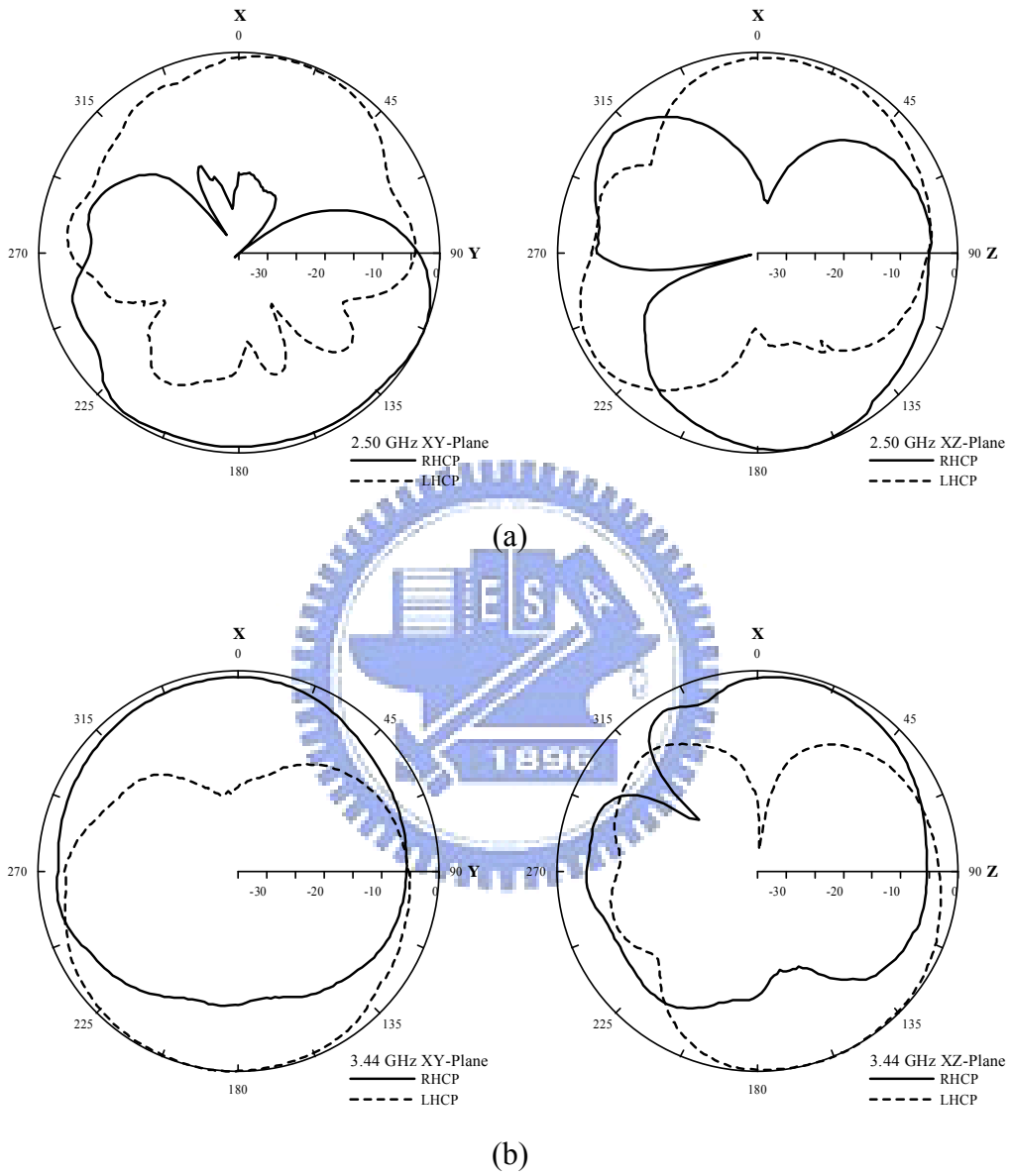
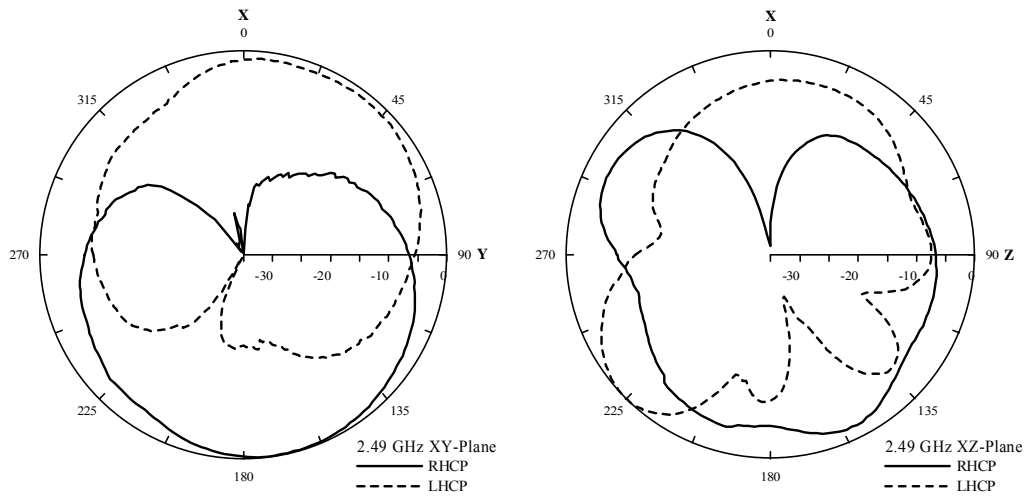
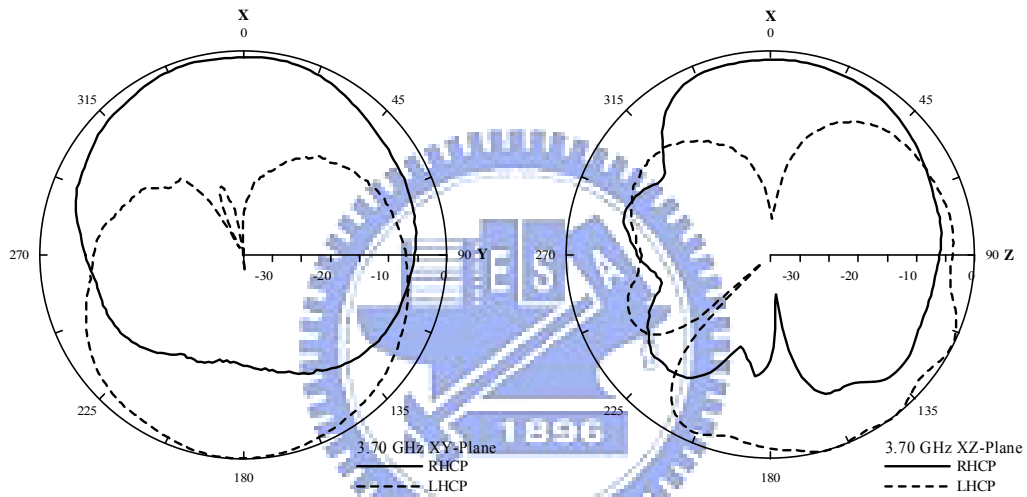


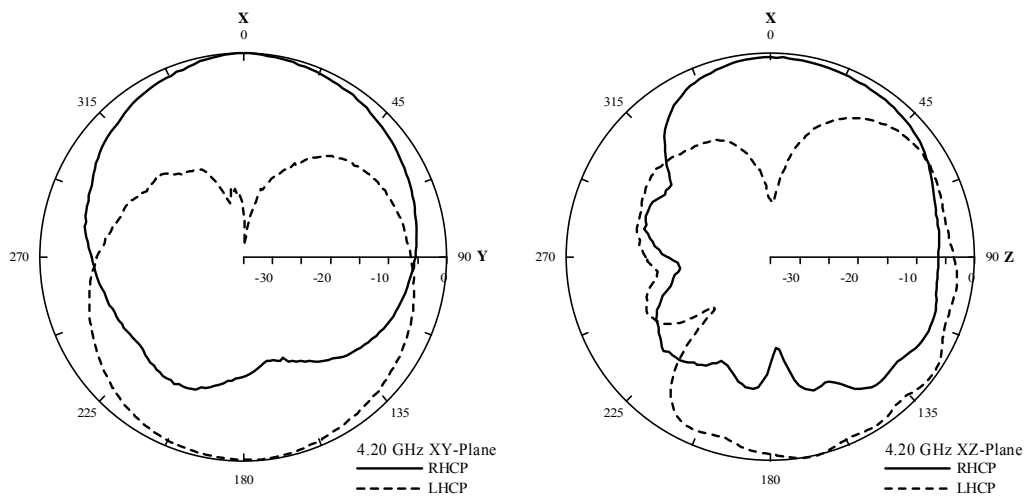
Fig. 2-16. Measured radiation patterns of Antenna 1 in the XY- and XZ-plane: (a) 2.50 GHz; (b) 3.44 GHz.



(a)



(b)



(c)

Fig. 2-17. Measured radiation patterns of Antenna 2 in the XY- and XZ-plane: (a) 2.49 GHz; (b) 3.70 GHz; (c) 4.20 GHz.

2.5 Summary

The broadband monopole antennas with dual-band circular polarization have been developed. In Antenna 1 design, an inverted-L slit embedded in the ground plane can not only be used to enhance the impedance-bandwidth, but also to excite dual-band circularly polarized radiation waves. The measured impedance-bandwidth is 102.5% from 2.12 to 6.58 GHz, and the 3-dB AR-bandwidths of dual-band CP wave are about 6.0% for LHCP at the lower band and 6.7% for RHCP at the upper band. Furthermore, a method used to enhance the impedance- and AR-bandwidth is proposed. Antenna 2 demonstrates by embedding an I-shaped slit in the rectangular radiator and by adding an I-shaped stub in the ground plane can further increase the impedance-bandwidth and AR-bandwidth of the upper band. The measured results show that the impedance-bandwidth was enhanced from 102.5% to 118.4%, and the 3-dB AR-bandwidth at the upper band was improved from 6.7% to 23.1%. The proposed antennas, which have simple structure, excellent performances, and fabricated easily, are very suitable for the modern wireless communication system.

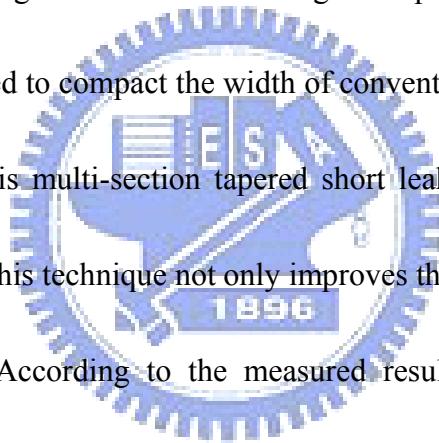
2.6 References

- [2-1] W. L. Stutzman and G. A. Thiele, *Antenna Theory and Design*, 2nd ed. New York: Wiley, 1998.
- [2-2] D. K. Cheng, *Field and Wave Electromagnetics*, 2nd ed. Addison-Wesley Publishing Company, Inc., 1989.
- [2-3] G. I. Igwe, "Axial ratio of antenna illuminated by an imperfectly circularly polarized source," *IEEE Trans. Antennas Propag.*, vol. AP-35, no. 3, pp. 339-342, Mar. 1987.
- [2-4] B. Y. Toh, R. Cahill, and V. F. Fusco, "Understanding and measuring circular polarization," *IEEE Trans. Edu.*, vol. 46, no. 3, pp.313-318, Aug. 2003.
- [2-5] T. G. Ma and S. J. Wu, "Ultrawideband band-notched folded strip monopole antenna," *IEEE Trans. Antennas Propag.*, vol. 55, no. 9, pp. 2473-2479, Sep. 2007.
- [2-6] M. J. Ammann and Z. N. Chen, "A wide-band shorted planar monopole with bevel," *IEEE Trans. Antennas Propag.*, vol. 51, no. 4, pp. 901-903, Apr. 2003.
- [2-7] *High Frequency Structure Simulator (HFSS) Version 10.0*, Ansoft Corporation, USA.

CHAPTER 3

COMPACT WIDEBAND LEAKY-WAVE ANTENNA

A compact wideband leaky-wave antenna (LWA) with etched slot elements and tapered structure is studied. The proposed antenna is composed of an asymmetric-fed multi-section tapered short leaky-wave antenna with two embedded slots and a ground plane with etched slot elements. Base on the concept of LWA, the asymmetric-fed is utilized to excite the first higher order mode. By etching slot elements on the ground plane, the current distribution of this antenna can be influenced to compact the width of conventional LWA. In order to achieve the impedance matching, this multi-section tapered short leaky-wave antenna is embedded with two rectangular slots. This technique not only improves the impedance matching but also suppresses the back lobe. According to the measured results, the impedance bandwidth achieves about 1.30 GHz for 7-dB return loss, which covers the range from 3.30 to 4.60 GHz, and the scanning angle of the measured main beam is about 36° , which covers the range from 17° to 53° . This short LWA is only about $1.14 \lambda_0$ at 3.4 GHz, and the back lobe can be suppressed by 7.5 dB at 4.3 GHz. Due to the etched slot elements on the ground plane, the frequency of the radiation angle is shifted to lower frequency by 750 MHz, which can compact the width of LWA by more than 20 %.



3.1 Leaky-Wave Antenna Theory

Leaky-wave antenna (LWA), which used an asymmetric feed line to excite the first higher order mode (TE_{01} , leaky mode), was presented by Menzel in 1979 [3-1]. In general, the radiation mode of commercial antenna is the dominant mode, which is a slow wave relative to radiating in free space. Comparing to the dominant mode, the first higher mode is a fast wave and excites the characteristics of narrow beamwidth and frequency scanning. Figure 3-1 shows the electric and magnetic fields of the dominant mode and the first higher order mode of open microstrip line [3-2]. In Fig. 3-1(a), the dominant mode, the electric field of which is an even symmetry about the axial centerline, is not a radiation mode of LWA. In Fig. 3-1(b), the first higher order mode, the electric field of which is an odd symmetry about the axial centerline, excites a radiating traveling wave.

The leakage theory and the phenomenon of leaky-wave antenna had been proposed by Oliner, such as the difference between the surface wave and the space wave, bound mode region, leakage region, and cutoff region in waveguide [3-3]~[3-5]. The leaky wave can be analyzed into surface wave and space wave, shown in Fig. 3-2 [3-6]. k_s is the surface wave number, and k_x and k_z are respectively the x direction and the z direction of the surface wave number. They can be expressed as

$$k_s^2 = k_x^2 + k_z^2 \quad (3-01)$$

$$k_z = \beta - j\alpha \quad (3-02)$$

where β and α are the phase and the attenuation constant. There, k_z is assumed that $k_z = \beta$.

For actual leakage, $k_x \geq 0$ and k_x is real. Therefore, we can find that

$$k_s \geq \beta \quad (3-03)$$

As β is less than k_s , the surface wave is formed. As β is less than k_s further, the space wave is then formed. When $\beta = k_0$, where k_0 is the free space wave number, the boundary can be defined. If $\beta < k_0$, the space wave will be leaked out [3-6].

As a rule, k_z is a complex propagation constant, like Eq. (3-02). The rigorous (Wiener-Hopf) solution mentioning [3-7]~[3-9] can be used to obtain the complex propagation constant of the first higher order mode. The variation of the normalized phase and attenuation constant are plotted in Fig. 3-3. In [3-10], the first higher order mode can be divided into four region:

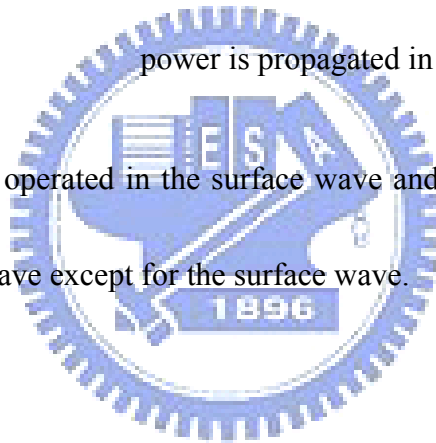
- 1) $\alpha = 0, \beta > k_s$, bound mode region. The power is propagated in the forms of the surface wave and the quasi-TEM wave.
- 2) α is small, $k_s > \beta > k_0$, surface wave leakage region. When $\beta = k_0$, the main beam is ideally radiated parallel to end-fire direction. The power on the LWA is reflected from the open end to produce a serious side lobe. When the length of

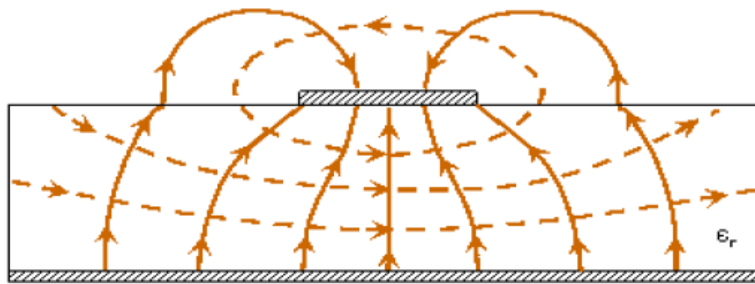
LWA is increased, the side lobe will be reduced.

3) α is small, $k_0 > \beta$, surface wave and space wave leakage region. The surface wave and space wave are excited. The beamwidth of main beam is like a pencil beam. The radiated power of side lobe is small.

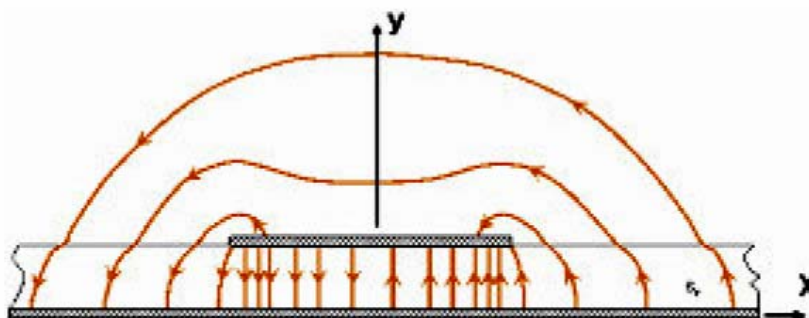
4) α is large, $k_0 > \beta$, cutoff region or reactive region. The first higher order mode is reactive below cutoff, and the small real power is propagated in the guided direction.

Leaky-wave antenna is operated in the surface wave and space leakage region, and the power leaks into the space wave except for the surface wave.





(a)



(b)

Fig. 3-1. Field diagram for the (a) dominant mode and (b) first higher order mode (E field: solid line, H field: dashed line) [3-2].

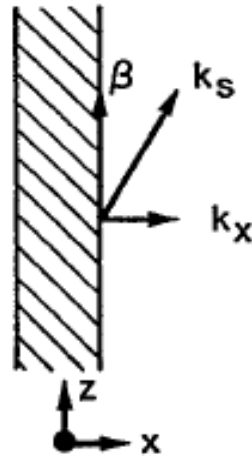


Fig. 3-2. Top view of the strip of microstrip line and dielectric region around it [3-6].

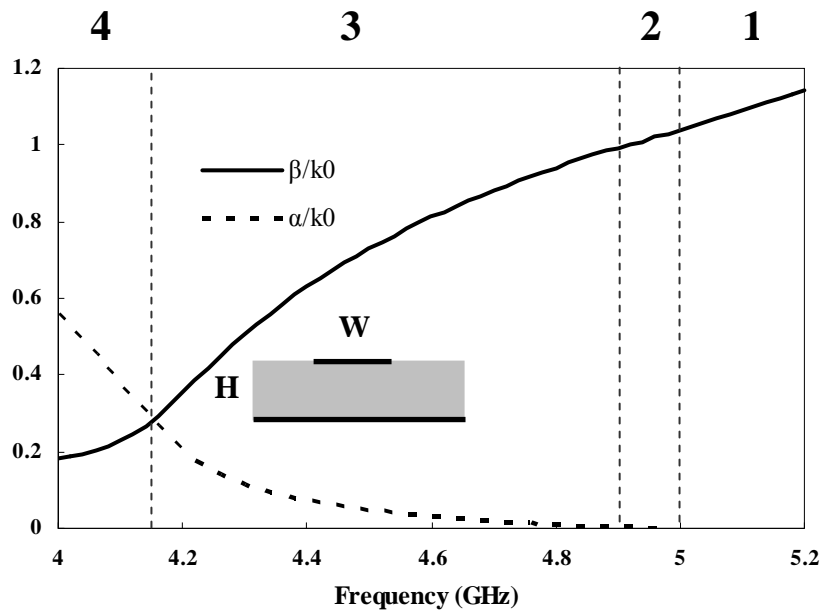


Fig. 3-3. Normalized complex propagation constants of the conventional microstrip LWA. $H = 1.6$ mm, $W = 15$ mm, and $\epsilon_r = 4.4$. k_0 is the free space wave number.

3.2 Procedure of Leaky-Wave Antenna Design

Figure 3-4 shows the proposed configuration of the compact leaky-wave antenna. The antenna is fabricated on FR4 substrate with a dielectric constant (ϵ_r) of 4.4, loss tangent ($\tan \delta$) of 0.024, and thickness (H) of 1.6 mm. The total length L_1 of the multi-section tapered short leaky-wave antenna is chosen to be 10.0 cm (about $1.14 \lambda_0$ at 3.4 GHz). The width and length of each section of the tapered LWA are listed in Table 3-1. Here, we embedded two rectangular slots with the sizes of $S_1 \times S_2$ (Slot-A) and $S_3 \times S_4$ (Slot-B) on the leaky-wave antenna. The etched slot elements with the size of $G_1 \times G_2$ are on the ground plane, and the gap between the slots is D. The dimensions of the geometric parameters are also displayed in Table 3-1. In this section, the design procedures of this antenna, which include the etched slot elements on the ground for reducing width of leaky-wave antenna, and the multi-section tapered short leaky-wave antenna with embedded Slot-A and Slot-B for increasing the impedance bandwidth and suppressing the back lobe, are introduced step by step.

3.2.1 Compact Leaky-Wave Antenna

Generally, the cutoff frequency of a conventional leaky-wave antenna is controlled by the normalized complex propagation constant which includes the normalized phase constant β/k_0 and the normalized attenuation constant α/k_0 , where k_0 is the free space wavenumber. In Fig. 3-5, as the normalized attenuation constant equals the normalized phase constant ($\alpha/k_0 = \beta/k_0$), the cutoff frequency can be defined. When the normalized phase constant is less than one ($\beta/k_0 < 1$), which is called fast wave ($\beta < k_0$), the radiation region can be found. The β/k_0 , α/k_0 , cutoff frequency, and radiation region can be determined by the width of leaky-wave antenna, dielectric constant, and substrate thickness. The theoretical β/k_0 and α/k_0 of the conventional microstrip LWA as a function of frequency are plotted in Fig. 3-5. They are calculated by employing a rigorous (Wiener-Hopf) solution [3-7] and [3-9]. The cutoff frequency is about 4.15 GHz, and the radiation region is operated from 4.15 to 4.9 GHz. In [3-11] and [3-12], the normalized constant β/k_0 and α/k_0 relate directly to the maximum radiation angle θ_m between the broadside direction and the main-beam direction, and the 3-dB radiation beamwidth $\Delta\theta$. These relations are given by

$$\sin \theta_m \cong \beta / k_0 \quad (3-04)$$

$$\Delta\theta \cong \frac{1}{(L/\lambda_0)\cos\theta_m} \quad (3-05)$$

and

$$L/\lambda_0 \cong \frac{0.183}{\alpha/k_0} \quad (3-06)$$

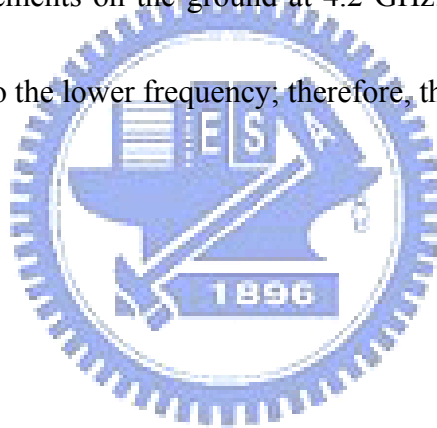
Figure 3-6(a) compares the theoretical θ_m of infinite length, and the simulated and measured θ_m of finite length (about $1.40 \lambda_0$ at 4.2 GHz) conventional LWA. The characteristics of the finite length conventional LWA were simulated by Ansoft High Frequency Structure Simulator software. Fig. 3-6(b) illustrates the theoretical $\Delta\theta$ of infinite length, and the simulated and measured $\Delta\theta$ of finite length conventional LWA. The values of theoretical θ_m and $\Delta\theta$ are determined in Eq. (3-04)~(3-06) by the values of theoretical β/k_0 and α/k_0 . The theoretical, simulated, and measured radiation angles of convention LWA are respectively about 16° , 22° , and 15° at the cutoff frequency of 4.15 GHz; therefore, it can be seen that the length of LWA does not influence the value of θ_m and β/k_0 much (see Eq. (3-04)). However, from Fig. 3-6(b) we can see that the 3-dB radiation beamwidth, $\Delta\theta$, of the theoretical calculation of infinite length LWA, and the simulated and measured results of finite length LWA are respectively about 95° , 43° , and 60° at 4.15 GHz. This result agrees very well with the thesis in [3-12] that the length of LWA can vary the value of $\Delta\theta$ and α (see Eq. (3-05) and (3-06)). Furthermore, since the cutoff frequency can be controlled by the width of leaky-wave antenna, the width of LWA can be reduced by reducing the value of β/k_0 and α/k_0 or the cutoff frequency.

In order to compact the leaky-wave antenna size, the slot elements with the size of $G_1 \times G_2$ are etched on the ground plane of the conventional LWA. This method of etching slot

elements on the ground plane can change the current distribution on the ground to reduce the frequency of the first higher order mode. Therefore, the radiation angle θ_m and 3-dB radiation beamwidth $\Delta\theta$ are also varied. Figure 3-7(a) and (b) show the simulated radiation angle and 3-dB radiation beamwidth results with different number of slot elements. The slot elements are 0, 4, 7, and 10 elements, respectively. For the results of Fig. 3-7(a), we can find that the frequency of θ_m is strongly dependent on the number of the slot elements. As they are increased to 7 elements, the frequency of 22° radiation angle is decreased from 4.15 to 3.33 GHz. Furthermore, the frequency of 22° radiation angle is converted from 3.33 to 3.25 GHz when the number of the slot elements is increased from 7 to 10. In Fig. 3-7(b), the characteristic of shifting to lower frequency of the $\Delta\theta$ is similar to that of the θ_m . As the cutoff frequency is shifted to lower frequency, the β/k_0 and α/k_0 has been varied; therefore, the width of LWA is reduced. For conventional LWA, if it is operated at lower frequency, obviously, the width of LWA must be increased. However, using this technique of etched slot elements on the ground plane, the LWA can be operated at lower frequency without increasing the width of LWA. From these simulated results, it can clearly be concluded that the cutoff frequency is decreased about 900 MHz from 4.15 to 3.25 GHz. Therefore, by this technique, we can compact the width of conventional LWA by more than 20 %.

The θ_m and $\Delta\theta$ are changed because the current distributions are influenced by etching slot elements on the ground plane. The simulated surface current distributions of the

conventional LWA and the LWA with 10 etched slot elements on the ground at 4.2 GHz are illustrated in Fig. 3-8(a) and Fig. 3-8(b). Comparing the surface current distributions on the LWA of Fig. 3-8(a) with that of Fig. 3-8(b), it can be found that the wavelength on the LWA is different. The LWA with 10 etched slot elements on the ground is less than half of the wavelength of the conventional LWA. Since the current distributions of ground plane are affected by the slot elements, the wavelength on the LWA is decreased. This phenomenon is explained that the fast wave ($\beta < k_0$) of the conventional LWA is changed to the slow wave ($\beta > k_0$) by etching the slot elements on the ground at 4.2 GHz. The cutoff frequency and the radiation region are shifted to the lower frequency; therefore, the width of LWA is reduced.



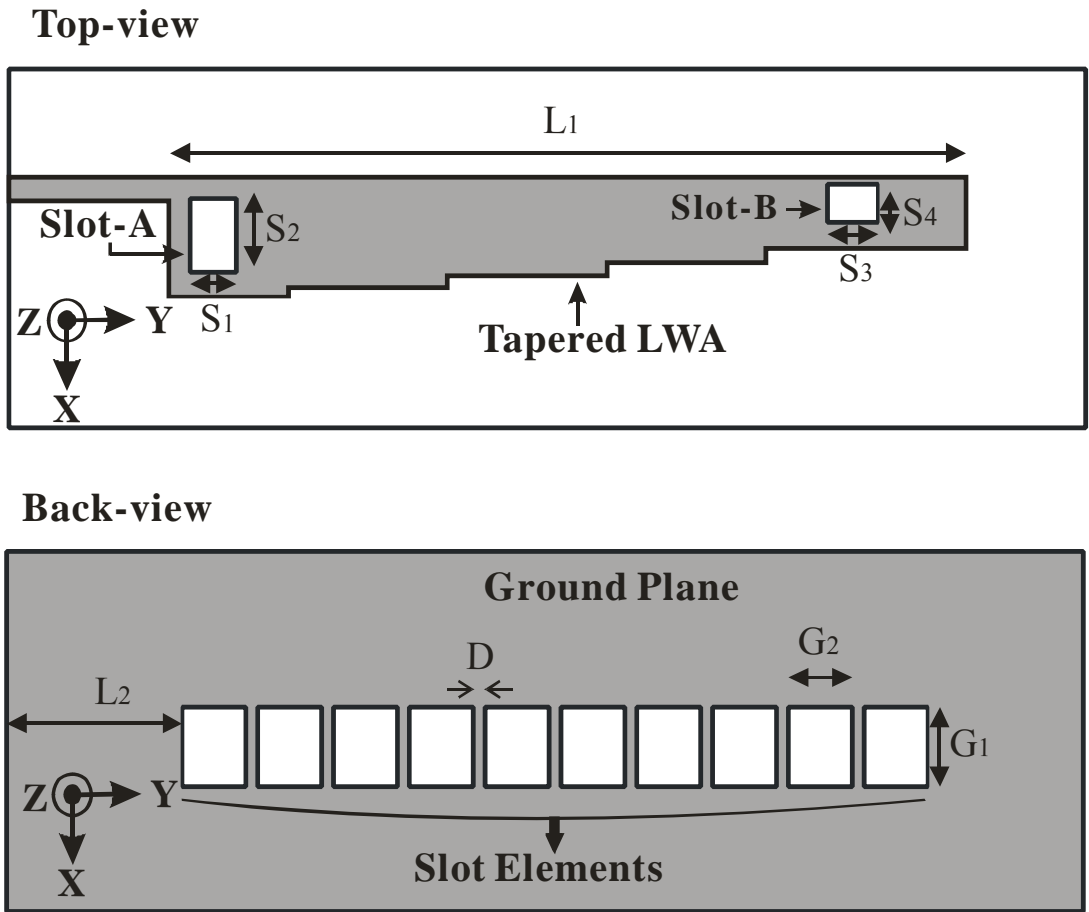


Fig. 3-4. Configuration of the proposed leaky-wave antenna.

TABLE 3-1
DIMENSIONS OF THE PROPOSED LEAKY-WAVE ANTENNA.

L_1	10.0 cm	S_1	7.0 mm
L_2	22.0 mm	S_2	13.0 mm
G_1	10.0 mm	S_3	8.0 mm
G_2	8.0 mm	S_4	7.0 mm
D	1.5 mm	H	1.6 mm
Width of Section 1	15.0 mm	Length of Section 1	15.0 mm
Width of Section 2	14.5 mm	Length of Section 2	20.0 mm
Width of Section 3	14.0 mm	Length of Section 3	20.0 mm
Width of Section 4	13.3 mm	Length of Section 4	20.0 mm
Width of Section 5	11.8 mm	Length of Section 5	25.0 mm

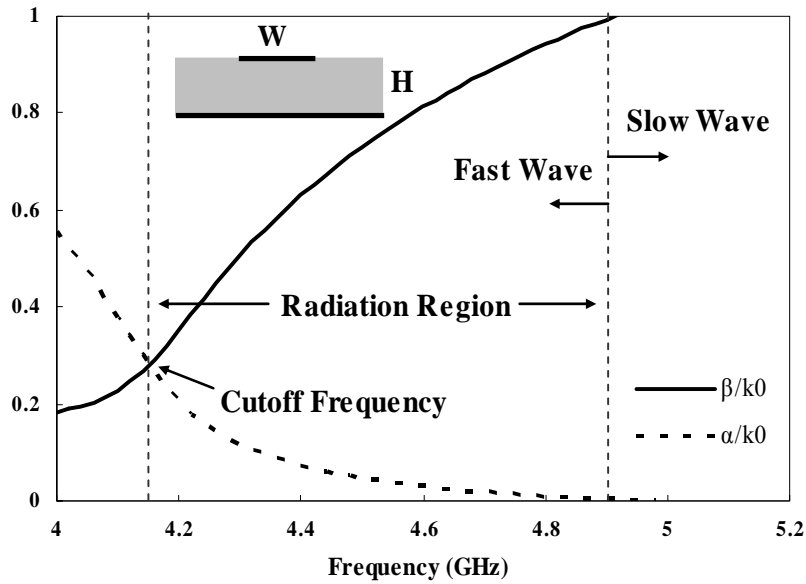
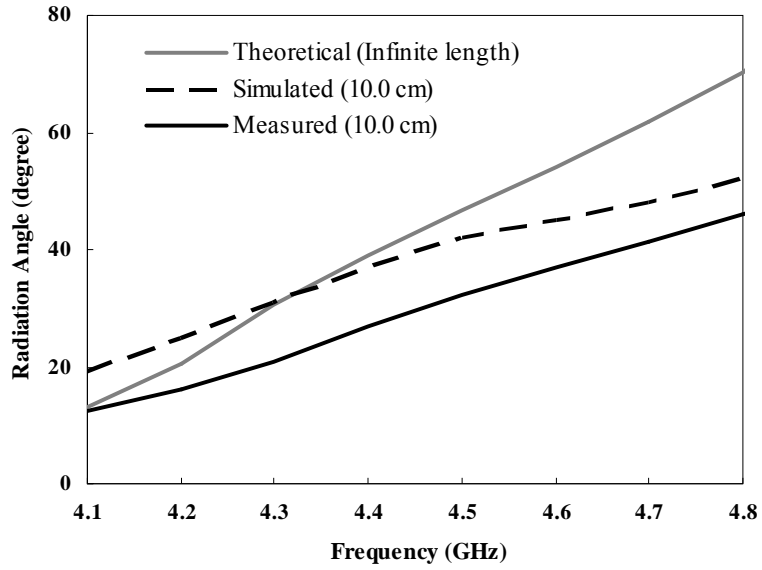
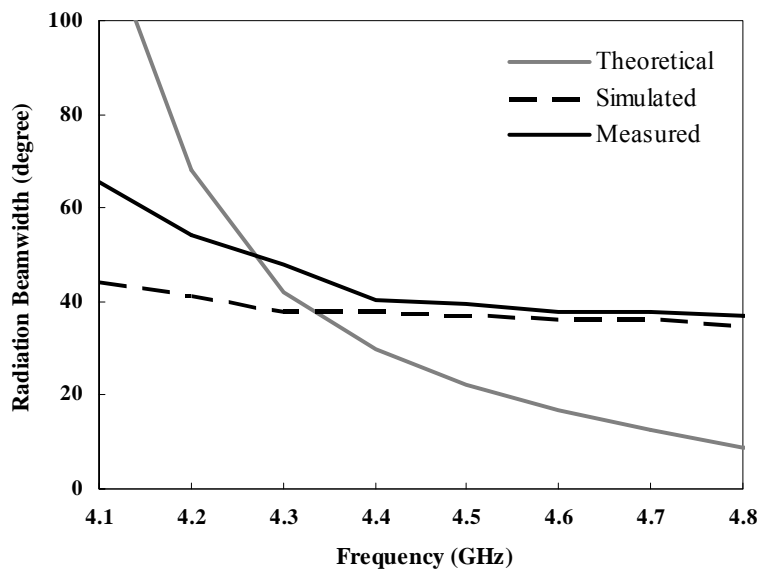


Fig. 3-5. Normalized complex propagation constants of the conventional microstrip LWA. $H = 1.6$ mm, $W = 15$ mm, and $\epsilon_r = 4.4$. k_0 is the free space wave number.

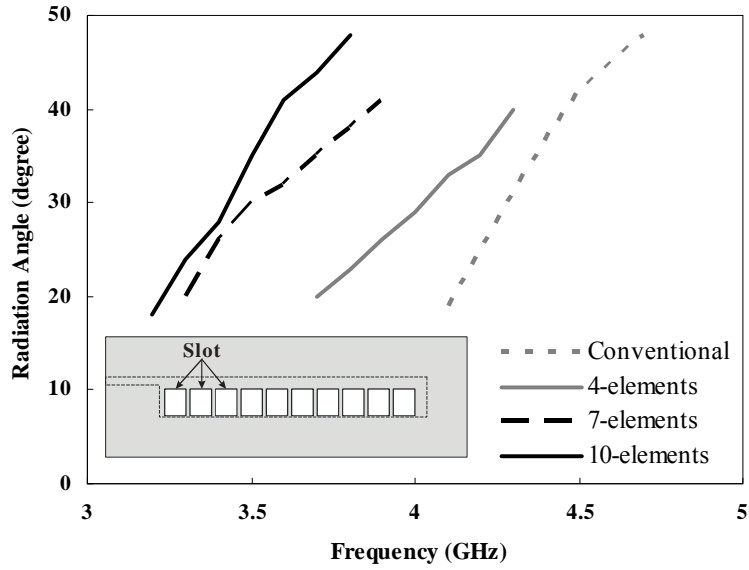


(a)

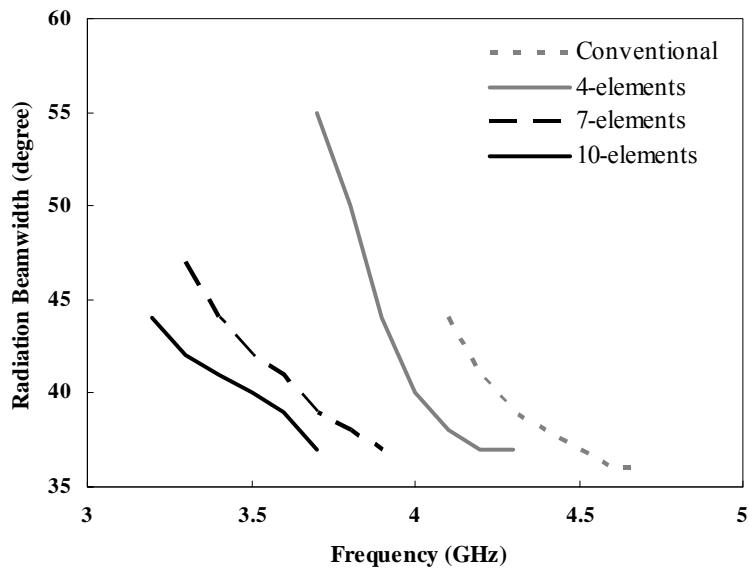


(b)

Fig. 3-6. Comparison of the theoretical, simulated, and measured θ_m and $\Delta\theta$ of a conventional LWA: (a) Radiation angle θ_m ; (b) Radiation beamwidth $\Delta\theta$.

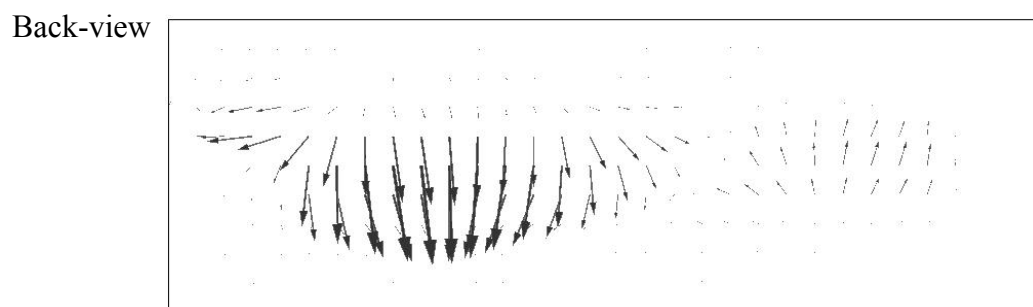
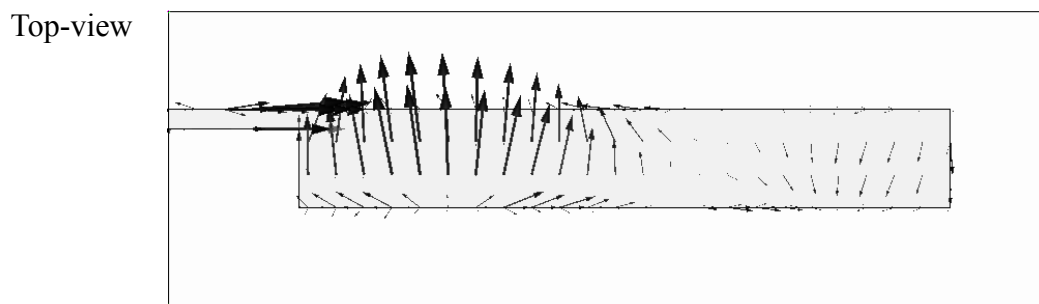


(a)

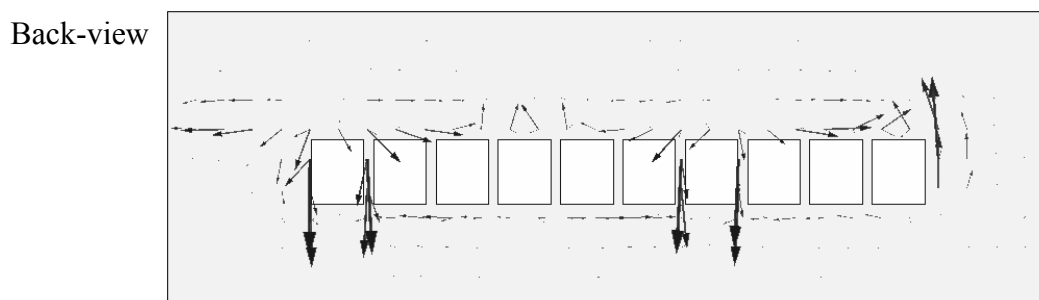
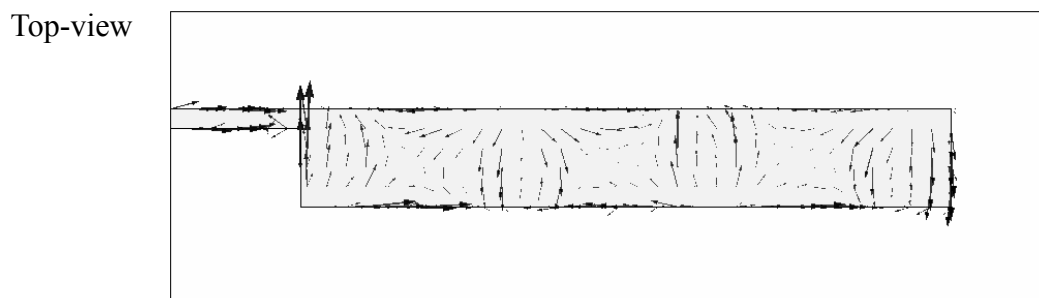


(b)

Fig. 3-7. Simulated radiation angle and 3-dB radiation beamwidth of LWA with etched slot elements: (a) Radiation angle θ_m ; (b) Radiation beamwidth $\Delta\theta$.



(a)



(b)

Fig. 3-8. Simulated surface current distributions at 4.2 GHz: (a) conventional LWA; (b) LWA with 10 slot elements.

3.2.2 Parameter Study of Etched Slot Elements

Due to the coupling effect between the LWA and the slot elements on the ground plane, this antenna can excite dual-beam radiation pattern, which includes the radiations of LWA above the substrate and radiation below the ground plane with etched slot elements. Figure 3-9 exhibits the simulated normalized radiation patterns by adjusting the width of slot elements (G_1) in the YZ-plane at 3.7 GHz as the number and length of the slot elements are respectively 10 and 8 mm. Notice that the energy of the current distributions at the end of the short LWA with 10 etched slot elements on the ground is strong (see Fig. 3-8(b)); therefore, the induced back lobe was excited. As can be seen from Fig. 3-9, the radiation angle of the main beam at 3.7 GHz is increased from 20° to 44° as the width is increased from 4 mm to 10 mm. The 3-dB radiation beamwidth of the main lobe and the gain of the back lobe above the substrate are slightly affected by the width of slot elements. Nevertheless, this gain of back lobe is almost independent of the width of slot. The side lobe below the substrate is radiated because the power of the ground is coupled by the LWA and radiates through the slot; consequently, the size of slot can influence the side lobe. In this case, the gain of the side lobe is enlarged as the width is increased from 4 mm to 7 mm, and it can be found that the radiation angle is depending on the radiation angle of main lobe. The simulated normalized radiation patterns of 3.7 GHz in the YZ-plane at the different length of slot elements (G_2) are shown in Fig. 3-10 as other parameters are fixed. As shown in Fig. 3-10, the 3-dB radiation

beamwidth of the main lobe and the gain of back lobe are respectively narrowed and enlarged by increasing the length of the slot, and it can also be seen that the back lobe is mainly varied by the length of the slot.

The simulated return losses of the conventional LWA and the LWA with 10 slot elements on the ground plane are plotted in Fig. 3-11. The dimensions of the slot and the distance between the two slot elements are displayed in Table 3-1. The 7-dB impedance bandwidth of the conventional LWA is about 1.0 GHz from 4.4 to 5.4 GHz. When slot elements are etched on the ground plane, the initially frequency can be decreased from 4.4 to 3.4 GHz; nonetheless, the impedance mismatched from 3.4 to 4.3 GHz is caused by this method.

According to above discussions of etching slot elements on the ground plane, we can conclude that the numbers and the dimensions of these slot elements can reduce the frequency of the radiation angle, control the 3-dB radiation beamwidth, influence the back lobe, and excite the side lobe. Although reducing the width of LWA, the slot elements cause the impedance mismatching.

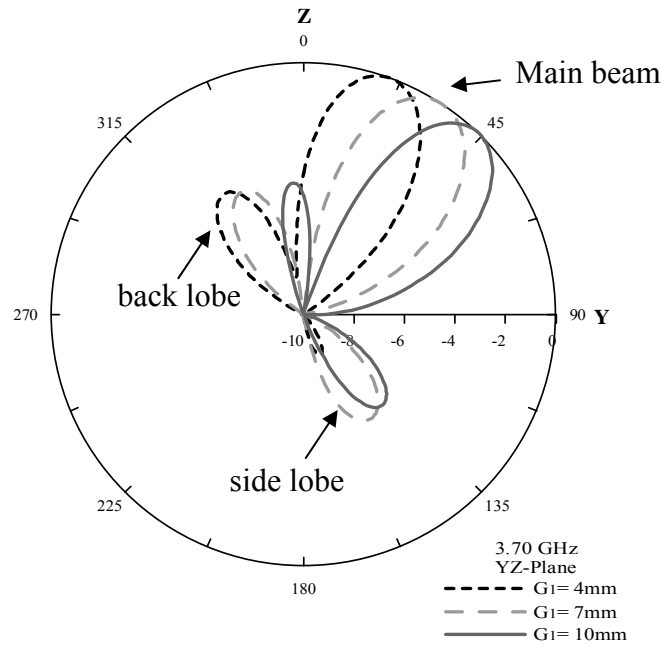


Fig. 3-9. Simulated radiation patterns of the slot widths, G_1 , in the YZ-plane at 3.70 GHz.

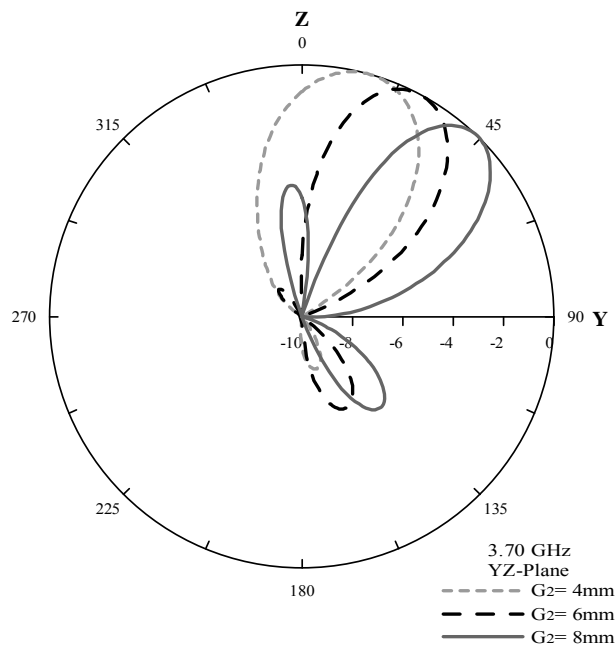


Fig. 3-10. Simulated radiation patterns of the slot lengths, G_2 , in the YZ-plane at 3.70 GHz.

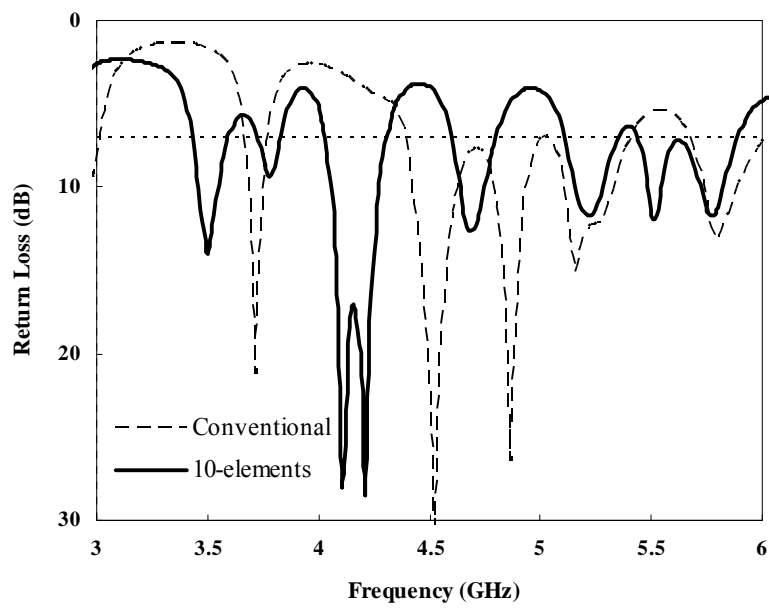


Fig. 3-11. Comparison the simulated return losses of conventional LWA and LWA with 10 slot elements on the ground plane.

3.2.3 Increasing Bandwidth and Suppressing Back Lobe

In order to achieve the impedance matching, the multi-section tapered leaky-wave antenna is utilized. Because the radiated frequency is determined by the width and length of each section of the tapered structure, the impedance and the radiation region can be improved [3-13]. However, this method of the multi-section tapered short leaky-wave antenna results in serious back lobes. To increase the impedance bandwidth further and reduce the serious back lobe, the Slot-A with the sizes of $S_1 \times S_2$ is embedded on this multi-section tapered short LWA to improve the impedance matching, and the Slot-B with the sizes of $S_3 \times S_4$ is utilized to suppress the back lobe. In this analysis here, the parameters of etched slot element on the ground plane are fixed.

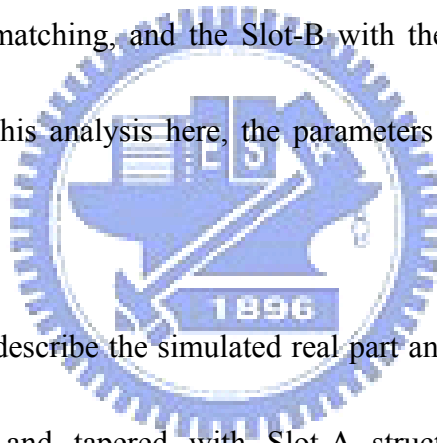
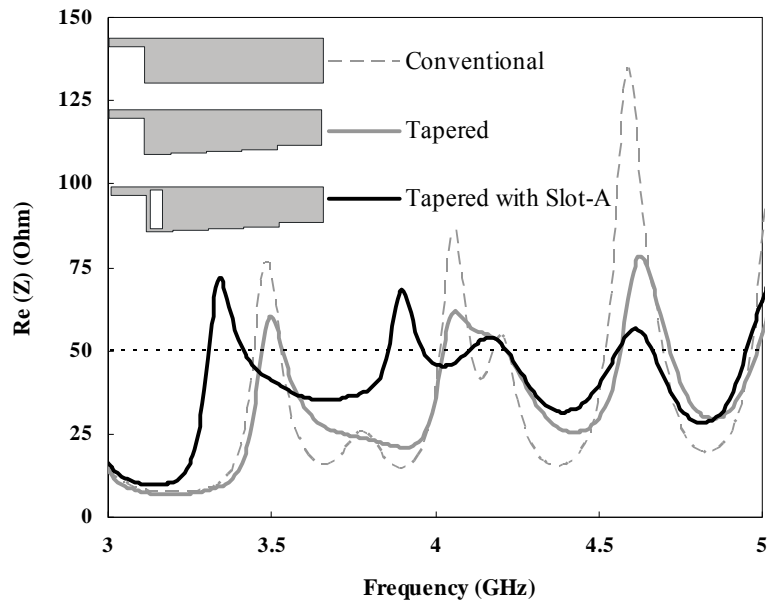


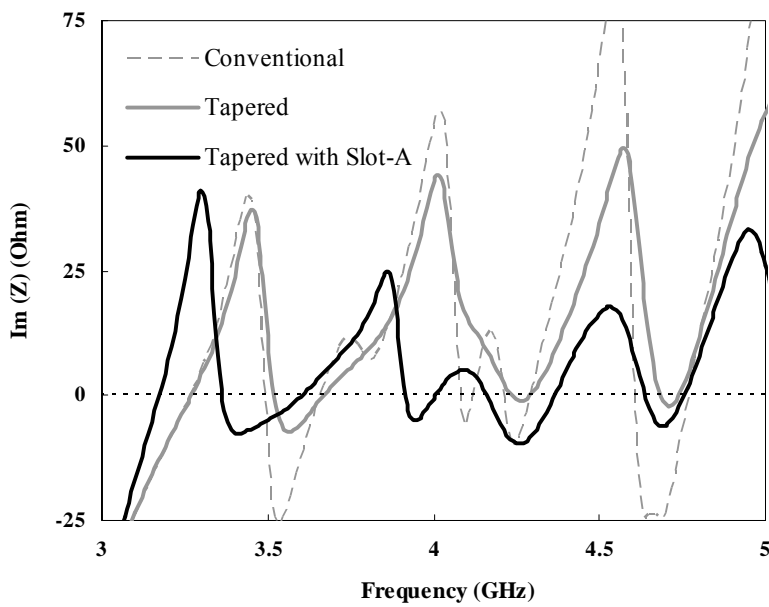
Figure 3-12(a) and (b) describe the simulated real part and imaginary part impedance of the conventional, tapered, and tapered with Slot-A structure. The dimensions of the multi-section tapered short LWA and Slot-A are listed in Table 3-1. In Fig. 3-12(a) and (b), we can see that the real part impedance of the conventional short LWA is almost less than 25Ω except the three peaks at 3.5, 4.1, and 4.6 GHz, and the imaginary part of the impedance tends to be inductive except the several deeps. When the LWA is changed from conventional to tapered, the three peaks are lowered, and the low impedance is increased in the real part impedance. The phenomenon of the imaginary part impedance which is inductive is lowered. Even though the real and the imaginary part impedance are improved by tapered structure, the

impedance matching is not widened. In order to achieve wideband impedance matching, the Slot-A is embedded on this multi-section tapered short LWA. It can be seen from Fig. 3-12, from 3.3 to 5.0 GHz, the real part impedance is changed to almost 50Ω , and the imaginary part of the impedance is decreased to approach 0Ω . Consequently, this method of the multi-section tapered short LWA with embedded Slot-A can improve the impedance bandwidth.

The simulated normalized radiation patterns in the YZ-plane of the tapered short LWA with no slot, that with only Slot-A, and that with both Slot-A and Slot-B embedded at 4.3 GHz are compared in Fig. 3-13. We can see that the gain of the back lobe of the tapered LWA with no slot embedded is only about 1.4 dB lower than the main beam at 4.3 GHz. It was observed that as the frequency was increased, the gain of the back lobe could be even larger than the main beam or even substitute for the main beam. As Slot-A was embedded on this tapered short LWA, the gain of back lobe can now be suppressed to about 2.5 dB at 4.3 GHz. Therefore, we can see that although embedding Slot-A can improve the impedance matching, but it still cannot suppress the back lobe effectively. To further suppress the back lobe, Slot-B is embedded on this tapered short LWA (as shown in Fig. 3-4). Finally, we can see the gain of back lobe is successfully be suppressed by 5.5 dB.



(a)



(b)

Fig. 3-12. Comparison the simulated impedance of the LWA of conventional, tapered, and tapered with Slot-A structure: (a) Real part; (b) Imaginary part.

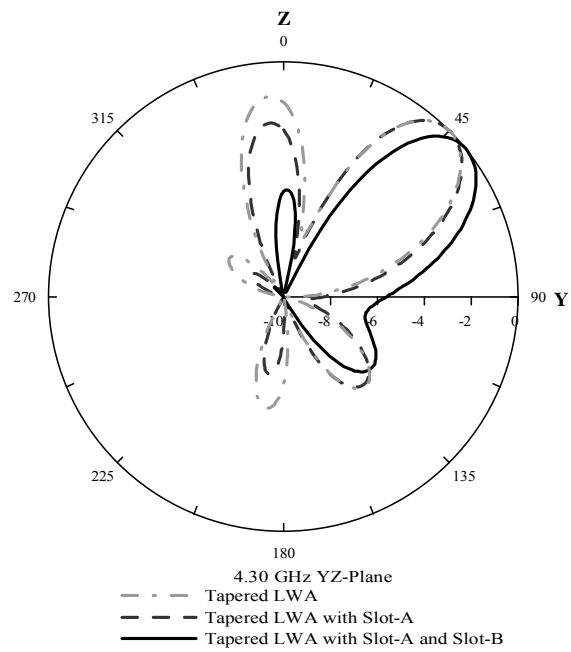


Fig. 3-13. Comparison the simulated radiation patterns of the multi-section tapered short LWA without slot, that with Slot-A, and that with Slot-A and Slot-B at 4.3 GHz.

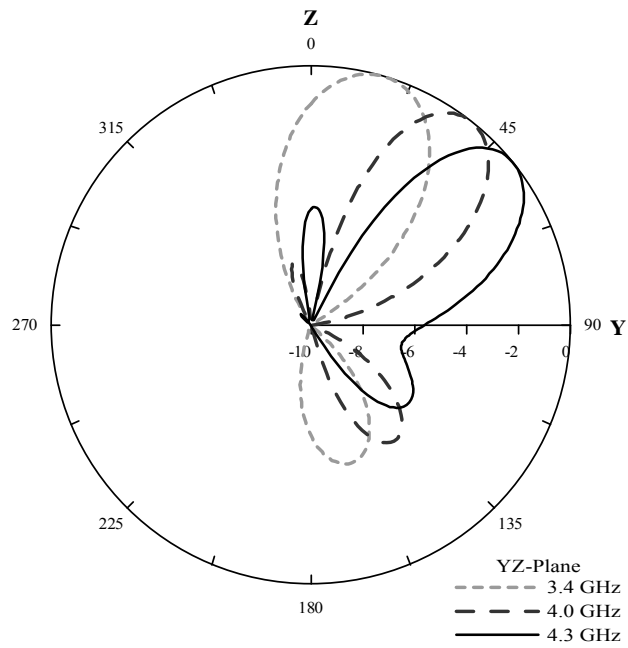
3.3 Simulation and Measurement Results

From the above discussion of antenna design, etching slot elements on the ground can reduce the frequency of the radiation angle, and the multi-section tapered short leaky-wave antenna with embedded Slot-A and Slot-B can achieve both the impedance matching and suppressing the back lobe. Fig. 3-14(a) and (b) respectively illustrate the simulated and measured normalized radiation patterns in the YZ-plane of the proposed antenna at 3.4, 4.0, and 4.3 GHz. The measured gain of the back lobe is 7.5 dB lower than the main beam at 4.3 GHz. The measured results of the characteristic of the radiation angle, 3-dB radiation beamwidth, and back lobe, are similar to the simulated results (see Fig. 3-14(b)). The scanning angle of the measured main beam is 36° from 17° to 53° as the operating frequency increases from 3.4 to 4.3 GHz. In addition, the measured 3-dB beamwidth of 46° at 4.3 GHz is larger because the main beam and the side lobe are combined to increase the 3-dB beamwidth. Comparing the measured results of the conventional short LWA (in Fig. 3-6) and the proposed LWA (in Fig. 3-14(b)), it can be inferred that the cutoff frequency of LWA is decreased about 750 MHz from 4.15 to 3.4 GHz; therefore, the width of conventional short LWA can be reduced by more than 20 %. Figure 3-15 shows the maximum measured gains. The gains are larger than 4.8 dBi from 3.4 to 4.4 GHz, and the gain variation is less than 1.6 dBi.

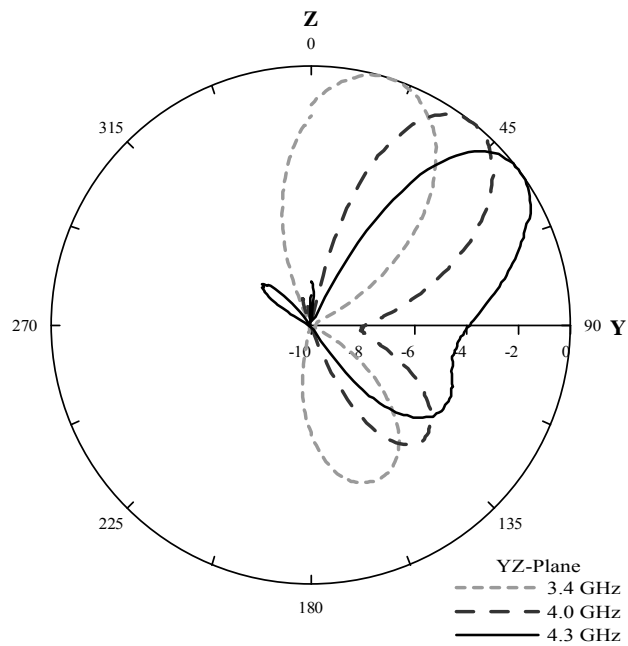
The simulated and measured return losses of the conventional LWA and our proposed

LWA are exhibited in Fig. 3-16. It has good agreement between the simulated and measured results of our proposed LWA. Comparing with the impedance bandwidth of about only 24 % for the conventional LWA, the measured 7-dB impedance bandwidth of our proposed LWA reaches about 33 % with respect to the center frequency at 3.95 GHz. In addition, the initially frequency is decreased about 1.12 GHz from 4.42 GHz of the conventional LWA to 3.30 GHz of the proposed LWA. From the measured results, it can be seen that this compact antenna, which is formed by the multi-section tapered short leaky-wave antenna with two slots and a ground plane with ten etched slot elements, not only creates a wideband impedance bandwidth and suppresses the back lobe, but also reduces the width of conventional LWA by 20%.





(a)



(b)

Fig. 3-14. Simulated and measured radiation patterns of the proposed LWA in the YZ-plane: (a) simulated patterns; (b) measured patterns.

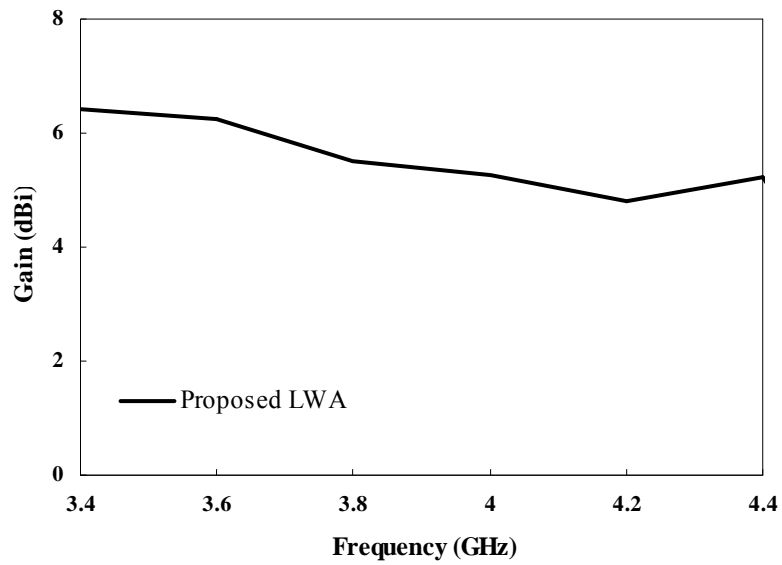


Fig. 3-15. Maximum measured gains of the proposed LWA.

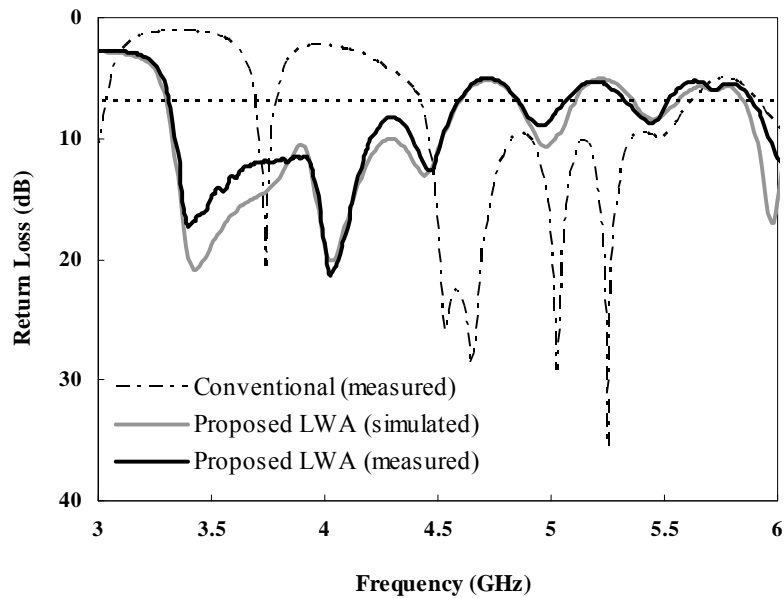


Fig. 3-16. Comparison the simulated and measured return losses of the conventional LWA and the proposed LWA.

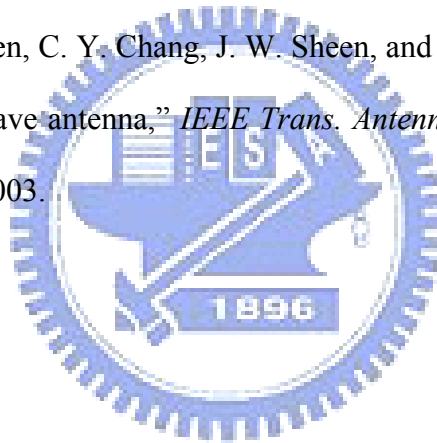
3.4 Summary

In this chapter, a novel compact leaky-wave antenna has been presented. The width of LWA was reduced by using the method of etching slot elements on the ground; it thus influenced the current distribution of leaky-wave antenna, reducing the frequency of the radiation angle and influencing the back lobe, and excited the side lobe. Furthermore, it causes impedance mismatching. As a result, we tapered this short leaky-wave antenna and embedded Slot-A and Slot-B to achieve both the impedance matching and suppressed the back lobe. With these methods, the 7-dB impedance bandwidth can be achieved from 3.30 to 4.60 GHz. The scanning angle of the measured main beam is 36° from 3.40 to 4.30 GHz. This compact LWA with length of only about $1.14 \lambda_0$ at 3.4 GHz not only successfully reduces the width of a conventional LWA by more than 20 %, but also suppresses the back lobe by 7.5 dB at 4.3 GHz. This compact LWA provides a lot of advantages such as compact size, low cost, and easy fabrication. It is suitable for the scanning systems, such as traffic control and collision avoidance system.

3.5 References

- [3-1] W. Menzel, "A new travelling-wave antenna in microstrip," *Archiv. Elektrnik, Ubertrag Tech.*, pp. 137-140, Apr. 1979. Band 33.
- [3-2] L. Kempel, S. Schneider, J. Radcliffe, D. Janning, and G. Thiele, "FE-BI analysis of a leaky-wave antenna with resistive sheet termination," in *IEEE ACES Int. Conf.*, Apr. 2005, pp. 670-673.
- [3-3] A. A. Oliner, "Leakage from various waveguides in millimeter wave circuits," *Radio Science*, vol. 22, no. 6, pp. 866-872, Nov. 1987.
- [3-4] A. A. Oliner, "Leakage from higher modes on microstrip with application to antennas," *Radio Science*, vol. 22, no. 6, pp. 907-912, Nov. 1987.
- [3-5] A. A. Oliner, "A new class of scannable millimeter wave antennas," in *Proc. 20th European Microwave Conf.*, 1990, pp. 95-104.
- [3-6] A. A. Oliner and K. S. Lee, "The nature of the leakage from higher modes on microstrip line," in *Microw. Symp. Digest, MTT-S Int.*, Jun. 1986, vol. 86, no. 1, pp. 57-60.
- [3-7] D. C. Chang and E. F. Kuester, "Total and partial reflection from the end of a parallel-plate waveguide with an extended dielectric loading," *Radio Sci.*, vol. 16, pp. 1-13, Jan. –Feb. 1981.
- [3-8] G. M. Zelinski, G. A. Thiele, M. L. Hastriter, M. J. Havrilla and A. J. Terzuoli, "Half width leaky wave antennas," *IET Microw. Antennas Propag.*, vol. 1, no. 2, pp. 341-348, Apr. 2007.
- [3-9] A. A. Oliner and K. S. Lee, "Microstrip leaky wave strip antennas," in *IEEE AP-S Int. Symp. Dig.*, Philadelphia, PA, Jun. 1986, pp. 443–446.

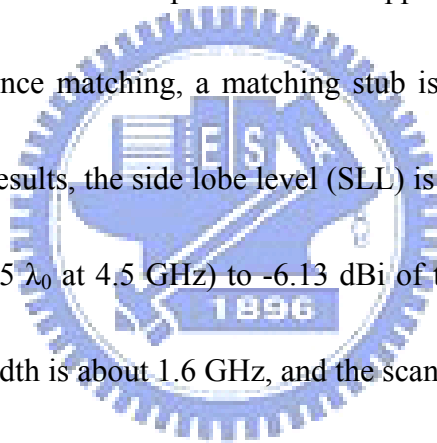
- [3-10] Y. D. Lin, J. W. Sdheen, and C. K. Tzuang, "Analysis and design of feeding structures of microstrip leaky-wave antenna," *IEEE Trans. Antennas Propag.*, vol. 44, no. 9, pp. 1540-1547, 1996.
- [3-11] J. L. Gómez-Tornero, A. d. l. T. Martínez, D. C. Rebenaque, M. Gugliemi, and A. Álvarez-Melcón, "Design of tapered leaky-wave antennas in hybrid waveguide-planar technology for millimetre waveband applications," *IEEE Trans. Antennas Propag.*, vol. 53, no. 8, pp. 2563-2577, Aug. 2005.
- [3-12] P. Lampariello, F. Frezza, H. Shigesawa, M. Tsuji, and A. A. Oliner, "A versatile leaky-wave antenna based on stub-loaded rectangular waveguide: part I-theory," *IEEE Trans. Antennas Propag.*, vol. 46, no. 7, pp. 1032-1041, Jul. 1998.
- [3-13] W. Hong, T. L. Chen, C. Y. Chang, J. W. Sheen, and Y. D. Lin, "Broadband tapered microstrip leaky-wave antenna," *IEEE Trans. Antennas Propag.*, vol. 51, no. 8, pp. 1922-1928, Aug. 2003.



CHAPTER 4

SUPPRESSING SIDE LOBE OF TAPERED SHORT LEAKY-WAVE ANTENNA

A method for suppressing side lobe of tapered short leaky-wave antenna (LWA) is demonstrated in this chapter. The proposed LWA contains a tapered microstrip radiator with a shorting pin and two rectangular slots. This design of two slots and a shorting pin can interfere with the current distribution of tapered LWA to suppress the radiation of side lobe. In order to achieve the impedance matching, a matching stub is added along the feeding line. According to the measured results, the side lobe level (SLL) is improved from 0.01 dBi of the tapered short LWA (about $1.5 \lambda_0$ at 4.5 GHz) to -6.13 dBi of the proposed LWA at 6.4 GHz. The 7-dB impedance bandwidth is about 1.6 GHz, and the scanning range is about 43° .



4.1 Tapered Leaky-Wave Antenna Theory

LWA can excite a wide bandwidth by the first higher order mode. The radiation bandwidth is mainly controlled by the width of LWA, the thickness of the substrate, and the dielectric constant. Therefore, the tapered LWA is proposed to increase the bandwidth [4-1] and [4-2]. The tapered LWA uses sections of different width and length to excite different operating frequency band, and then these bands are combined to increase impedance bandwidth. The theory of tapered LWA is that the wider width of LWA radiates in the lower frequency region and the narrower width enters into the reactive region not to radiate power, simultaneously. Similarly, the narrower width radiates in the higher frequency region and at the same time the wider width enters into the bound mode region. The width of each section of tapered LWA can be determined by the start and the end frequency. The equations of radiation region and cutoff frequency (f_c) of each section is expressed as

$$f_c = \frac{c}{2w_{eff}\sqrt{\epsilon_r}} \quad (4-01)$$

$$f_c < f < \frac{f_c\sqrt{\epsilon_r}}{\sqrt{\epsilon_r}-1} \quad (4-02)$$

where c is the speed of light in the vacuum, w_{eff} is the effective width of strip line, and ϵ_r is the dielectric constant of substrate. The length of each section can be designed by the survival power ratio (r) at the end of strip, which is defined as

$$r = e^{-2\alpha L} \quad (4-03)$$

where L is the length of a section. Therefore, we can use the Eq. (4-01) and (4-03) to design the width and the length of each section. Figure 4-1 shows three types of tapered LWA.

Because the impedance mismatch and the discontinuity effect are caused by the original tapered LWA (Type I), the bandwidth will be reduced and the side lobe level will be increased.

Type II and III are designed to improve the bandwidth.

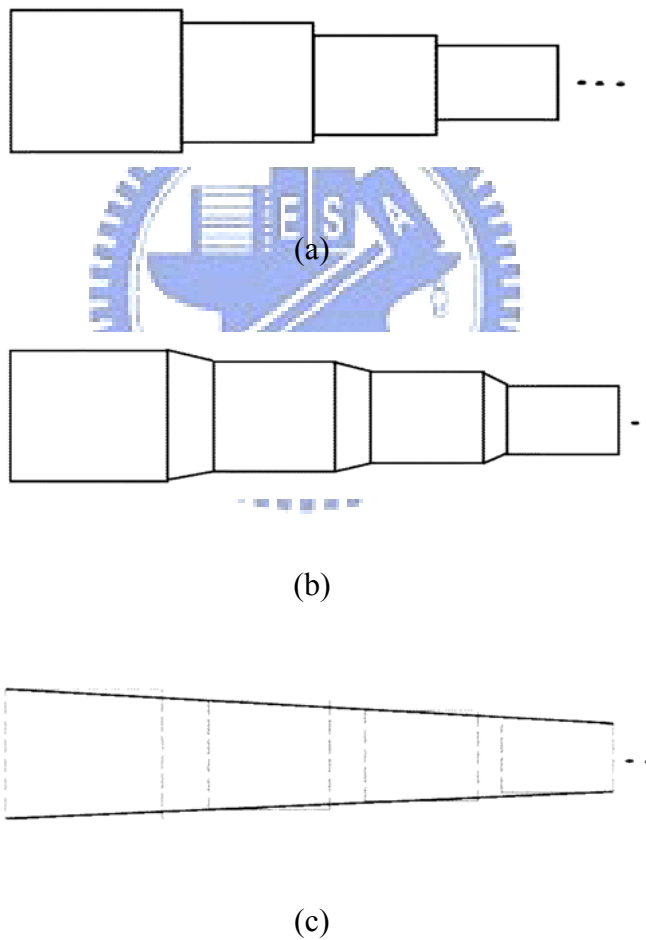


Fig. 4-1. Three structure of tapered LWA: (a) Type I, (b) Type II, (c) Type III [4-1].

4.2 Antenna Design

The structure of the proposed short length leaky-wave antenna is shown in Fig. 4-2. The antenna is printed on a 1.6 mm thick FR4 substrate, the dielectric constant and the loss tangent of which are 4.1 and 0.02. It is fed by microstrip feed line with a matching stub. The antenna is contained of a tapered microstrip radiator with a shorting pin and two rectangular slots (Slot 1 and Slot 2). The total length L_1 of the antenna is chosen to be 10.0 cm (about $1.5\lambda_0$ at 4.5 GHz, λ_0 is the free space wavelength), and the length of each section of the tapered LWA is 10.0 mm. The width of each section is listed in Table 4-1. The sizes of $S_1 \times S_2$ (Slot 1) and $S_3 \times S_4$ (Slot 2) are respectively $6.0 \times 12.0 \text{ mm}^2$ and $6.0 \times 7.5 \text{ mm}^2$. In this chapter, we utilize Ansoft High Frequency Structure Simulator to simulate our proposed antenna.

In general, the tapered leaky-wave antenna is utilized to increase the impedance bandwidth [4-1]. However, this method of the tapered short leaky-wave antenna excites serious side lobes, and even the main lobe is replaced by side lobe at higher frequency. The measured normalized radiation patterns of the conventional tapered short LWA are exhibited in Fig. 4-3. As can be seen from Fig. 4-3, the gain of the side lobe is greatly increased as the frequency is increased, and the gain of side lobe has been equal to the main lobe at 6.4 GHz.

In order to suppress the side lobe, the method of using two slots (Slot 1 and Slot 2) and a shorting pin is proposed. The Slot 1 is mainly used to suppress the excitation of the dominant mode. The simulated return losses of the conventional tapered short LWA and the

conventional tapered short LWA with Slot 1 structure are illustrated in Fig. 4-4. From these simulated results, they can be clearly seen that the dominant mode is successfully suppressed by embedded Slot 1 on the tapered short LWA. The Slot 2 and the shorting pin are designed to affect the reflected wave and reduce the radiation of side lobe. The structures of LWA and simulated radiation pattern in YZ-plane at 6.0 GHz are shown in Fig. 4-5. As can be seen from Fig. 4-5(e), the level of the side lobe is successfully suppressed by utilizing these methods. The simulated surface current distributions of the conventional tapered short LWA, with Slot 1, with Slot 1 and 2, and the proposed LWA at 6.0 GHz are plotted in Fig. 4-6(a), (b), (c), and (d), respectively. According to Fig. 4-6(a), the serious side lobe is generated by the strong power of current distribution at the end of the tapered short LWA. As the Slot 1 is embedded on the LWA, although the current distribution in Fig. 4-6(b) can be changed, the power at the end of the LWA with Slot 1 still radiate a serious side lobe. From Fig. 4-6(c) it can be shown that the path and the direction of current at the end of the LWA with Slot 1 and 2 are varied, and then the serious side lobe of the LWA with Slot 1 is separated into two weak side lobes, which is shown in Fig. 4-5(e). In order to reduce the power at the end of LWA with Slot 1 and 2, the shorting pin is design near the Slot 2. According to Fig. 4-6(d), because the power at the end is guided to the ground, the side lobe can be reduced. By using this method, the side lobe of the conventional tapered short LWA can be suppressed successfully. To achieve the impedance matching, a matching stub is added along the feeding line.

Figure 4-7 and 4-8 show the effects of the distance between Slot 1 and Slot 2 on radiation pattern in YZ-plane and current distribution at 6.0 GHz. As the distance is $0.75 \lambda_0$, the side lobe level is increased in Fig. 4-7, mainly because the power at the end of the LWA is larger in Fig. 4-8(a). However, the power and the direction of current at the end of the LWA can be varied in Fig. 4-8(b) as the distance is $1.0 \lambda_0$. According to these simulated results, the side lobe level is mainly varied by the distance between Slot 1 and Slot 2.

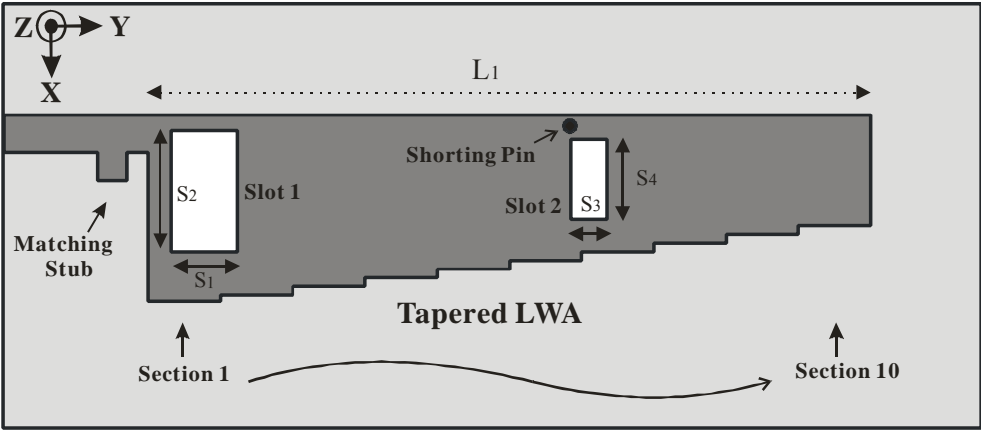


Fig. 4-2. Structure of the proposed short length LWA.

TABLE 4-1
DIMENSIONS OF THE PROPOSED TAPERED SHORT LWA.

Width of Section 1	15.0 mm	Width of Section 6	11.7 mm
Width of Section 2	14.5 mm	Width of Section 7	11.0 mm
Width of Section 3	13.8 mm	Width of Section 8	10.3 mm
Width of Section 4	13.1 mm	Width of Section 9	9.6 mm
Width of Section 5	12.4 mm	Width of Section 10	8.9 mm

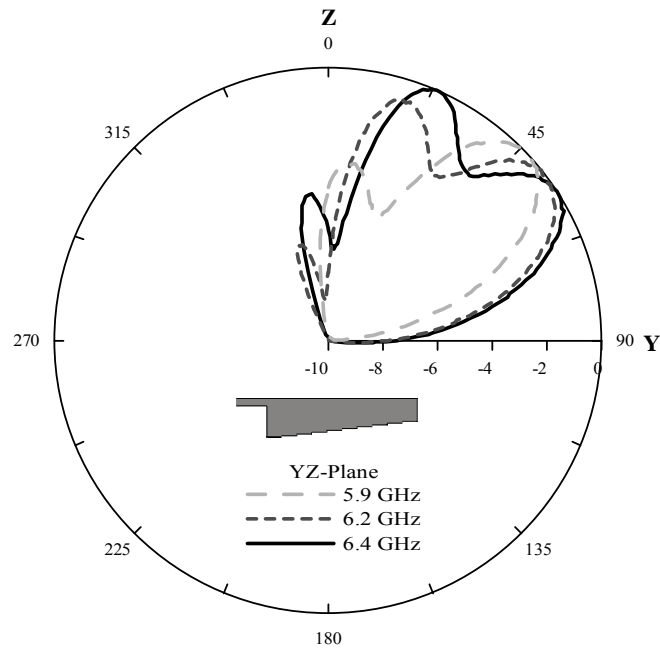


Fig. 4-3. Measured normalized radiation patterns of the conventional tapered short LWA.

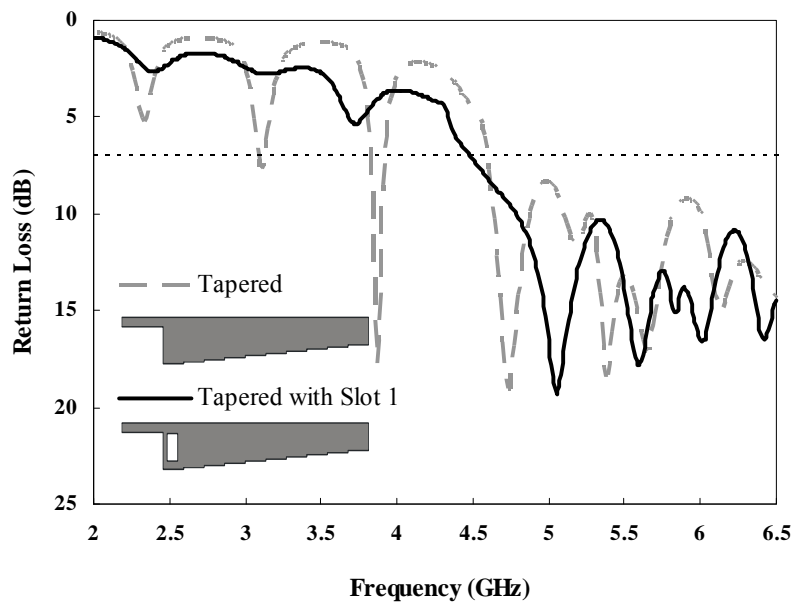


Fig. 4-4. Simulated return losses of the conventional tapered short LWA and the conventional tapered short LWA with Slot 1 structure.

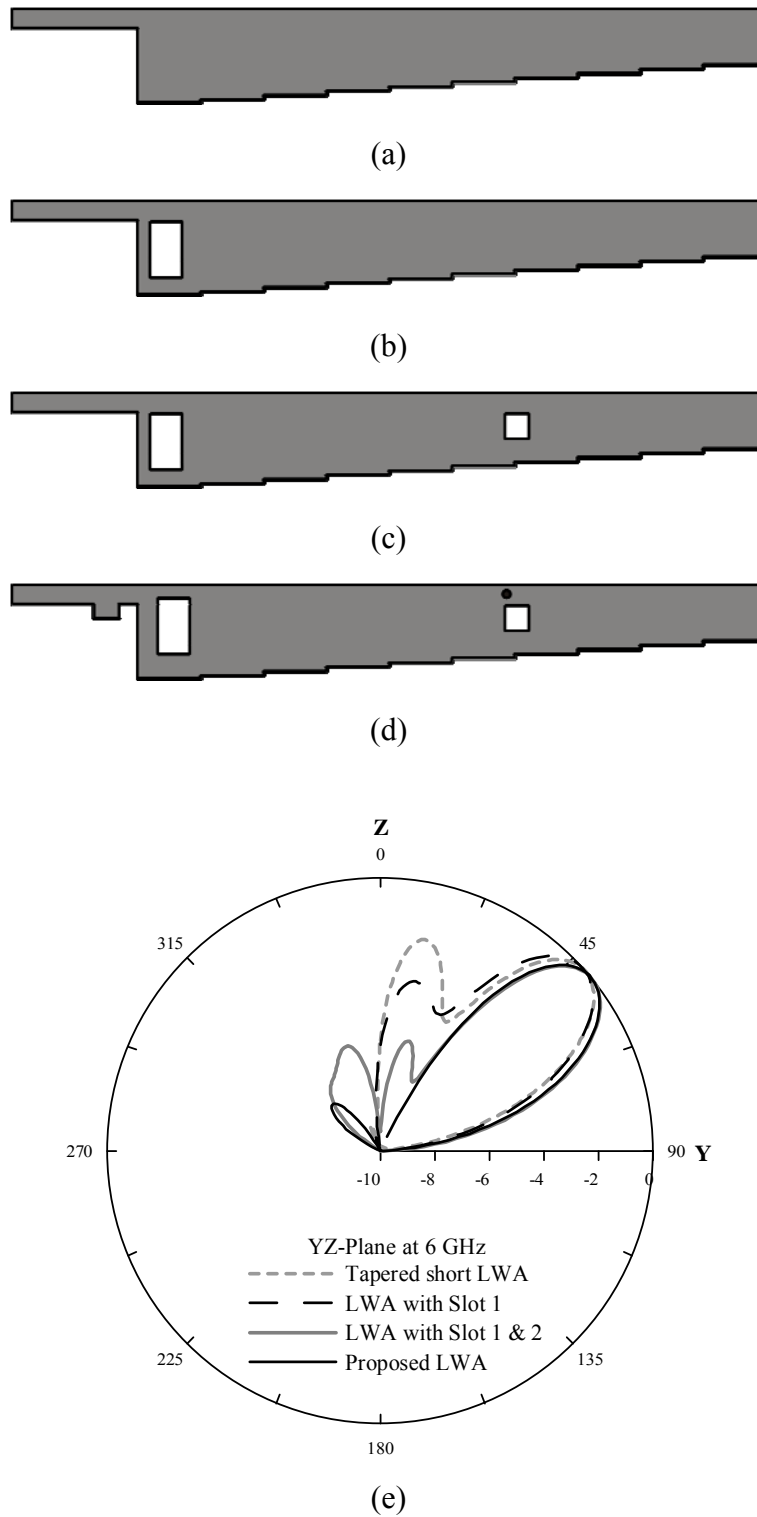
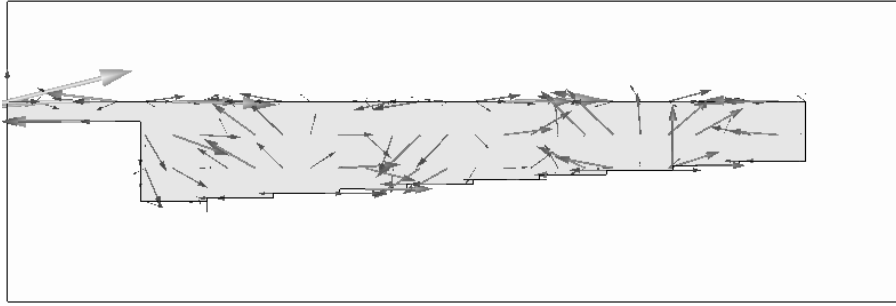
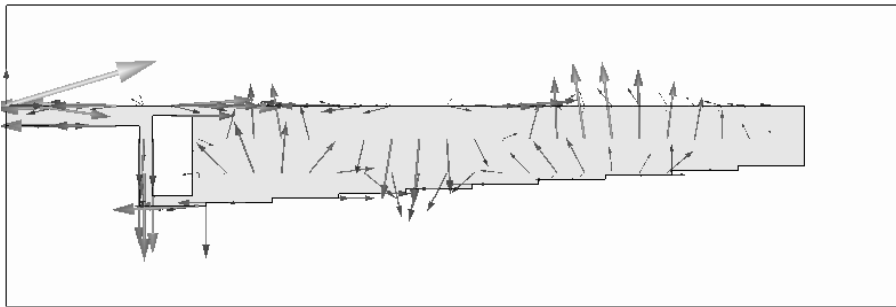


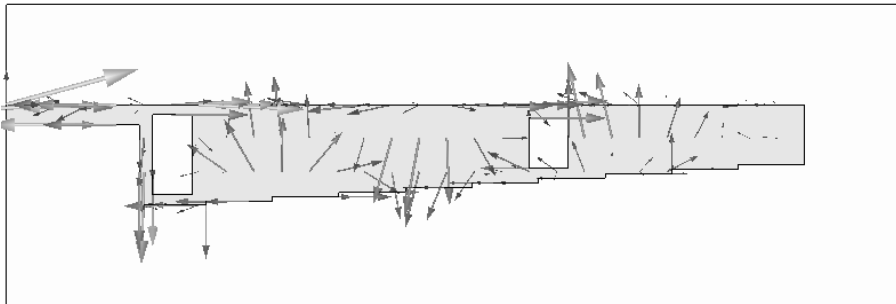
Fig. 4-5. Structures of LWA and simulated radiation pattern in YZ-plane at 6.0 GHz: (a) conventional tapered short LWA; (b) LWA with Slot 1; (c) LWA with Slot 1 and 2; (d) proposed LWA; (e) Radiation pattern.



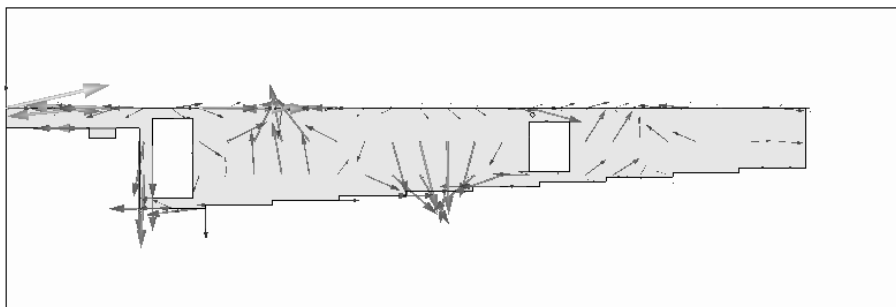
(a)



(b)



(c)



(d)

Fig. 4-6. Simulated surface current distributions at 6.0 GHz: (a) conventional tapered short LWA; (b) LWA with Slot 1; (c) LWA with Slot 1 and 2; (d) proposed LWA.

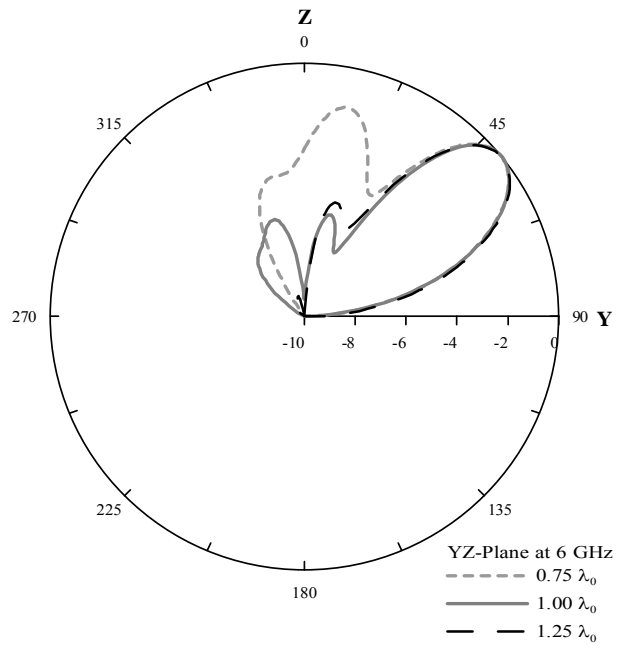
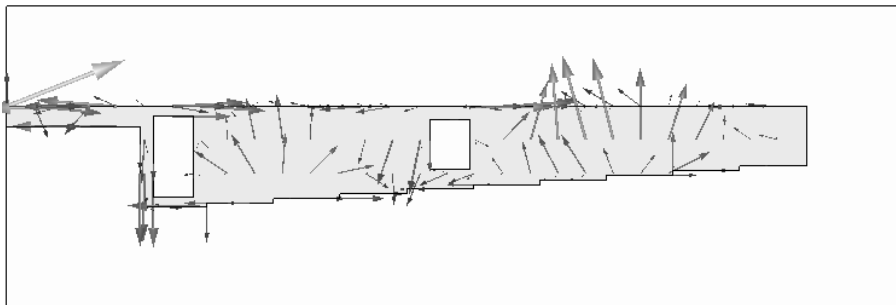
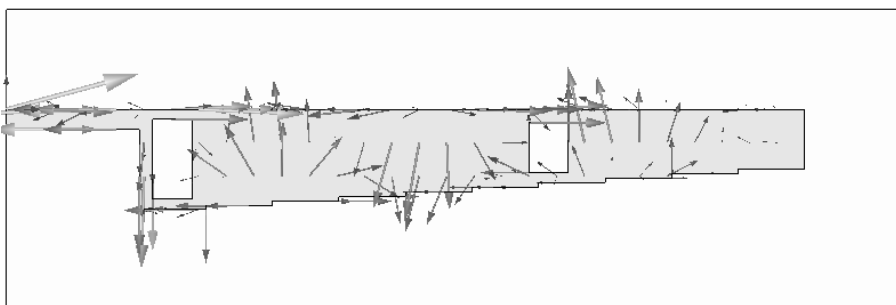


Fig. 4-7. Simulated radiation pattern in YZ-plane at 6.0 GHz.



(a)



(b)

Fig. 4-8. Simulated surface current distributions at 6.0 GHz: (a) $0.75 \lambda_0$ between Slot 1 and Slot 2; (b) $1.0 \lambda_0$ between Slot 1 and Slot 2.

4.3 Simulation and Measurement Results

The measured normalized radiation patterns of the proposed LWA at 5.9, 6.2, and 6.4 GHz are shown in Fig. 4-9. Comparing the measured radiation pattern of Fig. 4-3 with that of Fig. 4-9, it is found that the tapered short LWA and the proposed LWA are very similar in the characteristics of radiation angle and 3 dB radiation beamwidth within 6.2 GHz. However, the measured side lobe level (SLL) of the proposed LWA have been significantly improved from -0.01 to 6.13 dB at 6.4 GHz by using two slots and a shorting pin. The main lobe scanning angle of the proposed LWA is from 14° to 57° between 4.6 to 6.4 GHz. Fig. 4-10 exhibits the measured SLL, the SLL of the proposed LWA is less than -5 dB, and the variation of the SLL is independent on the frequency. Fig. 4-11 illustrates the measured maximum gains of the tapered LWA and the proposed LWA. The variation of maximum gain of the proposed LWA is slightly affected by this method, and the gains are larger than 4 dBi from 4.6 to 6.4 GHz. Fig. 4-12 plots the simulated and measured return losses. The 7-dB impedance bandwidth of measured result is about 1.6 GHz from 4.58 to 6.18 GHz. Although the bandwidth of the proposed LWA is narrower than the conventional tapered LWA (see Fig. 4-4), the proposed LWA can largely suppress side lobe level; therefore, it avoids the main lobe being replaced by the side lobe at higher frequency.

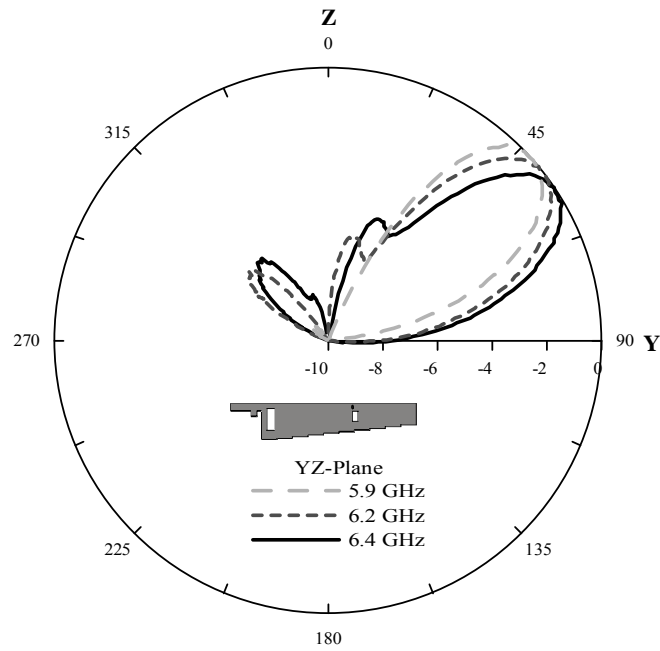


Fig. 4-9. Measured normalized radiation patterns of the proposed LWA.

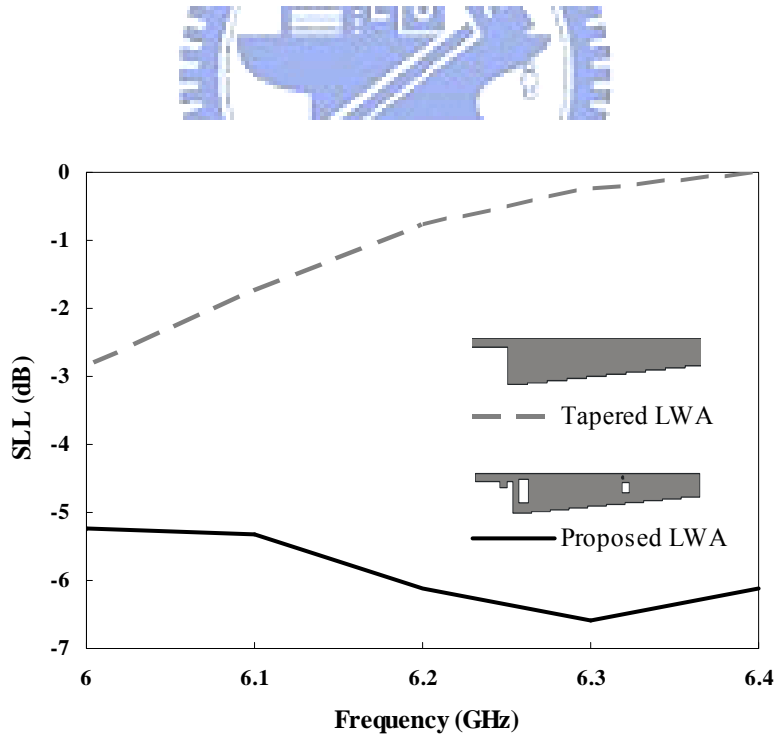


Fig. 4-10. Comparison of the measured side lobe level (SLL) of tapered LWA and proposed LWA.

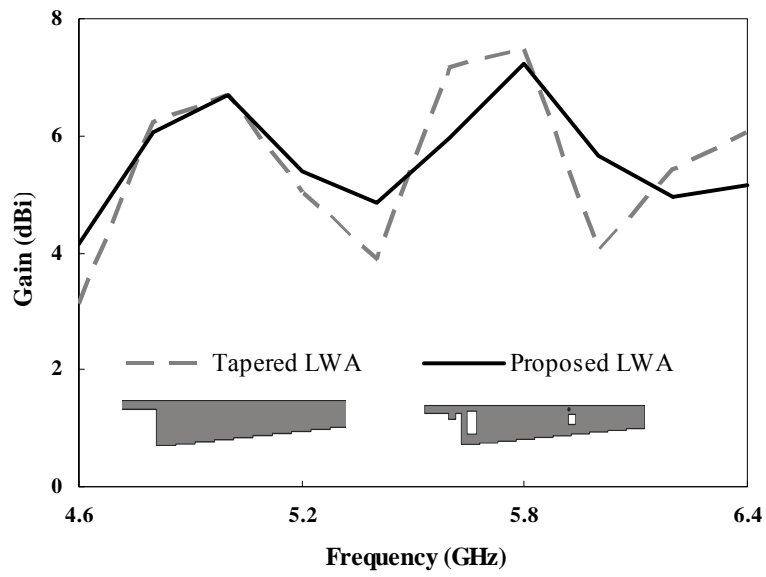


Fig. 4-11. Comparison of measured maximum gains of the tapered LWA and the proposed LWA.

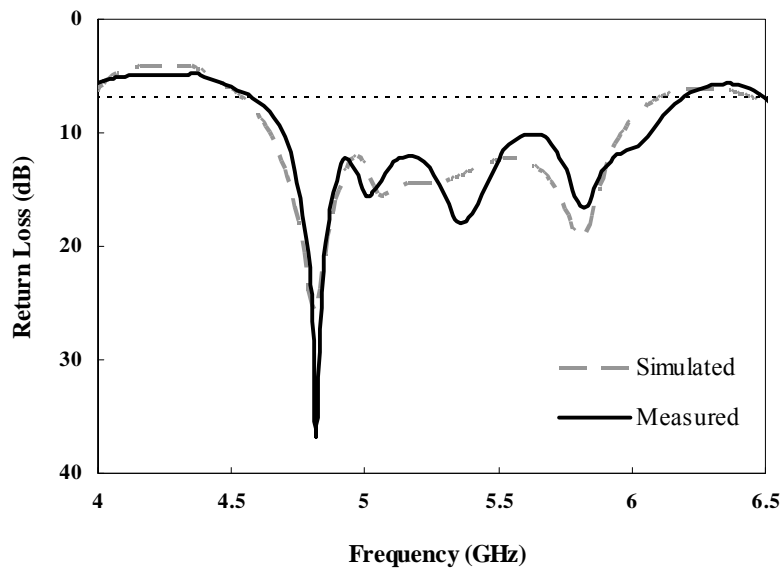
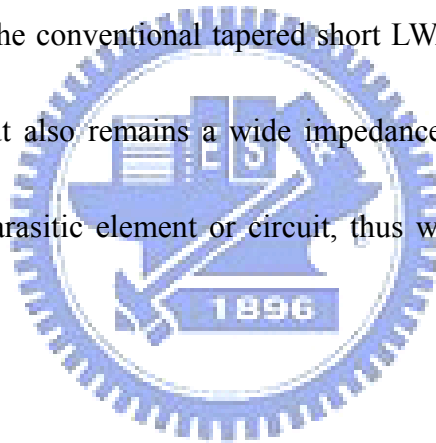


Fig. 4-12. Simulated and measured return losses of the proposed LWA.

4.4 Summary

In this chapter, a method is proposed to reduce the serious side lobe excited by the conventional tapered short LWA. By embedding two slots and a shorting pin, it can change the current distribution at the end of the tapered short LWA at higher frequency to reduce the radiation of the side lobe. According the measured results, the SLL of the proposed LWA maintains less than -5 dB from 6.0 to 6.4 GHz. The scanning range covers 43° from 14° to 57° , and the impedance bandwidth is achieved about 30% with respect to the center frequency at 5.38 GHz. Compared to the conventional tapered short LWA, the proposed LWA not only suppresses the side lobe, but also remains a wide impedance bandwidth. Furthermore, this method does not use any parasitic element or circuit, thus we can avoid enlarging antenna size.



4.5 References

- [4-1] W. Hong, T. L. Chen, C. Y. Chang, J. W. Sheen, and Y. D. Lin, "Broadband tapered microstrip leaky-wave antenna," *IEEE Trans. Antennas Propag*, vol. 51, no. 8, pp. 1922-1928, Aug. 2003.
- [4-2] V. Nalbandian and C. S. Lee, "Tapered leaky-wave ultra wide-band microstrip antenna," in *Proc. IEEE AP-S Int. Symp.*, 1999, pp. 1236-1239.



CHAPTER 5

END-FIRE RADIATED ON-CHIP MONOPOLE ANTENNA FOR WPAN APPLICATION

An end-fired radiated on-chip monopole antenna for wireless personal area network (WPAN) application is designed. The feeding network of coplanar waveguide (CPW) structure is proposed to feed the monopole antenna. The on-chip antenna is fabricated in TSMC 0.18- μm CMOS process. The architecture of this antenna inherits rectangular monopole antenna except for its asymmetric-fed, slit, and shorting path approaches. The asymmetric-fed is to provide dual-band around 60 GHz and end-fire radiation. In addition, by embedding a slit on the monopole antenna and a shorting pin on the ground plane, this antenna can achieve wide impedance bandwidth. According to the simulation results, the impedance bandwidth is 7.7 GHz for 10-dB return loss, which covers the range from 56.4 to 64.1 GHz. The simulated maximum gain is about 3.4 dBi, and the gain of end-fire direction is about 0.75 dBi at 60 GHz.

5.1 Coplanar Waveguide (CPW) Theory

In recent years, coplanar waveguide (CPW) structure is very widely used by microwave integrated circuits (MICs), monolithic microwave integrated circuits (MMICs), or RFIC system [5-1]~[5-3]. CPW, which was first proposed by C. P. Wen [5-4] in 1969, is fabricated on a dielectric substrate. Conventional CPW structure (see Fig. 5-1) consists of a center strip conductor with two semi-infinite ground planes on a dielectric substrate for the single input, called GSG. Furthermore, the metals of conventional CPW are on the same plane, and via holes are not required to fabricate [5-5] and [5-6]. CPW structure offers several advantages to replace microstrip structure [5-5] and [5-7]:

1. Cross talk effects are very weak because the signal line is existed between ground planes.
2. CPW has low dispersion to offer the wide band circuits and components.
3. As the signal is delivered on CPW, the radiation loss will be reduced.
4. Series and shunt connections are easy achieved.

The characteristic impedance of CPW is determined by the width of the signal line, w , and the width of the gap on either side, s . The approximate formula [5-8] is shown as

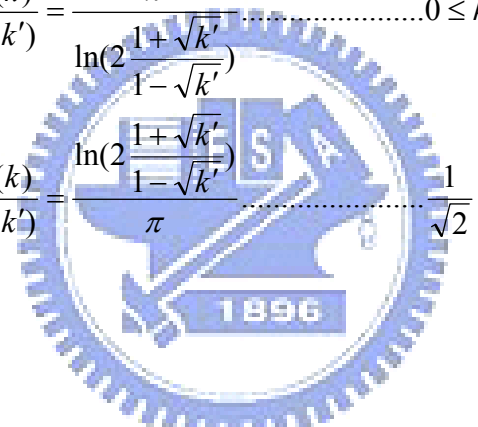
$$Z_0 = \frac{30\pi}{K(k)/K(k')} \cdot \frac{1}{\sqrt{\epsilon_{re}}} \quad (5-01)$$

where

$$\varepsilon_{re} = \frac{1 + \varepsilon_r}{2} \cdot (\tanh(1.785 \log(\frac{h}{s}) + 1.75) + \frac{ks}{h} (0.04 - 0.7k + 0.01(1 - 0.1\varepsilon_r)(0.25 + k))) \quad (5-02)$$

$$k = \frac{s}{s + 2w} \quad (5-03)$$

$$k' = \sqrt{1 - k^2} \quad (5-04)$$

$$\left\{ \begin{array}{l} \frac{K(k)}{K(k')} = \frac{\pi}{\ln(2 \frac{1 + \sqrt{k'}}{1 - \sqrt{k'}})} \dots\dots\dots 0 \leq k \leq \frac{1}{\sqrt{2}} \\ \frac{K(k)}{K(k')} = \frac{\ln(2 \frac{1 + \sqrt{k'}}{1 - \sqrt{k'}})}{\pi} \dots\dots\dots \frac{1}{\sqrt{2}} \leq k \leq 1 \end{array} \right. \quad (5-05)$$


where ε_r is the dielectric constant of the CPW structure. If the thickness of substrate is approximately infinite, the effective dielectric constant can be defined as

$$\varepsilon_{re} = \frac{1 + \varepsilon_r}{2} \quad (5-06)$$

According to these equations, the size of CPW structure can be designed.

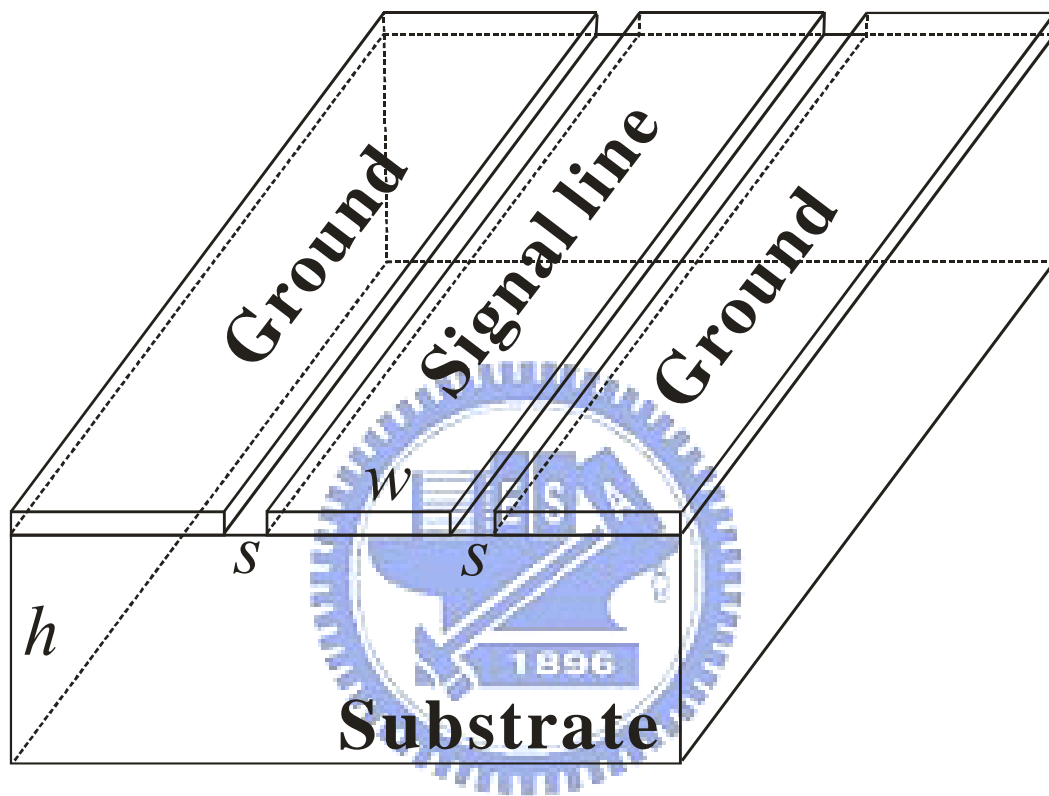
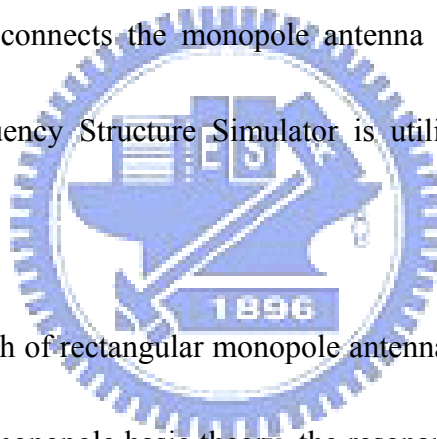


Fig. 5-1. 3D structure of conventional coplanar waveguide (CPW).

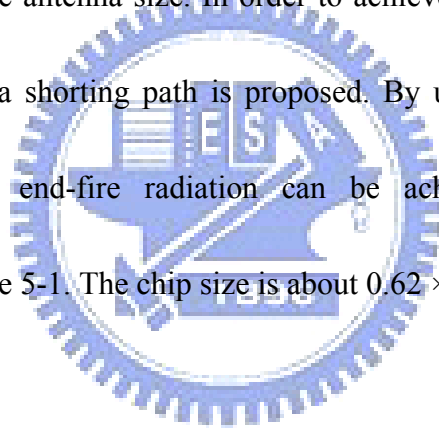
5.2 Antenna Design

The structure of the proposed on-chip monopole antenna is shown in Fig. 5-2. The on-chip antenna is fabricated in TSMC 0.18- μm CMOS process. The proposed antenna is etched on a silicon substrate with relative permittivity $\epsilon_r = 11.9$, thickness $H = 0.7$ mm, and $100 \Omega\text{-cm}$ material. The CPW structure is used for feeding network of this antenna. Besides, the gap and the width of the CPW matching feed line are respectively 40 and 80 μm . The antenna consists of three parts: a rectangular monopole antenna with a slit, an asymmetric-fed, and a shorting path which connects the monopole antenna and the ground plane. In this chapter, Ansoft High Frequency Structure Simulator is utilized to simulate the proposed antenna.



The length and the width of rectangular monopole antenna are respectively 0.35 mm and 0.75 mm. According to the monopole basic theory, the resonant frequency is excited at about 78.6 GHz, and the radiated direction is at the broadside direction. However, in order to reduce the resonant frequency and the radiated direction, an asymmetric-fed, which can cause different surface current distribution on the antenna, is applied. Figure 5-3 presents the surface current distribution of the monopole antenna with central-fed and asymmetric-fed. In Fig. 5-3(a), the current distribution of the central-fed can be divided into vertical and horizontal current, and two components with 180° out of phase are excited at the horizontal direction. Therefore, radiation at the horizontal direction in the far field is very weak, and

radiated direction is at the broadside direction. Asymmetric-fed, on the other hand, also generates the vertical and the horizontal currents in Fig. 5-3(b). Due to the current level, radiated direction is mainly caused by the horizontal current to generate end-fire radiation. Figure 5-4 shows the simulated normalized radiation patterns of the monopole antenna with asymmetric-fed at 60 GHz. It can be seen from Fig. 5-4 that the antenna generates the end-fire radiation. The simulated return losses of central- and asymmetric-fed are plotted in Fig. 5-5. The central-fed resonates a mode at 78.6 GHz, and the asymmetric-fed excites dual mode around 60 GHz to reduce the antenna size. In order to achieve the impedance matching, the method of using a slit and a shorting path is proposed. By using these methods, the wide impedance bandwidth and end-fire radiation can be achieved successfully. Detailed dimensions are listed in Table 5-1. The chip size is about $0.62 \times 1.00 \text{ mm}^2$.



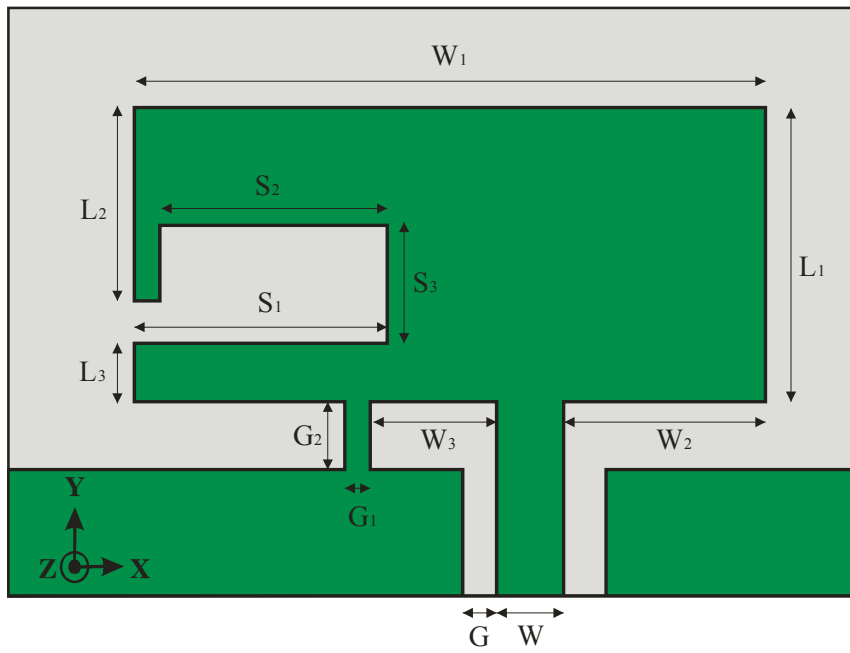
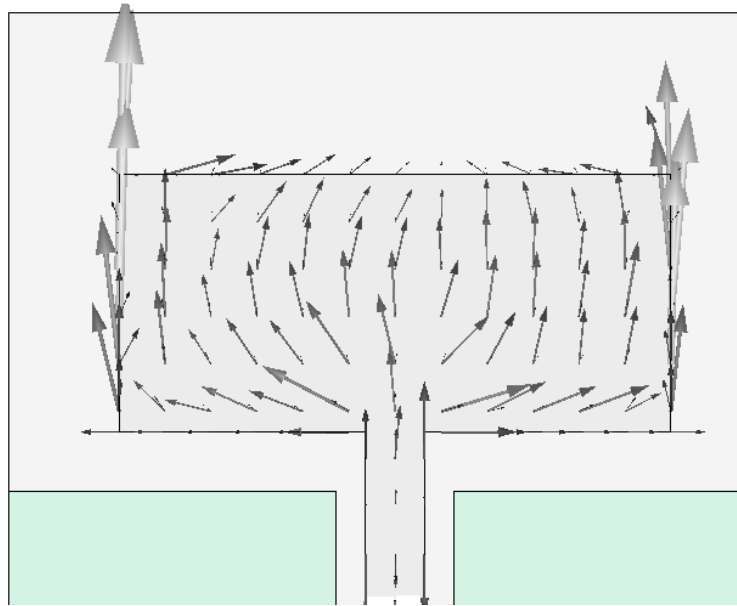
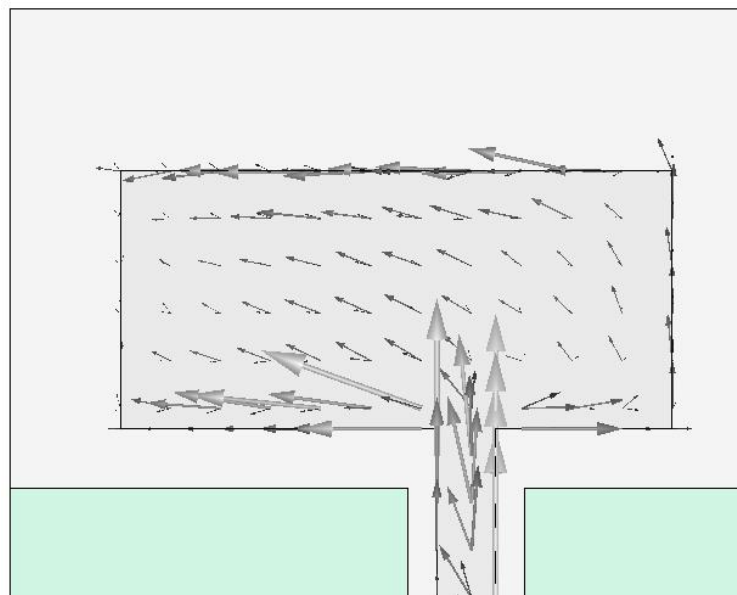


Fig. 5-2. Structure of the proposed on-chip monopole antenna.

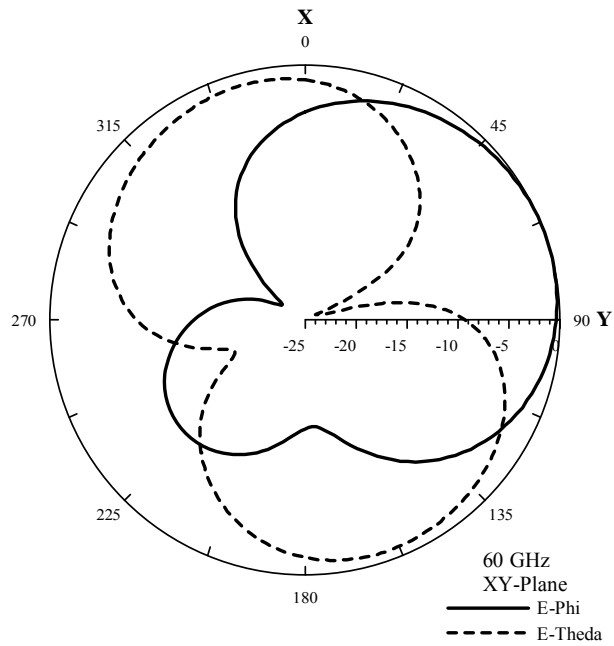


(a)

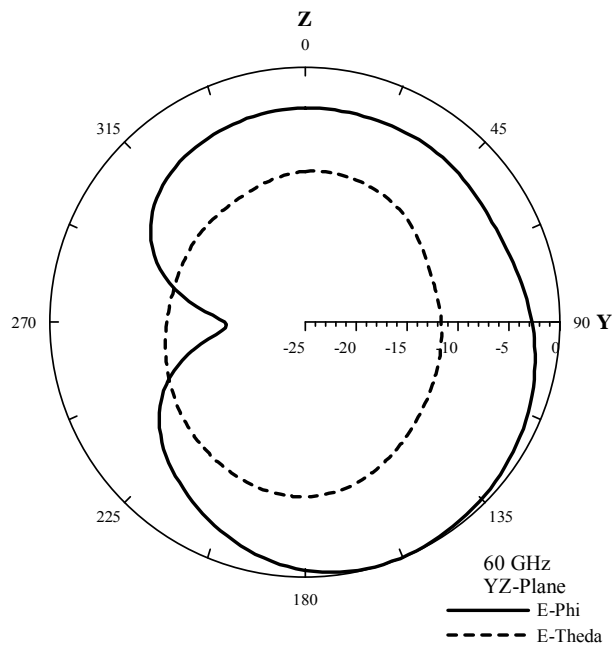


(b)

Fig. 5-3. Surface current distribution of the monopole antenna with central-fed and asymmetric-fed: (a) central-fed at 78.6 GHz; (b) asymmetric-fed at 60 GHz.



(a)



(b)

Fig. 5-4. Simulated normalized radiation patterns of the monopole antenna with asymmetric-fed at 60 GHz: (a) XY-Plane; (b) YZ-Plane.

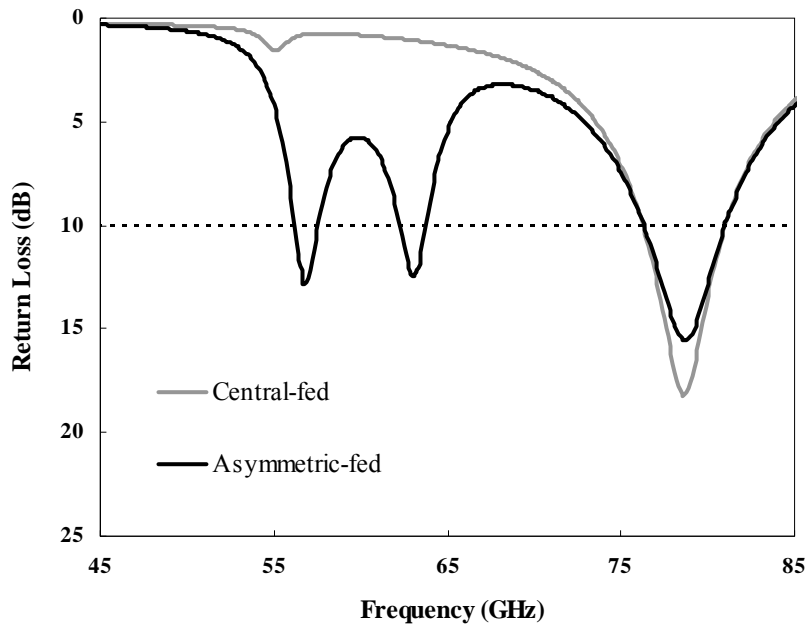


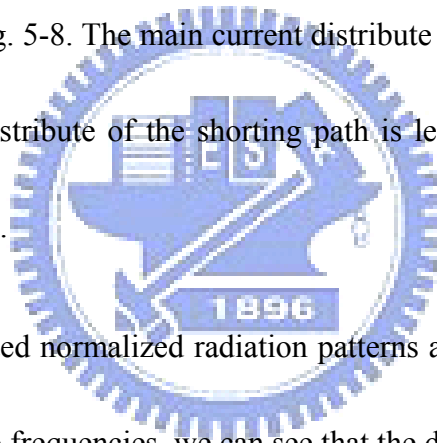
Fig. 5-5. Simulated return losses of central-fed and asymmetric-fed.

TABLE 5-1
DIMENSIONS OF THE PROPOSED MONOPOLE ANTENNA.

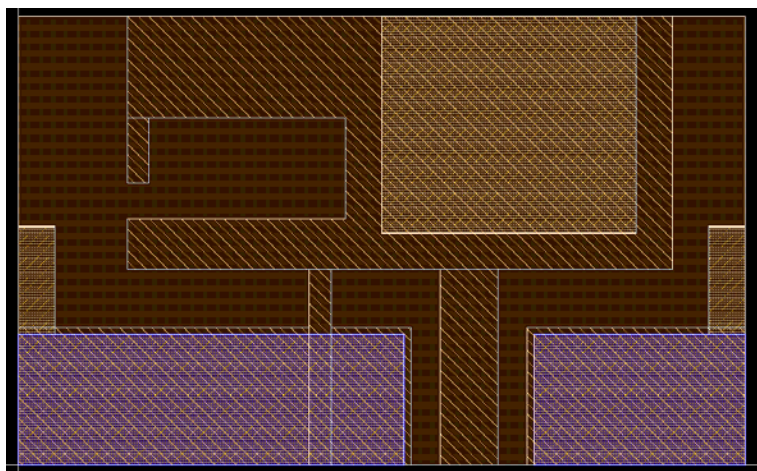
W	80 μm	G	40 μm
W ₁	0.75 mm	G ₁	30 μm
W ₂	0.24 mm	G ₂	80 μm
W ₃	0.15 mm	L ₁	0.35 mm
S ₁	0.3 mm	L ₂	0.23 mm
S ₂	0.27 mm	L ₃	70 μm
S ₃	0.14 mm		

5.3 Simulation Results

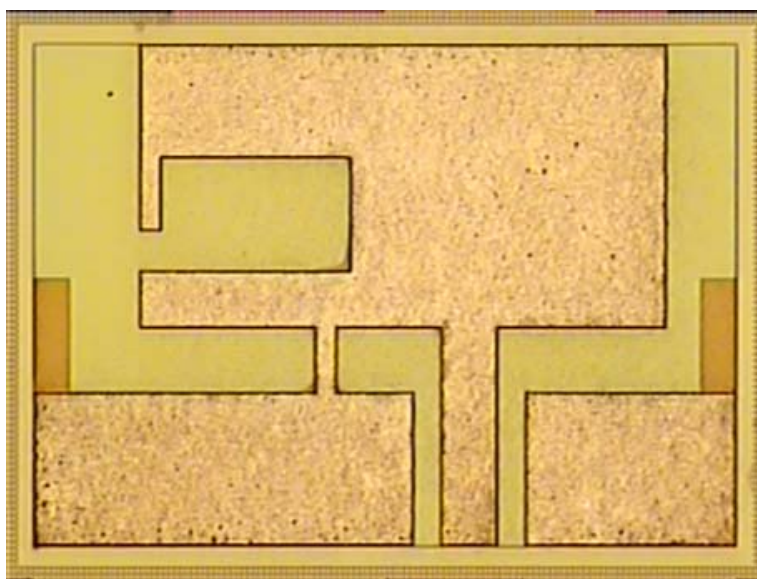
The layout photo and the micrographic of the on-chip antenna are shown in Fig. 5-6. Due to the dummy of 0.18- μm CMOS process, the structures of the layout photo and the proposed antenna have some different parts. However, these parts affect slightly the bandwidth and radiation pattern. Figure 5-7 plots the simulated return loss of the proposed antenna. The 10-dB impedance bandwidth of measured result is about 7.7 GHz from 56.4 to 64.1 GHz, and the minimum return loss is about 32 dB. The current distributions of the on-chip antenna at 58 and 63 GHz are shown in Fig. 5-8. The main current distribute is over the path of the slit at 58 and 63 GHz. The current distribute of the shorting path is less, so that the shorting path is used to match the impedance.



The 2D and 3D simulated normalized radiation patterns at 58 and 63 GHz are shown in Fig. 5-9 and 5-10. At the two frequencies, we can see that the direction of the pattern results is at end-fire direction. However, the simulated maximum gain of the proposed antenna is not at end-fire direction in YZ-Plane. As the result of the silicon substrate with 10 $\Omega\text{-cm}$ material, the input power is attracted to the substrate, and then the direction of the maximum gain is affect. Fig. 5-11 and Fig. 5-12 illustrate variation of the maximum gain and the gain at end-fire direction. Due to the silicon substrate of 100 $\Omega\text{-cm}$ material, the maximum gains and the gain at end-fire direction can be larger than 2.1 dBi and -0.5 dBi from 57 to 64 GHz.



(a)



(b)

Fig. 5-6. Proposed on-chip antenna: (a) layout photo; (b) micrographic.

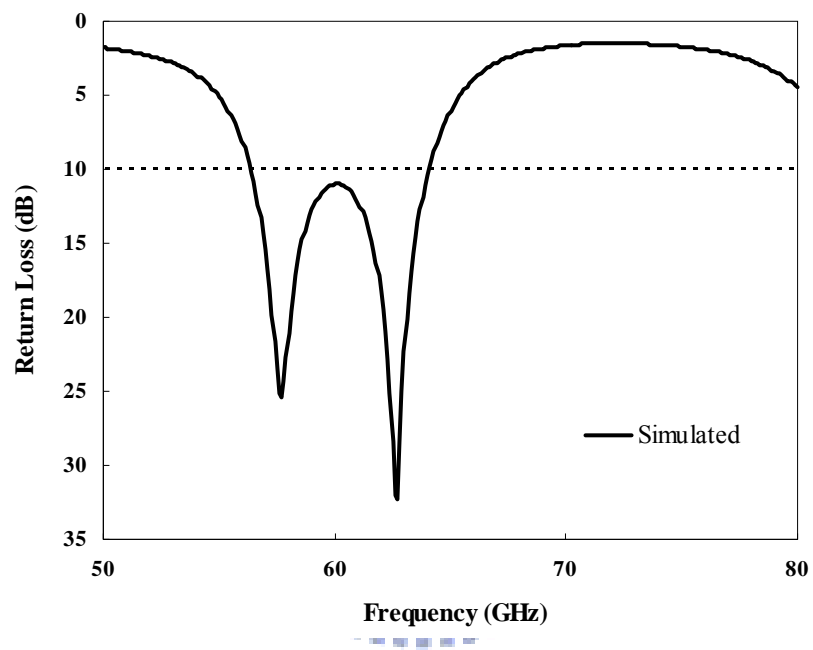
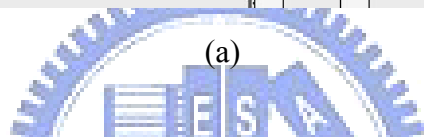
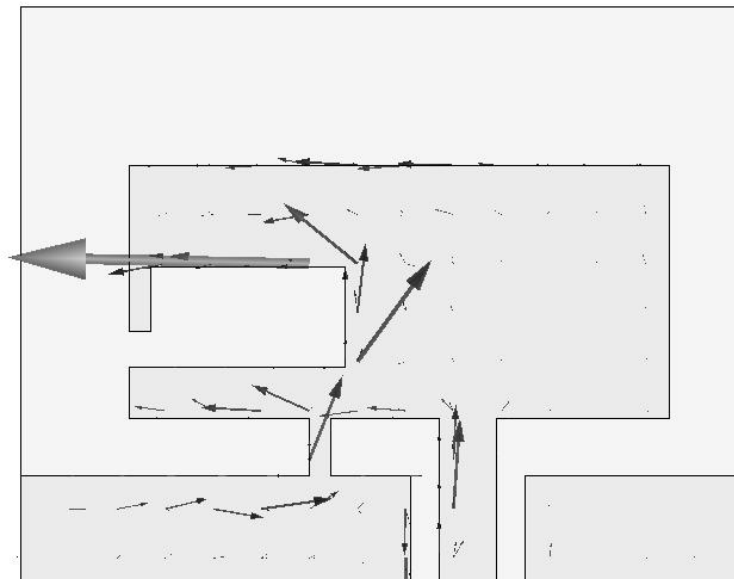
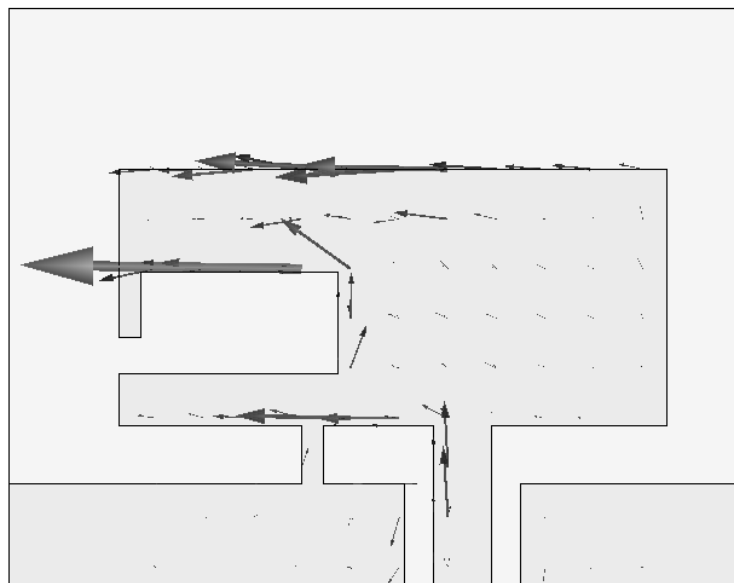


Fig. 5-7. Simulated return loss of the proposed antenna.



(a)



(b)

Fig. 5-8. Current distribution of the on-chip antenna: (a) 58 GHz; (b) 63 GHz.

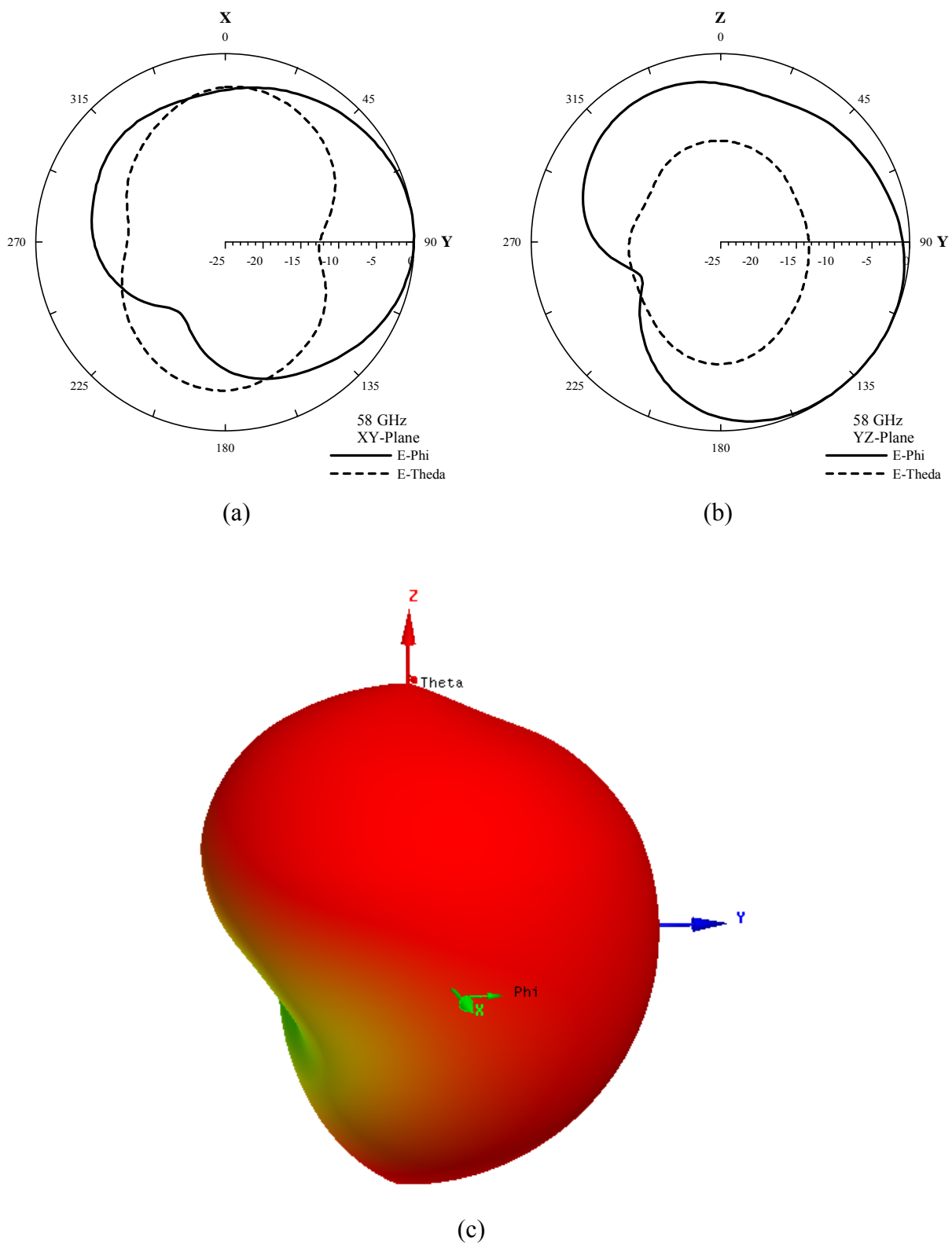


Fig. 5-9. Simulated normalized radiation patterns of on-chip antenna at 58 GHz: (a) XY-Plane; (b) YZ-Plane; (c) 3D.

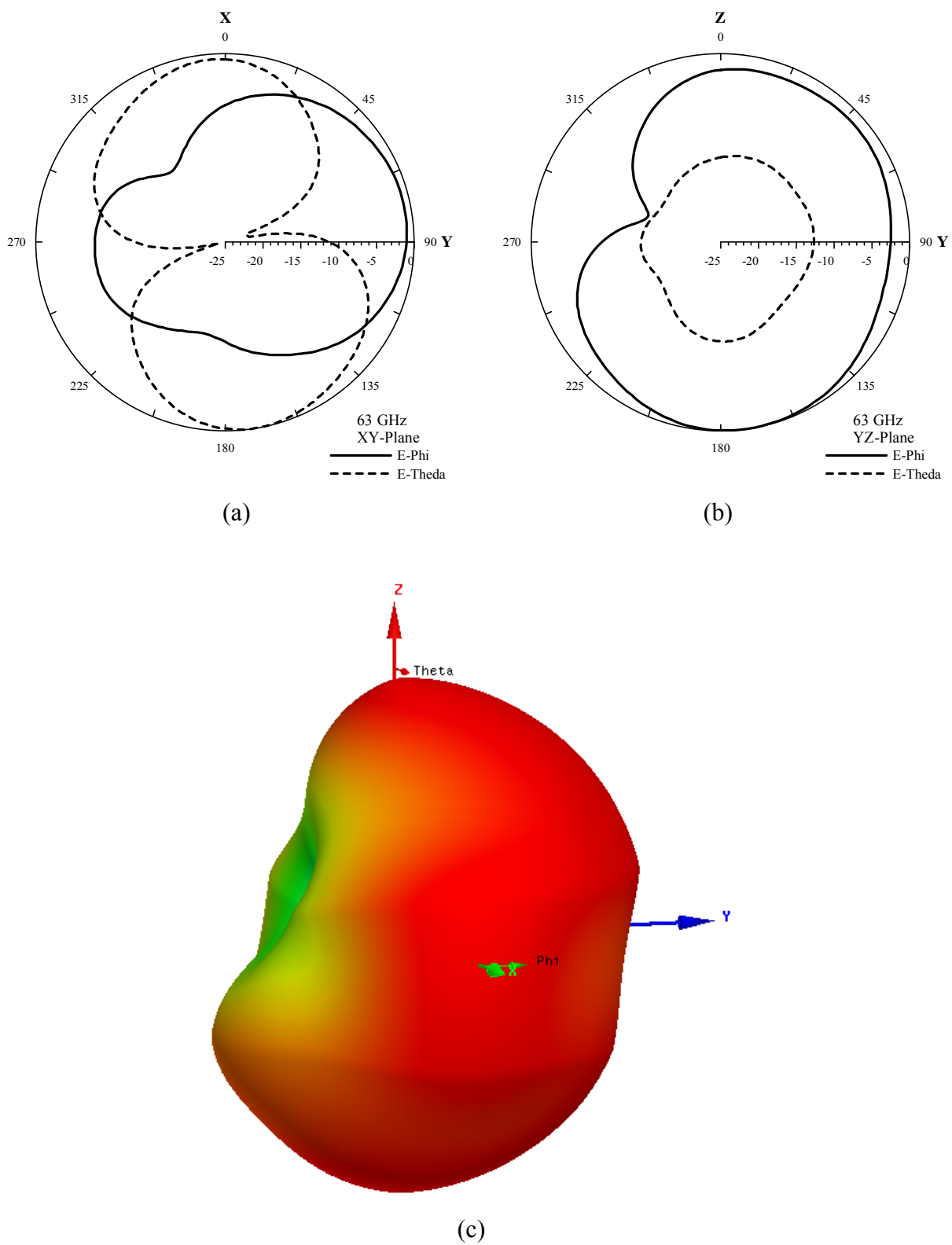


Fig. 5-10. Simulated normalized radiation patterns of on-chip antenna at 63 GHz: (a) XY-Plane; (b) YZ-Plane; (c) 3D.

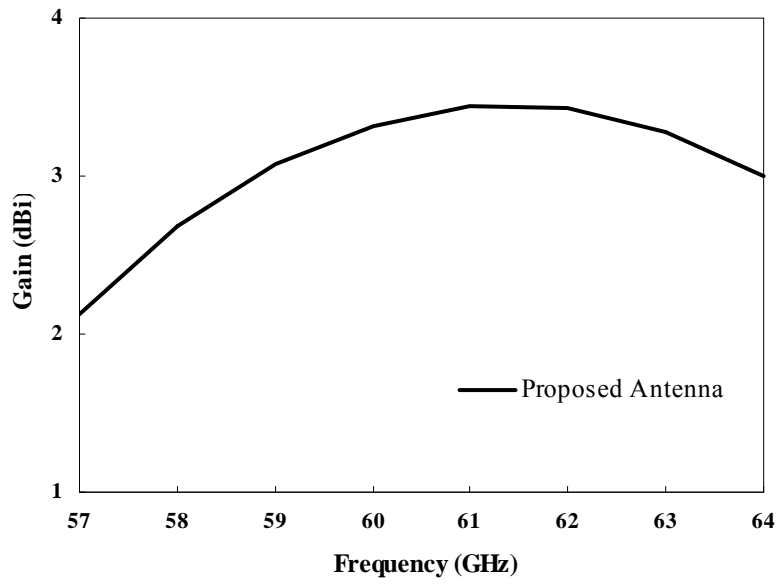


Fig. 5-11. Maximum simulated gain of the proposed LWA.

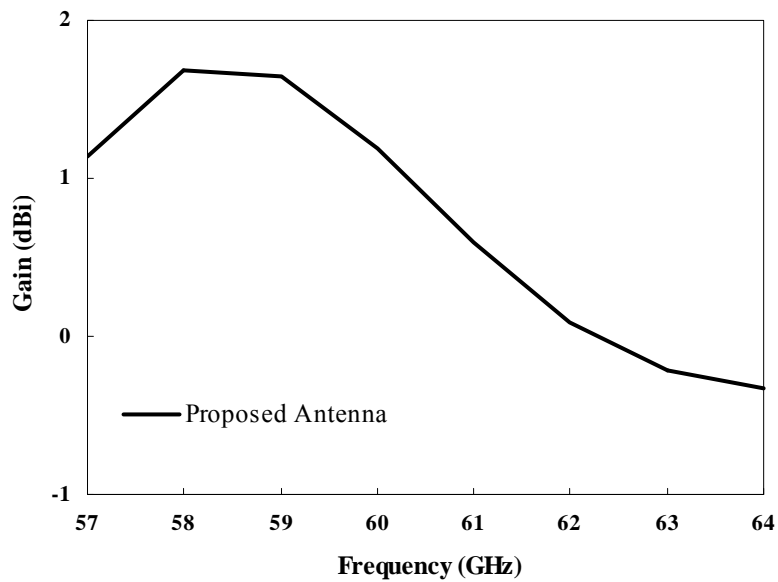
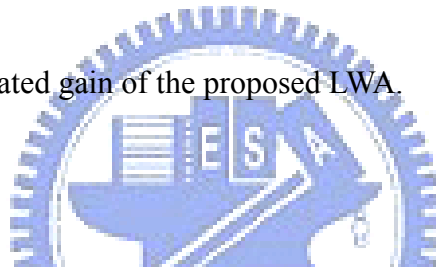
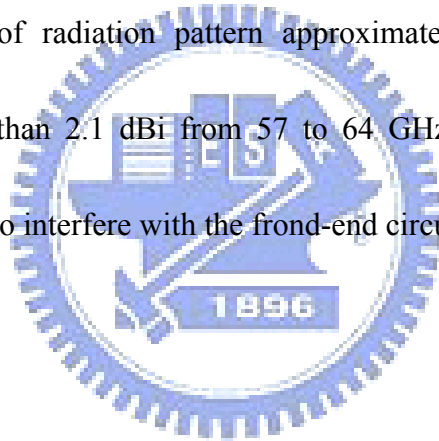


Fig. 5-12. Simulated gain of the proposed LWA at end-fire direction.

5.4 Summary

In this chapter, an on-chip CMOS monopole antenna is proposed to excite wide impedance bandwidth for wireless personal area network application and radiate to the end-fire direction. By using the asymmetric-fed, a slit on the monopole antenna, and a shorting pin on the ground plane, this antenna can achieve wide impedance bandwidth and end-fire radiation. The on-chip antenna size is only about $0.62 \times 1.00 \text{ mm}^2$. According the results, the impedance bandwidth is about 12.8 % with respect to the center frequency at 60.25 GHz, the direction of radiation pattern approximates end-fire direction, and the maximum gains are larger than 2.1 dBi from 57 to 64 GHz. This design can reduce the radiated power of back side to interfere with the frond-end circuit.



5.5 References

- [5-1] S. S. Hsu, K. C. Wei, C. Y. Hsu, and H. R. Chuang, "A 60-GHz millimeter-wave CPW-fed Yagi antenna fabricated by using 0.18- μm CMOS technology," *IEEE Electron Device Lett.*, vol. 29, no. 6, pp. 625-627, Jun. 2008.
- [5-2] A. Shamim, L. Roy, N. Fong, and N. G. Tarr, "24 GHz on-chip antennas and Balun on bulk Si for air transmission," *IEEE Trans. Antennas Propag.*, vol. 56, no. 2, pp.303-311, Feb. 2008.
- [5-3] C. Cao, Y. Ding, X. Yang, J. J. Lin, H. T. Wu, A. K. Verma, J. Lin, F. Martin, and K. K. O, "A 24-GHz transmitter with on-chip dipole antenna in 0.13- μm CMOS," *IEEE J. Solid-State Circuits*, vol. 43, no. 6, pp.1394-1402, Jun. 2008.
- [5-4] C. C. Lin, S. S. Hsu, C. Y. Hsu, and H. R. Chuang, "A 60-GHz millimeter-wave CMOS RFIC-on-chip triangular monopole antenna for WPAN applications," in *Proc. IEEE AP-S Int. Symp.*, Jun. 2007, pp. 2522-2525.
- [5-5] C. H. Doan, S. Emami, A. M. Niknejad, and R. W. Brodersen, "Design of CMOS for 60 GHz applications," in *IEEE Proc. Solid-State Circuits Conf.*, 2004, pp. 440-449.
- [5-6] D. Bhattacharya, "Characteristic Impedance of Coplanar Waveguide," *Electron. Lett.*, vol. 21, no. 13, pp. 557, Jun. 20, 1985.
- [5-7] F. L. Lin and R. B. Wu, "Computations for radiation and surface-wave losses in coplanar waveguide bandpass filters," *IEEE Trans. Microw. Theory Technol.* Vol. 47, no. 4, 385-389, Apr. 1999.
- [5-8] R. N. Simons, *Coplanar Waveguide Circuits, Components, and Systems*, John Wiley & Sons, Inc., 2001.

CHAPTER 6

FUTURE STUDY

The proposed designs have achieved the CP monopole antenna, reduced the LWA size, solved the problem of serious side lobe, and designed on-chip antenna. Therefore, some topologies will be proposed in this section.

6.1 Radiation of Dual-Beam

In chapter 3, the slot-lobe is radiated through the slot of the proposed LWA and the measured gain of the slot-lobe is about 4 dB lower than the main beam. If the slot-lobe level is increased, the top and the bottom position will be simultaneously scanned by difference operating frequency. We propose a topology to approach this requirement. Figure 6-1 shows the schematic configuration of the topology. Some stubs are added into bigger slots of ground plane to couple the power of LWA. The power is coupled into these stubs to increase the radiation of bottom position. Furthermore, we can use switches [6-1], which are shown in Fig. 6-2, to achieve large scanning region.

6.2 Integration of Front-End

In chapter 5, an on-chip CMOS monopole antenna is proposed to excite wide impedance bandwidth for wireless personal area network application and radiate to the end-fire direction. In order to further the application, the on-chip antenna can be integrated into front-end circuit such as receiver and transmitter front-end in [6-2] and [6-3] (see Fig. 6-3). The impedance matching and the effects of electromagnetic interference (EMI) will be considered in the integrated process. These problems are not alike the commercial produce, front-end circuit and antenna of which are individually designed, so that the effects of EMC and EMI can be solved by many methods and experiences. However, because the on-chip antenna and the front-end circuit are integrated into a chip, these problems will be a period of critical challenge.

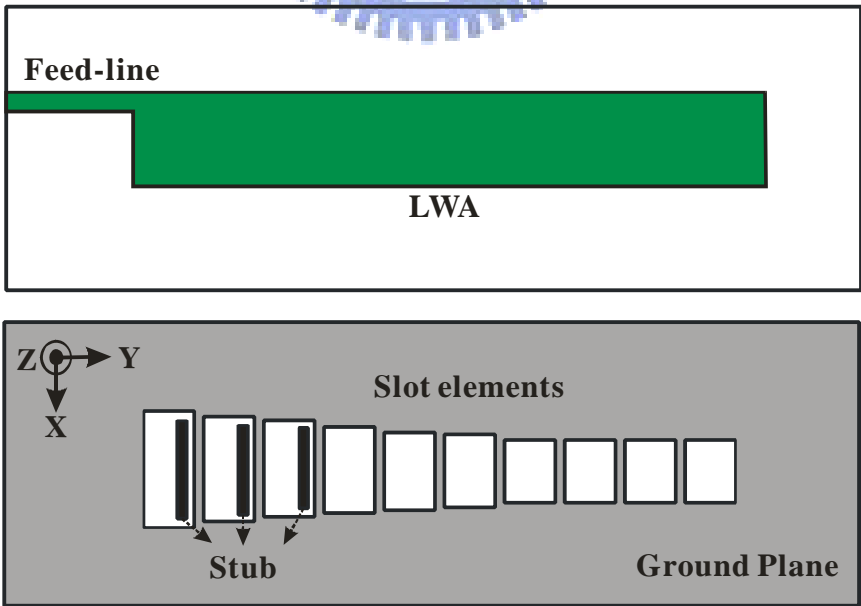


Fig. 6-1. Schematic configuration of the topology for dual-beam radiation.

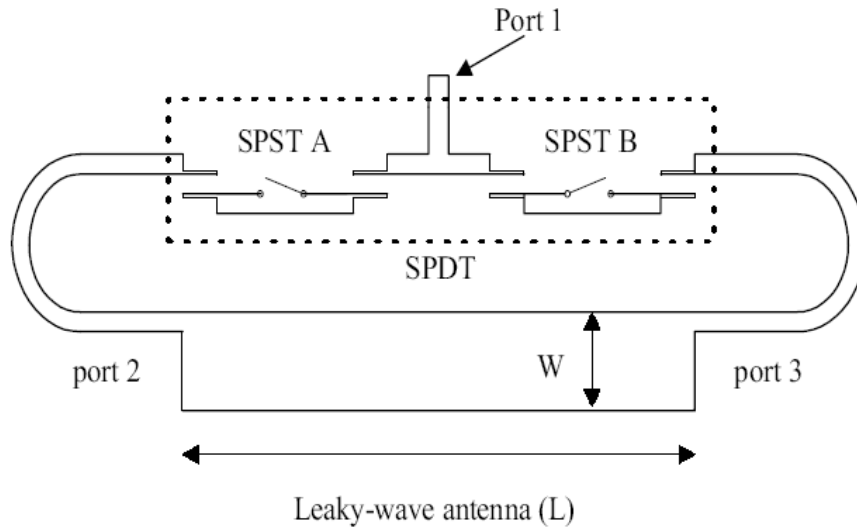
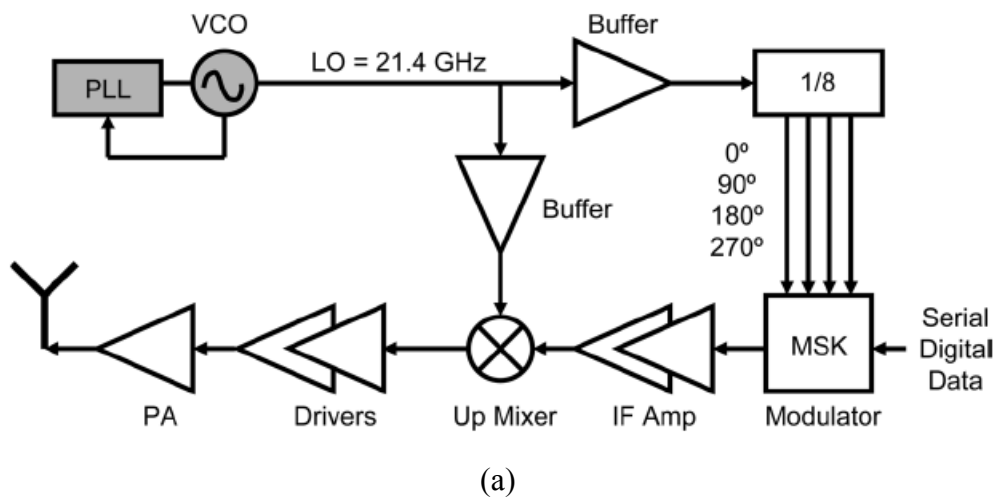
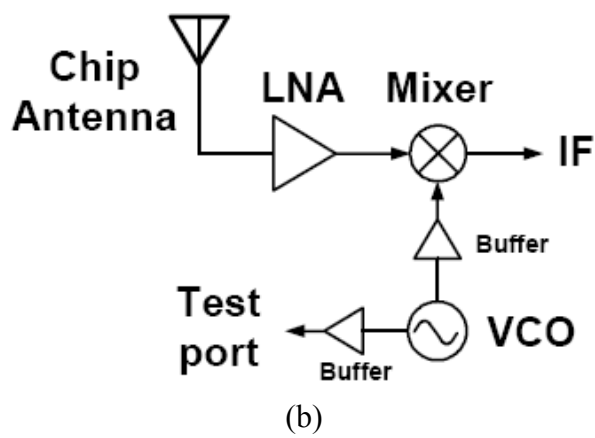


Fig. 6-2. Configure of a beam-switchable scanning LWA [6-1].



(a)



(b)

Fig. 6-3. Configure of frond-end: (a) transmitter [6-2], (b) receiver [6-3].

6.3 References

- [6-1] C. J. Wang, Y. C. Shin, and C. F. Joe, "Beam-switchable scanning leaky-wave antenna," *Electron. Lett.*, vol. 36, no. 7, pp. 596-597, Mar. 30, 2000.
- [6-2] C. Cao, Y. Ding, X. Yang, J. J. Lin, H. T. Wu, A. K. Verma, J. Lin, F. Martin, K. O. Kenneth, "A 24-GHz transmitter with on-chip dipole antenna in 0.13- μm CMOS," *IEEE J. Solid-State Circuits*, vol. 43, no. 6, pp.1394-1402, Jun. 2008.
- [6-3] C. S. Wang, J. W. Huang, S. H. Wen, S. H. Yeh, and C. K. Wang, "A CMOS RF front-end with on-chip antenna for V-band broadband wireless communications," in *IEEE European Solid State Circuits Conference*, Sep. 2007, pp. 143-146.

